Aus der Medizinische Klinik mit Schwerpunkt Hämatologie, Onkologie
und Tumorimmunologie (Campus Virchow-Klinikum) der
Medizinischen Fakultät Charité – Universitätsmedizin Berlin

DISSERTATION

T-cell surveillance of therapy-induced senescent lymphoma cells in the presence of anti-CD19/CD20 × CD3 bispecific antibodies

T-Zell-Überwachung von therapieinduzierten seneszenten Lymphomzellen in Gegenwart von Anti-CD19/CD20 × CD3 bispezifischen Antikörpern

zur Erlangung des akademischen Grades
Doctor medicinae (Dr. med.)

vorgelegt der Medizinischen Fakultät
Charité – Universitätsmedizin Berlin

von

Xiurong Cai
aus Guangdong, China

Datum der Promotion: 30.11.2023

Table of Contents

List of Figures

List of Tables

List of Abbreviations

5-FU	5-fluorouracil
ANOVA	Analysis of variance
ASF1A	Anti-silencing function protein 1 homolog A
AURKA	Aurora A Kinase
Bcl2	B-cell lymphoma 2
BiTE	Bispecific T cell engager
BRD4	Bromo and extra terminal domain protein 4
BSA	Bovine serum albumin
BsAbs	Bispecific antibodies
BSD	Blasticidin
CARD11	Caspase Recruitment Domain Family Member 11
CAR-T cell	Chimeric antigen receptor T cell
CCL2/MCP-1	C-C chemokine ligand 2/Monocyte chemoattractant protein-1
CCR2	C-C chemokine receptor type 2
CDK	Cyclin-dependent kinase
CDKN1A	Cyclin Dependent Kinase Inhibitor 1A
CDKN2A	Cyclin Dependent Kinase Inhibitor 2A
CIITA	Class II Major Histocompatibility Complex Transactivator
COX2	Cyclooxygenase-2
CR	Complete response
Crebbp	CREB Binding Protein
CSF1	Colony Stimulating Factor 1
CTX	Cyclophosphamide
CXCL14	Chemokine (C-X-C motif) ligand 14
CXCR1/2	C-X-C chemokine receptor 1/2
DAVID	Database for Annotation, Visualization and Integrated Discovery
DDR	DNA damage response
DLBCL	Diffuse large B cell lymphoma
DMEM	Dulbecco's Modified Eagle Medium
DMSO	Dimethyl sulfoxide
DPP4	Dipeptidyl peptidase 4
EGFR	Epidermal growth factor receptor
ERK	Extracellular signal-regulated kinase
ETS1/2	ETS proto-oncogene 1/2
FACS	Fluorescence-activated cell sorting
FASL	FAS ligand
Fc	Fragment crystallizable region
FCM	Flow cytometry
FcR	Fc receptors

FcγR	Fc-gamma receptors
FFS	Forward scatter
FMO	Fluorescence minus one
GFP	Green fluorescent protein
GO	Gene Ontology
GSEA	Gene Set Enrichment Analysis
H3K9	histone H3-lysine 9
HBS	HEPES-buffered saline
HIRA	Histone cell cycle regulator
HLA-E	Major Histocompatibility Complex, Class I, E
ICAM-1	Intercellular adhesion molecule–1
IDO	Indoleamine-pyrrole 2,3-dioxygenase
IFN-γ	Interferon-γ
IgG	Immunoglobulin G
IL-1β	Interleukin 1β
IL-2	Interleukin 2
IL-6	Interleukin 6
IL-8	Interleukin 8
IMDM	Iscove's modified Eagle's medium
JAK2	Janus Kinase 2
JMJD2C	Jumonji domain-containing protein 2C
L1	LINE-1
LB medium	Luria-Bertani medium
LCs	Lymphoma cells
LFA-1	Lymphocyte function-associated antigen 1
LSD1	Lysine-specific demethylase 1A
MAF	Mafosfamide
MAPK	Mitogen-activated protein kinase
MDM2	Mouse double minute 2 homolog
MDSCs	Myeloid-derived suppressor cells
MFI	Mean fluorescence intensity
MHC-I	Major histocompatibility complex class I
MHC-II	Major histocompatibility complex class II
MICA	MHC class I chain-related protein A
MICB	MHC class I chain-related protein B
MMPs	Matrix metalloproteinases
MSCV	Murine stem-cell retrovirus
mTOR	Mammalian target of rapamycin
MyD88	Myeloid differentiation primary response 88
NES	Normalized enrichment score
NF-κB	Nuclear factor kappa-light-chain-enhancer of activated B cells
NK cells	Natural killer cells

NKG2A	Natural Killer Group 2A
NKG2D	Natural Killer Group 2D
NOTCH	Neurogenic locus notch homolog protein 1
ORR	Overall response rate
PARPi	poly (ADP-ribose) polymerase 1 inhibitor
PBS	Phosphate buffered saline
PD-1	Programmed cell death protein 1
PD-L1	Programmed death-ligand 1
PFA	Paraformaldehyde
PGE2	Prostaglandin E2
PI3K	Phosphoinositide 3-kinase
PTEN	Phosphatase and tensin homolog
puro	Puromycin
R/R DLBCL	Refractory or relapsed DLBCL
Rb	retinoblastoma protein
R-CHOP	Rituximab, cyclophosphamide, doxorubicin hydrochloride, vincristine (Oncovin) and prednisolone
SAHF	Senescence-associated heterochromatin foci
SAS	Senescence-associated stemness
SASP	senescence-associated secretory phenotype
SA-β-gal	Senescence-associated beta-galactosidase
scFvs	Single chain variable fragments
SD	Standard deviation
SIRPα	Signal-regulatory protein-α
SPF	Specific pathogen-free
SSC	Side scatter
STAT3	Signal transducer and activator of transcription 3
STING	Stimulator of interferon genes
Suv39h1	Suppressor of variegation 3-9 homolog 1
TAAs	Tumor-associated antigens
TGF-β	Transforming growth factor-β
TIS	Therapy-induced senescence
TNF–α	Tumor necrosis factor–α
Tregs	Regulatory T cells
uPAR	Urokinase-type plasminogen activator receptor
Wnt	Wingless and Int-1
X-Gal	5-bromo-4-chloro-3-indolyl-beta-D-galacto-pyranoside

Abstract (English)

Background

Molecular heterogeneity and variable treatment sensitivity largely account for patients with diffused large B-cell lymphoma (DLBCL) failing curative Rituximab- CHOP therapy, leading to refractory/relapsed DLBCL with dismal outcomes despite novel next-line options. Therapy-induced state switches such as cellular senescence may affect the long-term outcome but remain understudied. Therapy-induced senescence (TIS) can be marked a double-edged sword, as it is beneficial as a stable arrest program but detrimental due to a senescence-associated pro-inflammatory secretome and stem-like reprogramming. Especially, the T-cell surveillance of senescent B-cell lymphoma deserves further investigation. This study explores how T cells can be harnessed to eliminate TIS lymphoma cells, with a specific view on the immunostimulation of anti-CD19/CD20 × CD3 bispecific antibodies (CD19-BsAb and CD20-BsAb, respectively) in this process.

Methods

Our published microarray-based gene dataset was used for gene set enrichment analysis, functional annotation and clustering analysis. A well-established TIS model, treating Bcl2-protected *Eμ-myc* lymphoma cells with mafosfamide (MAF), was used in co-culture with unstimulated pan T cells from lymphoma-naïve strain-matched donor mice (unstimulated T cells) in the presence or absence of CD19-BsAb or CD20-BsAb. The viability of lymphoma cells and phenotypes of co-cultured T cells were measured by flow cytometry.

Results

TIS lymphoma cells exhibited enriched immune response-related genetic signatures, with an increased expression of MHC-I/II, co-stimulatory factors (CD80, CD86) and PD-L1 on the cell surfaces. Unstimulated T cells preferentially killed TIS lymphoma cells, which were prone to interact with and activate the T cells. The CD19-BsAb and CD20-BsAb boosted the interaction of T cells with TIS lymphoma cells, resulting

in enhanced T-cell activation, proliferation and anti-lymphoma cytotoxicity. In addition, CD19-BsAb facilitated T cells to interact with proliferating lymphoma cells, leading to some immunogenic cell death of non-chemo-exposed lymphoma cells. PD-L1^{high} TIS lymphoma cells were less sensitive to T-cell killing *ex vivo*, even in the presence of CD20-BsAb. These findings indicate PD-L1/PD-1 immune checkpoint blockade as a critical co-strategy to enhance T-cell killing against TIS lymphoma cells.

Conclusion

This study depicted the immunostimulatory and immunoinhibitory signatures in TIS lymphoma cells. The T-cell-redirecting CD19-BsAb facilitated unstimulated T cells to kill proliferating as well as TIS lymphoma cells, while CD20-BsAb selectively boosted the T-cell killing of TIS lymphoma cells. Furthermore, PD-L1 blunted T-cell cytotoxicity towards TIS lymphoma cells, suggesting the therapeutic application of PD-L1/PD-1 blockade to de-repress senolytic T-cell activity. This study is likely to inspire future clinical research on the T-cell-redirecting BsAb in DLBCL care with the aim to target TIS lymphoma remainders.

Abstract (German)

Hintergrund

Die molekulare Heterogenität und die unterschiedliche Behandlungssensitivität sind der Grund dafür, dass die kurative R-CHOP-Therapie bei Patienten mit diffus großzelligem B-Zell Lymphom (DLBCL) versagt. Therapieinduzierte Seneszenz (TIS) kann den langfristigen Therapieerfolg beeinflussen, ist aber noch nicht ausreichend erforscht. Als stabiles Arrestprogramm ist TIS vorteilhaft, aber aufgrund eines Seneszenz-assoziierten proinflammatorischen Sekretoms und einer stammzellähnlichen Reprogrammierung auch nachteilig, was sie zu einem zweischneidigen Schwert macht. Die T-Zell-Überwachung des seneszenten Lymphoms bedarf weiterer Untersuchungen. In dieser Studie wird untersucht, wie T-Zellen genutzt werden können, um TIS-Lymphomzellen in Gegenwart von bispezifischen Anti-CD19/CD20 × CD3-Antikörpern (BsAb) zu eliminieren.

Methoden

Unser veröffentlichter, Microarray-basierter Genexpressions-Datensatz wurde für die Analyse der Anreicherung von Gensätzen, funktionelle Annotation und Clustering-Analysen verwendet. Bcl2-geschützte *Eμ-myc* Lymphomzellen, die mit Mafosfamid behandelt wurden, dienten als TIS-Modell, und wurden mit unstimulierten T-Zellen von Lymphom-naïven Mäusen in An- oder Abwesenheit von CD19-BsAb oder CD20-BsAb ko-kultiviert. Die Viabilität der Lymphomzellen und der Phänotyp der T-Zellen wurden mittels Durchflusszytometrie gemessen.

Ergebnisse

TIS-Lymphomzellen zeigten angereicherte genetische Signaturen im Zusammenhang mit der Immunantwort und zeigten eine erhöhte Oberflächenexpression von MHC-I/II, CD80, CD86 und PD-L1. Unstimulierte T-Zellen töteten bevorzugt TIS-Lymphomzellen, die dazu neigten, mit den T-Zellen zu interagieren und sie zu aktivieren. Die CD19-BsAb und CD20-BsAb verstärkten die Interaktion der T-Zellen mit den TIS-Lymphomzellen, was zu einer erhöhten T-Zell-Aktivierung, Proliferation

und Anti-Lymphom-Zytotoxizität führte. CD19-BsAb erleichterte es den T-Zellen, proliferierende Lymphomzellen bis zu einem gewissen Grad abzutöten. TIS-Lymphomzellen mit hohem PD-L1-Gehalt waren selbst in Gegenwart von CD20-BsAb weniger empfindlich gegenüber der T-Zell-Tötung *ex vivo*.

Fazit

In dieser Studie wurden die immunstimulierenden und immunhemmenden Signaturen in TIS-Lymphomzellen dargestellt. CD19-BsAb erleichterte unstimulierten T-Zellen die Abtötung der proliferierenden sowie der TIS-Lymphomzellen. CD20-BsAb hingegen verstärkte selektiv die T-Zell-Tötung von TIS-Lymphomzellen. Darüber hinaus schwächte PD-L1 die Zytotoxizität der T-Zellen gegenüber TIS-Lymphomzellen ab, was eine therapeutische Anwendung der PD-L1/PD-1-Blockade zur Derepression der T-Zell-Aktivität nahelegt. Diese Studie dürfte die künftige klinische Forschung zu den T-Zell-umlenkenden BsAbs in der DLBCL-Behandlung inspirieren, mit dem Ziel, TIS-Lymphomreste zu bekämpfen.

1. Introduction

1.1. Cellular senescence in lymphoma

Aggressive non-Hodgkin lymphoma, including its most prevalent subtype diffuse large B-cell lymphoma (DLBCL), is diagnosed at a median age of 67 years old [1]. Genetic aberration of Bcl2 family members, especially Bcl2 and Bcl6, has been revealed to be involved in the pathogenesis of DLBCL [2]. The conventional treatment for patients with DLBCL is the R-CHOP regimen (rituximab, cyclophosphamide, doxorubicin/hydroxyldaunorubicin, vincristine (oncovin) and prednisolone), with around 60% of patients achieving cure after this immunochemotherapy [3]. However, due to the heterogeneous pathological features of DLBCL, a sizeable proportion of patients fails first-line therapy. Refractory or relapsed lymphoma requires salvage regimens such as high-dose chemotherapy with autologous stem cell transplantation or chimeric antigen receptor T-cell (CAR T-cell) therapy in curative intent, although the majority of these patients will succumb to their disease [4, 5]. Various molecular mechanisms and corresponding strategies have been proposed to understand and overcome treatment resistance in these patients, such as the usage of pharmaceutical therapies to target aggressive mutations. In particular, a general fail-safe process, cellular senescence, has been uncovered to play a central role in DLBCLs during disease development and as a component of the treatment response [6, 7].

Cellular senescence was initially described as a steady cell cycle arrest at the G1 phase, which was first discovered in the primary cells that exhibited proliferation limitation in the *in vitro* culture [8]. This phenomenon is termed “replicative senescence”, resulting from continuous telomere shortening during cell division [9]. Later, similar phenotypes were found in cells exposed to other stimuli, including oncogene activation [10], oxidative damage, and irradiation- and chemotherapy-induced DNA damage, which are termed “stress-induced senescence” [11]. These stimuli trigger DNA damage response (DDR), leading to the activation of the p53 pathway and the ERK/ETS1/2 pathway, which ultimately induce the expression of $p21^{CIP1}$ (also known as CDKN1A) and

$p16^{INK4a}$ (also known as CDKN2A), respectively [12, 13]. With the overexpression of these two molecules as the blockers of cell cycle progression, cells fail to enter the S phase from the G1 phase. Furthermore, unsolvable DDR activates the retinoblastoma (Rb) and p53 pathways, and promotes the formation of promyelocytic leukemia nuclear bodies, which ultimately leads to senescence-associated heterochromatin foci (SAHF) through the ASF1A and HIRA chaperones [14, 15]. Additionally, Suv39h1 (suppressor of variegation 3-9 homolog 1), an H3K9 methyltransferase, can bind to the hypophosphorylated Rb-E2F complex and initiate H3K9me3 decoration to the promoters of the E2F target genes, thereby preventing transcription of the E2F target genes and the subsequent S-phase entry [7, 16].

Senescence and apoptosis are equally important intrinsic cellular programs that terminate the successive expansion of the deleterious mutation-harboring cells, thereby serving as a fail-safe to prevent precancerous neoplasms and malignancies [17]. Senescent cells, unlike apoptotic cells, are still viable, metabolically active and capable of secreting multiple types of soluble factors, known as the senescence-associated secretory phenotype (SASP) [18]. Composed of matrix-modifying enzymes, growth factors, chemokines and inflammatory cytokines, SASP allows senescence to act as a double-edged sword, exerting distinct functions depending on its temporal-spatial regulation feature and the state of SASP-recipient cells [19]. Besides the ability to communicate with adjacent or distant cells via SASP, senescent cells can establish crosstalk with their neighboring cells by modulating protein expression as well as antigen presentation on cell surfaces [20], and secreting biologically active materials via microvesicles and exosomes [21]. Through intricate cell-cell communication, senescent cells create either a pro-inflammatory or anti-inflammatory microenvironment that dynamically influences tissue homeostasis and malignant transformation in many cancers including lymphoma [19, 22].

The impact of senescence on tumor development and anti-cancer therapy has been studied in the past, especially in lymphoma as a model entity by our research group [6, 23-25]. Oncogene-induced senescence (OIS) operates as an anti-tumor barrier; specifically, *N-RAS* drives OIS as an obstacle to lymphoma onset through deceleration

of invasive T-cell lymphoma outgrowth in *Eμ-N-Ras* transgenic mice [7]. *Suv39h1* or *p53* is required to limit lymphoma occurrence by stroma-derived TGF-β-induced senescence and *N-RAS*-induced senescence [7, 25], and also to maintain TIS in the *Eμ-myc* transgenic Bcl2-overexpressed lymphomas [26]. Even though senescence is depicted as a steady cell cycle arrest to limit aberrant cell cycle progression, our group has shown the intrinsic nature of senescent cells to reprogram into *de novo* stemness – senescence-associated stemness (SAS), in addition to the extrinsic model of SASP-induced stemness [26]. By using conditional genetic switch models that allow control of essential senescence mediators such as *Suv39h1*, *p53*, *JMJD2C* and *LSD1* to allow cell cycle re-entry of senescent cells, we showed that cells harboring a history of senescence (post-senescence) exhibit elevated clonogenic growth and malignant phenotype in both mouse lymphoma and human melanocyte models [26, 27]. More importantly, the SAS-relevant *Wnt* marker β-catenin was found enriched in the relapsedtumors of DLBCL patients, suggesting the actual physiological relevance of SAS in human cancer and relapse. In addition to cell-intrinsic changes, senescent tumor cells modulate neighboring cells within the tumor microenvironment. One important findingfrom our group is that transplanting *MyD88-L265P*-bearing *Eμ-myc* transgenic hematopoietic stem cells into immunocompetent mice accelerates the occurrence of systemic lymphomas. The manifest primary lymphomas harboring either *MyD88- L265P* or *CARD11-L244P* mutants are found to be senescence-prone and able to avoid the adaptive immune surveillance through up-regulating PD-L1 on the lymphoma cells and the recruited macrophages in the lymphoma lesions [23]. This is the first demonstration of a direct senescence-selective tumor-controlling T-cell surveillance against senescent cells. Furthermore, senescence-derived signature *SUVERNASS* has been shown to predict the clinical outcome of patients with lymphoma [6]. The SAS and immune surveillance evasion may play independent or synergistic roles in promoting disease refractoriness or relapses. Given the persisting nature of senescent cells and their complex intercellular interaction with other cell types, particularly immune cells, an in-depth exploration of senescence cells and their environmental biology is undoubtedly

essential to dissect the impacts of chemotherapy-induced senescent lymphoma cells on the treatment outcome of DLBCL and hence, ultimately, therapeutic precisions.

1.2. Immune response to senescent cells

Through the inflammatory factors of SASP and the senescence-associated proteins on the cell surface, senescent cells attract multiple types of immune cells and trigger diverse immune responses. The innate immune response serves as the first barrier to combat pathogens, as well as the fundamental process for recognizing and clearing senescent cells, which involves natural killer cells (NK cells), monocytes/macrophages and neutrophils [28]. Senescence induced by the CDK4/6- and MAPK-inhibitors in *K-RAS*-mutant lung cancer cells can activate NK cells via TNF-α and ICAM-1 (two components from SASP), which subsequently leads to the clearance of senescent lung cancer cells, and hence tumor regression *in vivo* [29]. Furthermore, reactivation of *p53* in established hepatocellular carcinoma induces senescence, followed by immunosurveillance activation of NK cells, which were mobilized by CCL2 and activated by NKG2D ligands, and ultimately tumor regression [28, 30]. Additionally, senescent hepatic stellate cells with functional *p53* expression secrete IL-6 and IFN-γ, thereby inducing macrophage differentiation into an immune-activating M1 phenotype to phagocytize senescent cells [31]. The evidence here demonstrates clearly that innate immune response plays a necessary part in eliminating senescent cells.

In addition to innate immunity, the adaptive immune response towards senescent cells has also been studied in different senescence models. Preliminary evidence for senescence-triggered T-cell response came from the studies of Petti et al. [32] and van Tuyn et al. [33]. Petti et al. found that $NRAS^{Q61R}$ and $BRAF^{V600E}$ double-mutant melanoma cells enter senescence status and exhibit enhanced expression of MHC-I molecules, which enable malignant cells to be lysed by the IL-2-activated nonspecific killer cells and also the educated specific T cells *in vitro* [32]. Tuyn et al. reported that MHC-II molecule is transcriptionally up-regulated in the $NRAS^{Q61K}$- and $BRAF^{V600E}$-induced senescent human melanocytes as a result of the CIITA expression and IL-1β signal,

which leads to T-cell proliferation *in vivo* and *in vitro* [33]. Immunosurveillance of senescent cells was reported to rely on the persistence of aberrantly expressed p21, a critical mediator for regulating cell cycle arrest via Rb signaling. Rb signaling induces the secretion of CXCL14 in the mouse model with *K-RAS*^{G12V}-induced senescent hepatocytes as a way to polarize macrophages into an M1 phenotype which, as a potential primer, correlates with the infiltration by cytotoxic T cells, presumably further contributing to the killing of oncogene-bearing hepatocytes [34]. More direct evidence of senescence-triggered T-cell response was published by our group in 2021. We found that OIS lymphoma-experienced T cells preferentially killed senescent lymphoma cells, and achieved their massive lysis of lymphoma cells when receiving the anti-PD-L1/PD-1 blockade [23]. Hence, T cells are able to participate in the senescence-associated immune response, but further investigation is required to elucidate the impact of senescent cells on T cells, as well as the T-cell subsets that are involved in the senescence surveillance.

Due to the dynamic nature of senescence as well as the different contexts in its surrounding microenvironment, SASP factors mobilize various immune cells in both immune-enhancing and immune-suppressive directions, to eliminate the harmful cells in the acute senescence outburst or create a neoplasm-permissive microenvironment in the chronic senescence scenario [35]. Therefore, controversial findings exist among different studies of the senescence-triggered immune response. Kang TW et al. discovered that *N-RAS*^{G12V}-induced senescent hepatocytes evoke a *Ras*-mutant (but not necessarily senescence-specific) adaptive $CD4^+$ helper T-cell response, which further recruited and activated monocytes/macrophages to eliminate the pre-cancerous senescent hepatocytes, thereby preventing the occurrence of hepatocellular carcinoma [36]. However, Eggert T et al. uncovered the bidirectional impacts of senescence-triggered immune response on livers with or without neoplasms [37]. In detail, senescent hepatocytes secreted CCL2 to attract $CCR2^+$ immature myeloid cells, which differentiated into macrophages and eradicated the pre-neoplastic senescent hepatocytes, thereby avoiding malignancy occurrence. In contrast, the co-existing hepatocellular carcinoma cells impeded the differentiation process of these recruited

myeloid cells, which in turn suppressed the cytotoxicity execution of NK cells, hence establishing a tumor-promoting microenvironment for hepatocellular carcinoma to further progress. Another example of a SASP component with two-way functions in regulating senescence immunosurveillance is COX2, which is secreted by the *N-RAS*^{G12V}-induced senescent hepatocytes. In this setting, COX2 suppressed the recruitment and activation of immature myeloid cells and $CD4^+$ regulatory T cells (Tregs), which play immunosuppressive roles in senescence surveillance [38]. This immunomodulatory function of COX2 was achieved partly by its downstream molecule PGE_2. However, in a different experimental setting, the COX2/PGE_2 pathway in senescent thyrocytes and thyroid cancer cells can induce the differentiation of peripheral blood-derived human monocytes towards an immunosuppressive M2 phenotype, which executed a pro-tumor function *in vitro* [39]. Hitherto, the senescence-triggered immune response can lead to either an anti-tumor or pro-tumor outcome. Delineating the decisive mechanism of how senescent cells contribute to good and poor disease outcomes is of critical importance to facilitating immunoclearance of senescent cells and controlling senescence-induced chronic inflammation with invalid immunosurveillance.

SASP and senescence-associated proteins on the cell surface play major roles in the failure of senescence immunosurveillance. For instance, HLA-E, a non-classical MHC molecule, was induced in senescent cells via SASP (IL-6, CCL2/MCP-1, IL-8, etc.). HLA-E binds to the inhibitory receptor NKG2A on NK cells and $CD8^+$ T cells, resulting in the suppression of their effector function, which leads to the clearance failure of senescent cells [40]. MMPs from SASP can mediate the shedding of NKG2D ligands, which were orchestrated with the impediment of NKG2D receptor-regulated killer cell activation, as a way for senescent cells to elude immunosurveillance [41]. More importantly, our group reported that PD-L1 was upregulated in the senescence-prone lymphomas harboring either *MyD88-L265P* or *CARD11-L244P* mutants during the process of OIS-triggered T-cell-restricted tumor development [23]. PD-L1, an immune checkpoint protein, can inhibit the uncontrolled activation of effector T cells by binding to PD-1 on the activated cells [42]. We discovered that OIS-induced PD-L1 on

lymphoma cells inhibits the cytotoxic $CD8^+$ T-cell response in the senescence immunosurveillance. The PD-L1/PD-1 immune checkpoint blockade releases these dysfunctional $CD8^+$ T cells from cytotoxicity suppression, and lyses preferentially, but not exclusively, senescent lymphoma cells [23]. Furthermore, the SASP from the therapy-induced senescent prostate cancer cells with a defective *PTEN* gene generates an immunosuppressive microenvironment, which recruits $CD11b^+Gr\text{-}1^+$ myeloid cells (granulocytic myeloid-derived suppressor cells, MDSCs) while retaining a small number of dysfunctional NK cells, $CD4^+$ T cells and $CD8^+$ T cells [43]. These infiltrating MDSCs inhibit the proliferation of $CD8^+$ T cells *ex vivo* [43]. This finding was reproducible in the $p27^{Kip1}$-induced senescent stromal cell model, which causes the recruitment of granulocytic MDSCs and Tregs via IL-6 (a critical component of SASP) to restrain the anti-tumor T-cell response [44]. Moreover, CSF1 and IL-1β (SASP components) from *PTEN* loss-induced inflammatory response trigger expansion of MDSCs in the prostate, resulting in the failure of tumor immunosurveillance [45]. Conclusively, SASP contributes to the immune escape of senescent cells in an internal manner by up-regulating the immunosuppressive proteins while reducing the immunostimulatory proteins on the cell surfaces, or in an external manner to recruit immune cells with immunosuppressive function (e.g., MDSCs, Tregs and M2-like macrophages). The PD-L1/PD-1 axis serves as a brake in the immunosurveillance of OIS lymphoma and a potential therapeutic target for lymphoma, which requires further investigation on the role of the PD-L1/PD-1 axis in other senescence models including therapy-induced senescence (TIS).

1.3. Immunotherapy targeting senescent cells

Given the aforementioned bi-directional roles of senescent cells and their secretary phenotypes on tumor promotion and prevention, the eradication of detrimental senescent cells after chemotherapy or manipulation of SASP towards an anti-tumor direction mayimprove treatment outcomes in cancers.

To achieve the concept of exclusive senescence elimination, our group demonstrated a senescence-selective elimination method (so-called senolytics) using glucose

utilization blocker and autophagy inhibitor to target the metabolic, reprogrammed therapy-induced senescent (TIS) cells [24]. Other senolytics that target the inactive apoptosis pathways in senescent cells have been shown to be effective to improve cancer control [46], especially in sequential cancer therapy complementary with senolytic regimens [47]. Major senolytics include the Bcl2 family antagonist ABT-263 (Navitoclax), multi-kinase antagonist Dasatinib, p53-regulated apoptosis inducers FOXO4-DRI and UBX0101 (MDM2 antagonist), as well as PI3K-mediated survival inhibitors Quercetin in combination with Dasatinib, and Fisetin [48]. In various types of solid tumors (melanoma, breast cancer and ovarian cancer), the Bcl2 family-targeting antagonists, including ABT-263, ABT-199 (Venetoclax) and ABT-737, were administered as a sequential therapeutic following senescence-inducing anti-cancer treatments, which include chemotherapy (doxorubicin or etoposide), ionizing radiation, Aurora kinase inhibitor, poly (ADP-ribose) polymerase 1 inhibitors (PARPi) and CDK4/6 inhibitor (Palbociclib). This sequential treatment has been shown to improve therapeutic outcomes as well as reduce the toxicity of anti-cancer treatments [49-55]. Furthermore, the MDM2 inhibitor functions synergistically with a mitotic kinaseAurora A (AURKA) inhibitor in leveraging the disease control of melanomas [56]. This treatment modality triggers not only the intrinsic apoptosis process of senescent melanoma cells but the extrinsic lysis of these cells by mobilizing the cytotoxic immune cells through SASP [56]. Due to their weak specificity to deleterious senescent cells, senolytics may cause extensive elimination of senescent cells *in vivo*, leading to unwilling serious side effects in clinical trials [57, 58]. Therefore, senomorphics have been designed to modulate precisely one of the components or regulators of SASP. Senomorphics are a group of compounds that remodel the senescence microenvironment by altering SASP without disturbing the integrity of senescent cells and their anti-tumor features [59]. One strategy to modify or reduce SASP production is to manipulate the critical regulators of SASP, such as mTOR (rapamycin) [60, 61], p38-MAPK (BIRB-796 and UR-13756) [62], NF-κB (BAY 11-7082) [63], JAK2/STAT3 (ruxolitinib) [64] as well as other small molecules that target BRD4, L1 and STING [20]. However, the therapeutic value of these compounds is ambivalent due to the

controversial properties of SASP in influencing cancer development at different disease stages. Hence, targeting specific components of SASP, such as IL-6 or IL-8, serves as another strategy to reverse the tumor-propagating or enhance the tumor-suppressing functions of SASP. For instance, the IL-6R neutralizing antibody Tocilizumab, which blocks the binding of IL-6 to its receptor, exhibited feasibility and safety in patients with recurrent epithelial ovarian cancer when in combination with carboplatin/doxorubicin in a phase I trial [65]. Moreover, siRNA-based suppression of IL-8 retards the development of ovarian cancer xenografts [66]. Reparixin, an antagonist for the IL-8 receptors CXCR1/2, was found to be safe with therapeutic potential when administered in combination with paclitaxel in a phase Ib clinical investigation of metastatic breast cancer [67]. Using a virus-induced senescence (VIS) model, our group found that senolytics including Navitoclax, and Quercetin plus Dasatinib, selectively eliminate VIS cells, hence leading to successful alleviation of damage-causing inflammation responsein the lungs of SARS-CoV-2-infected hamsters and mice [68]. Other antagonists targeting the immunosuppressive components of SASP, such as TGF-β [69] and NOTCH [70], as well as the agonists that enhance the immunostimulating effects of SASP (STING [71]), are also under pre-clinical and clinical investigation. Despite the fact that these SASP components are not exclusively expressed or secreted by senescent cells, the targeted regulation of these molecules may indeed yield promising outcomes following the senescence-inducing anti-cancer therapies, especially after the precise spatial-temporal description of SASP in different tumor entities.

Senescence-inducing therapy combined with immunotherapy is an alternative strategy to overcome senescence-associated immunosuppression and hence eradicate immuno-escaping malignant cells [20]. Increasing studies have shown altered expression of senescence-associated surface proteins on senescent cells, including some immunoregulatory factors, which inspires the investigation of novel immunotherapies to target senescent cells. For instance, up-regulated HLA-E expression on senescent cells suppresses the effector function of NK cells and $CD8^+$ T cells by binding to its receptor NKG2A on these immune cells [40]. Anti-NKG2A neutralizing antibody (Monalizumab) has been demonstrated to boost NK cells to lyse malignant cells in

combination with EGFR-inhibitor (Cetuximab), and to further restore the cytotoxicity of $CD8^+$ T cells when in combination with anti-PD-L1 blocking antibody (Durvalumab) [72]. Another study also showed that MICA and MICB (NKG2D ligands) are proteolytically cleaved in senescent cells and hence allow senescent cells to escape immunosurveillance [41], which can be abolished by the antibody that targets the α3 domains of MICA/MICB and prevents their shedding [73]. Immune checkpoint proteins are another group of senescence-associated proteins that can be targeted to eliminate senescent malignant cells. Our previous work showed that PD-L1 was upregulated in the senescence-prone lymphomas with either *MyD88-L265P* or *CARD11-L244P* mutants [23]. We found that the PD-L1/PD-1 blockade can de-repress the cytotoxic potential of senescence-specific $CD8^+$ T cells, leading to lymphoma cell lysis *ex vivo* and disease control *in vivo*, thereby demonstrating for the first time the potential of targeting adaptive immune response by immune checkpoint blockade as new "endogenous immunological senolytics" [23]. Furthermore, the therapeutic application of the PD-L1/PD-1 blockade has been verified in CDK4/6 inhibition-induced senescence scenarios in various malignancies including melanoma [74, 75], lung cancer [76] and pancreatic cancer [77].

Apart from targeting the immunoregulatory molecules, targeting specific senescence-associated proteins on the cellular membranes by antibody- or immune-cell-based immunotherapies is an alternative approach to restoring functional immunosurveillance of senescent cells. For example, DPP4 was reported to be expressed exclusively on senescent fibroblasts. Hence, specific anti-DPP4 antibody results in antibody-dependent NK cell-mediated cytotoxicity against senescent cells [78].

Another senescence-specific surface protein uPAR was discovered by data mining of the RNA sequence from three independent senescence models (replication-/oncogene-/therapy-induced senescence) [79]. Based on this finding, uPAR-specific CAR-T cells were generated and reported to effectively eliminate senescent cells in the benign disease as well as the malignancy models, leading to the alleviation of liver fibrosis and survival extension of mice with lung adenocarcinoma after chemotherapy [79]. The

promising achievement of this novel CAR-T cell therapy encourages scientists to dissect the surfaceome of senescent cells, especially focusing on the senescence-associated or -specific peptides presented by MHC molecules on the cell surfaces. Correspondingly, the identification of senescence-specific T-cell clones and their TCR sequences may foster the development of immunotherapy to eliminate undesirable senescent cells [80]. Moreover, the immunogenicity alteration of senescent cells suggests the potential of T cell-redirecting bispecific antibodies in the clearance of senescent cells.

1.4. T cell-redirecting bispecific antibodies in lymphoma treatment

The bispecific antibodies (BsAbs) were first introduced and recombined by A. Nisonoff and M. M. Rivers, using two different antigen-binding fragments from polyclonal antibodies to form $F(ab')_2$ molecules in 1961 [81]. As antibody-engineering platforms have advanced, more than 100 formats of BsAbs have been manufactured so far to simultaneously target two types of antigens on the same cells (*cis*-co-engagement) or on different cells (*trans*-co-engagement) [82, 83]. The most widely studied BsAbs are constructed to bridge immune effector cells (NK cells, T cells and myeloid cells) to tumor cells, thereby attracting, redirecting, activating and/or derepressing the immune cells to lyse tumor cells [83].

The concept of redirecting T cells to target cells using BsAbs was first applied in cancer immunotherapy. T cell-redirecting BsAbs have one arm binding to the extracellular subunits of CD3 (usually CD3ε) on T cells and the other arm binding to the tumor-associated antigens (TAAs) on malignant cells [84]. Upon bridging the tumor cells and T cells, the T cell-redirecting BsAbs activate T cells while bypassing the MHC-specificity restriction, leading to lysis of the engaged tumor cells. These recruited T cells are mostly non-tumor-specific T cells, which execute their cytotoxicity efficiently after the formation of immunological synapses that are different from the naturally formed immunological synapses [85]. The activation of the BsAb-engaged T cells is independent of the specific recognition and interaction of TCRs to their matched

peptide-MHC complexes, therefore overcoming the immune evasion property of tumor cells with downregulated surface expression of MHC molecules [86].

Blinatumomab is an anti-CD19 × CD3 bispecific T-cell engager (BiTE) with small-sized single-chain variable fragments (scFvs), which are constructed by connecting the variable regions of the immunoglobulin heavy and light chains with a peptide linker [87]. Due to a lack of the Fc domain, blinatumomab has a short serum half-life (around 1.2 hours) in patients receiving a continuous intravenous infusion [88]. Blinatumomab is the first BsAb approved by the FDA for the salvage treatment of refractory/relapsed B-cell acute lymphoblastic leukemia (R/R B-ALL) [89]. Four independent clinical trials of blinatumomab in refractory/relapsed B-cell non-Hodgkin lymphoma (R/R B-NHL) have revealed an overall response rate (ORR) of 37% to 69% and even durable disease alleviation in some patients, but results in DLBCL have been overall moderate and rather disappointing [90-93]. Moreover, a higher dose of blinatumomab is needed to treat R/R B-NHL than R/R B-ALL, partly because of its short half-life [94]. This disadvantage may be overcome by introducing a modified Fc fragment without the capacity to be captured by Fc receptors, such as the Fc-silent domain. Mosunetuzumab (Lunsumio), a humanized anti-CD20 × CD3 BsAb, has been authorized by the European Medicines Agency for the treatment of adult relapsed/refractory follicular lymphoma [95]. Other types of anti-CD20 × CD3 IgG1-like BsAbs are still under clinical investigation for thetreatment of B-cell lymphoma, including Epcoritamab [96], Odronextamab (REGN1979)[97] and Glofitamab (RG6026) [98]. These BsAbs show promising efficacy as a salvage therapy for R/R B-cell NHL patients who had been heavily pretreated with conventionaltreatment modalities and even CAR-T cell infusion, achieving an ORR of 20% to 76% and a complete response (CR) rate of 14% to 48% in the DLBCL subgroup. Mosunetuzumab was also tested as a first-line treatment for elderly DLBCL patients who were ineligible for standard immunochemotherapy [99]. This clinical trial (NCT03677154) showed that mosunetuzumab is well tolerated among the treated patients and yields an ORR of 58% (11/19) and a CR rate of 42% (8/19). Most BsAbs are administered intravenously, hence the subcutaneously administered BsAb epcoritamab offers applicable convenience, lowers the possibilities of severe cytokine release syndrome and was shown to yield an

ORR of 76% (19/25) with a CR rate of 32% (8/25) in patients with R/R DLBCL [100].

In our previous study, we clearly demonstrated the use of the TIS signature "SUVARNESS" to predict the prognosis of DLBCL patients [6].

Having acknowledged the elevated immunogenicity of senescent tumor cells as well as their altered profile of immunoregulatory surface molecules on the cell surface, along with our previous observation that senescent cells elicited the T-cell response, the evidence collectively pinpoints the potential use of T cell-redirecting BsAbs as senolytics to eliminate post-treatment senescent cells, which may lower post-treatment inflammationand possibly prevent cancer recurrence. However, whether or not BsAbs may facilitate the clearance of chemotherapy-induced senescent cells is unknown, and, hence, the focus of this thesis.

2. Hypothesis

The scientific objective of this dissertation is to understand how chemotherapy-induced senescent B-cell lymphoma cells react to T-cell surveillance *ex vivo*, and the efficacy of anti-CD19 × CD3 and anti-CD20 × CD3 BsAbs (hereafter CD19-BsAb and CD20-BsAb, respectively) in influencing the cytotoxic function of unstimulated T cells towards senescent lymphoma cells.

Malignant B cells from lymphoma express both MHC-I and MHC-II molecules, therefore being recognized as one particular cancer type with antigen-processing functions [101] and the potential to prime T cells to initiate adaptive immunosurveillance. However, several strategies were used by these malignant B cells to escape immunosurveillance via "hiding" or "defending" themselves [102]. The "hiding" strategy refers to the intrinsic changes of tumor B cells to become less recognizable to immune cells. For instance, B-cell lymphoma cells lose or down-regulate their surface expression of MHC-I/MHC-II molecules for lesser antigen presentation, the co-stimulatory factors (CD80, CD86) for weakening the signal 2 of T-cell activation, and the adhesion molecule ICAM-1 (CD54) for reducing binding to LFA-1 on immune cells [103]. Approximately 55% to 75% of DLBCL lesions lose the surface expression of MHC-I due to the mutations of the β2-microglobulin gene (*B2M*) [104] or the loss of the *MHC-I* gene [105]. MHC-II loss was found in 20% of DLBCL lesions [106] as a result of *Crebbp*-mutant-causing transcriptional deregulation [107] or cytoplasmic mislocalization of MHC-II molecules [108], the latter of which was associated with the double overexpression of the *C-myc* and *Bcl2* genes. The "defending" strategies for lymphomas to survive immunosurveillance include their acquisition of apoptosis resistance and expression of inhibitory factors that lead to a suppressive immunoenvironment. The loss or mutations of the *Fas* (CD95) gene [109-111], which encodes a receptor for the FAS/FASL extrinsic cell death pathway, were found in around 50% of the extra-nodal DLBCL lesions and associated with a poorer prognosis for DLBCL patients. The intrinsic apoptosis pathway is predominantly modulated by

the Bcl2 family proteins [89], with Bcl2 protein as the principal anti-apoptosis regulator. The t(14;18) translocation is one of the critical genetic features in a subgroup of DLBCLs, occurring in 34% of the germinal center B-cell-like DLBCL [112]. The t(14;18) translocation results in a genetic tandem of the enhancer of the immunoglobulin heavy- chain (*IgH*) gene with the *Bcl2* gene, leading to an overexpression of Bcl2 that protects malignant B cells from the intrinsic apoptosis pathway triggered by various stimuli [113]. Furthermore, malignant B cells can express or secrete an abundance of molecules to inhibit the tumor immunosurveillance. For instance, PD-L1/L2 proteins are frequently expressed in DLBCL lesions, including the malignant B cells themselves and their surrounding immune cells [23, 114]. The expression of PD-L1, either locating on the cell surfaces or being a soluble protein, is a prognosis marker predicting the poor treatment outcomes of DLBCL patients [115-118]. Moreover, tumor B cells can express CD47 to interact with signal-regulatory protein-α (SIRPα) and provide a "don't eat me" signal to the macrophages [119, 120], or express FasL to induce cell death to their engaging immune cells [71-74, 121]. Last but not least, some cytokines or molecules (IL-10, TNF-α and IDO) can generate an immunosuppressive microenvironment [122, 123]. Generally, the immune microenvironment in the majority of DLBCLs is "non-inflammatory" or "non-inflamed", and only a small proportion of DLBCL cases exhibit an "inflammatory"or "inflamed" immune landscape [124]. Steen C et al. conducted large-scale profiling of cell states and cellular ecosystems to uncover the functionally relevant clusters of distinct immune microenvironments in DLBCLs, and provided a comprehensive evaluation system (Lymphoma EcoTyper) for identifying therapeutic targets of DLBCLs [125]. This classifier of DLBCLs integrates the cell states of malignant B-cell and 12 other cell lineages within the lymphoma microenvironment with the interactions between different cell types, depicting the relevance of the DLBCL ecosystems to the heterogenicity of clinical outcomes, which further emphasizes the unneglectable role of the tumor microenvironment, especially the immune microenvironment, in the treatment response of DLBCLs. Since the immune landscape of DLBCL is shaped by a complex molecular or cellular network, a more in-depth characterization of the altered

immunogenicity of DLBCL before and after anti-cancer therapy is also required.

Besides the endogenous features of malignant B cells, the R-CHOP-based chemo-immunotherapy can also alter the immune landscape of DLBCL lesions by influencing the tumor cells and their neighboring cells. On one hand, chemotherapy triggers the apoptosis and senescence of malignant cells to alleviate tumor burden, which is accompanied by the release of tumor-specific- or tumor-associated antigens that may be presented by cross-primed bystander cells, leading to the potential initiation of immunosurveillance. On the other hand, malignancy-induced- or chemotherapy-triggered immunosuppression can undermine the surveillance of immune cells towards the damaged or intact tumor B cells. The chemotherapy-induced phenotypic changes of tumor cells, e.g., chemotherapy-induced senescence, can be exploited by malignant B cells for reprogramming to acquire a senescence-associated stemness, leading to disease recurrence [26]. Furthermore, TIS may generate alternative surface proteins and SASP that contain a variety of pro-inflammatory cytokines, which potentially alters the immune landscape of malignancies including B-cell lymphomas, providing new targets for novel immunotherapies in the clinical management of malignancies.

The T cell-redirecting bispecific antibodies (BsAbs), with one arm targeting CD3 on T cells and the other arm targeting tumor-associated antigens on malignant cells, mediate the interaction of tumor cells with T cells, including tumor-specific T cells and non-tumor-specific T cells, the latter of which is in the majority. Upon bridging T cells to tumor cells, BsAbs help to form the “artificial” immunological synapses between T cells and tumor cells in the presence of appropriate costimulatory signals, which bypass the specificity restriction of the peptide-MHC complexes to their specific TCRs [126]. Afterwards, these polyclonal T cells are activated and able to execute their cytotoxic function towards their engaging tumor cells. The CD19-BsAb and CD20-BsAb are designed to redirect T cells to target lymphoblastic leukemia cells and lymphoma cells. Humanized CD19-BsAb and CD20-BsAb exhibited efficacies and certain promising outcomes in heavily pre-treated R/R DLBCL patients and elderly DLBCL patients without pre-treatment (see **Introduction 1.4** for more details). These findings inspired us to study the senolytic effects of CD19-BsAb and CD20-BsAb on the TIS lymphoma

cells.

The T cell-redirecting CD19-BsAb and CD20-BsAb in this study were obtained from Absolute Antibody [127, 128]. These recombinant monoclonal BsAbs are constructed based on murine IgG2a, with one Fab segment (≈50kDa) targeting mouse CD19 (Clone 6D5) or CD20 (Clone 18B12), one single-chain Fv (scFv) segment (≈25kDa) targeting mouse CD3ε (Clone 145-2C11), and the Fc segment (≈50kDa) (**Figure 1**). The heterodimeric BsAbs (Fab/scFv-Fc), therefore, are monovalent with two specificities. The Fc segments of CD19-BsAb and CD20-BsAb in this study bear knob-into-hole (KIH) and Fc Silent™ mutations. The KIH strategy introduces mutations in the heavy chains to change amino acids at the CH3 domain on monoclonal antibody 1 (mAb1) and the CH2 domain on monoclonal antibody 2 (mAb2), thereby creating the "knob" and "hole" on the heavy chains of mAb1 and mAb2, respectively. The KIH mutation enables a preferential formation of heterodimers rather than homodimers [129]. The Fc Silent™ mutation minimizes the binding of BsAbs to Fc receptors (FcR and FcγR). Therefore, the Fc Silent™ mutation abrogates the unspecific binding of BsAbs to non-target cells and reduces the antibody-mediated phagocytosis and cytotoxicity of effector cells towards BsAb-binding non-target cells. Moreover, the Fc Silent™ mutation can extend the half-life of IgG-like BsAbs *in vivo* compared to BiTEs without Fc domains. In this study, we hypothesize that therapy-induced senescent lymphoma cells exhibit an immunostimulatory feature to trigger primary T-cell surveillance, which can be amplified by the application of CD19-BsAb and CD20-BsAb, leading to immunogenic senescence elimination.

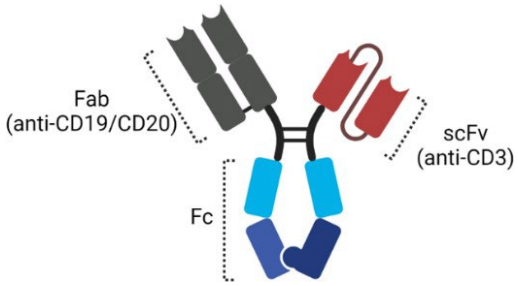

Figure 1. Schematic of anti-CD19 × CD3 and anti-CD20 × CD3 bispecific antibodies.

3. Materials and methods

3.1. Materials

3.1.1. Equipment

Equipment	Full name	Provider
Autoclave	Laboklav	SHP Steriltechnik AG
Balance	Analytical balance (ABS 120-4N)	Kern
	Mettler PE 1600	Mettler Toledo
Cell counter	LUNA® automated cell counter	Logos Biosystems
Cell imagers	IncuCyte® Live-Cell Analysis Instrument (SX1)	Sartorius
Cell imagers	EVOS™ XL Core Imaging System	Thermo Fisher Scientific
Centrifuges	Heraeus Fresco 17 centrifuge	Thermo Scientific
	Heraeus Megafuge 16R centrifuge	Thermo Scientific
	Megafuge 1.0R	Heraeus
	Cytospin centrifuge Rotina 35R	Hettich
	Sorvall™ Legend™ Micro 21 Microcentrifuge	Thermo Scientific
	Mini centrifuge	Nippon Genetics Europe GmbH
	Mini star microcentrifuge	VWR
CO_2-incubator for cells	Series CB-S Solid. Line | CO_2 incubator	Binder
Fluorescence microscope	Olympus CKX41	Olympus
Flow cytometer	Guava easyCyte™ 12HT Systems	Luminex
Freezer	-20°C ProfiLine freezer	Liebherr
	-86°C ultralow temperature freezer	Glacier
Freezing container	Mr. Frosty	Thermo Fisher Scientific
Fume hood	Variolab mobilien w90	Waldner
Glass devices	beaker (mL, mL and mL)	Duran® Hirschmann® EM Technology Germany
	Duran Bottles (mL, mL and mL)	
	Erlenmeyer flask (mL, mL and mL)	
	Glass Pipettes (5 mL)	
	Graduated Cylinder	
Heated magnetic stirrer	Heidolph MR Hei-Tec heatable magnetic stirrer	Fisher Scientific
Hemocytometer	0.0025mm^2	OPTIK-Labor
Hood for cell culture	Labgard class II biological safety cabinet	Nuaire
Incubator for bacteria	Bacteria incubator (Function Line)	Heraeus Instruments
Liquid nitrogen container	MVE 1500 Series-190°C high efficiency freezer	Chart

MACS dissociator	gentleMACS Dissociator	Miltenyi Biotec
Magnet	-	Miltenyi Biotec
Magnetic stand	-	Miltenyi Biotec
Microscopes	Compact inverted microscope	ZEISS Primovert
NanoDrop Spectrophotometer	NanoDrop 2000™ Spectrophotometer	Thermo Fisher Scientific
pH-meter	MP220 Basic pH/mV/°C Meter	Mettler Toledo
Pipette controller	PIPETBOY acu 2	Integra Biosciences
Pipettes	Research® plus - mechanical Pipettes	Eppendorf
Refrigerator	-	Liebherr
Shaker for bacteria	Incubator shaker series	Eppendorf
Sorter	S3e Cell Sorter	Bio-Rad
Thermomixer	Thermomixer comfort 1.5ml Thermal shaker	Eppendorf
Vortex mixer	Vortex-Genie 2	Scientific Industries
Water bath	-	GFL

3.1.2. Plasmids

Plasmid	**Overexpressing gene**	**Antibiotic resistance gene**
Helper	-	-
MSCV-*Bcl2*	murine *Bcl2*	-
MSCV-*Bcl2*-GFP	murine *Bcl2*	-
MSCV-*Bcl2*-BSD	murine *Bcl2*	Blasticidin
MSCV- *Bcl2*-Puro	murine *Bcl2*	Puromycin
MSCV-empty-BSD	-	Blasticidin
MSCV-empty-Puro	-	Puromycin

3.1.3. Chemicals

Name	**Empirical Formula**	**Provider**
2-Mercaptoethanol	C_2H_6OS	Carl Roth
4-Hydroxytamoxifen	$C_{26}H_{29}NO_2$	Sigma-Aldrich
5-bromo-4-chloro-3-indolyl-β-D-galactosidase (X-β-Gal)	$C_{14}H_{15}BrClNO_6$	Carl Roth
Agar	-	Sigma-Aldrich
Calcium chloride dihydrate	$CaCl_2 \cdot 2H_2O$	Carl Roth
Chloroquine diphosphate salt	$C_{18}H_{26}ClN_3 \cdot 2H_3PO_4$	Sigma-Aldrich
Dimethyl Sulfoxide (DMSO)	$(CH_3)_2SO$	Sigma-Aldrich
Di-Sodium hydrogen phosphate dihydrate	$Na_2HPO_4 \cdot 2H_2O$	Carl Roth

Ethanol (absolute)	C_2H_6O	Carl Roth
Ethylenediaminetetraacetic acid (EDTA)	$(HO_2CCH_2)_2NCH_2CH_2N(CH_2CO_2H)_2$	Sigma-Aldrich
Glutaraldehyde	$OHC(CH_2)_3CHO$	Carl Roth
HEPES	$C_8H_{18}N_2O_4S$	Carl Roth
Hydrochloric Acid	HCl	Carl Roth
LB Medium	-	Carl Roth
Magnesium chloride hexahydrate	$MgCl_2 \cdot 6H_2O$	Carl Roth
Methanol	CH_3OH	Carl Roth
Neomycin sulfate	$C_{23}H_{46}N_6O_{13} \cdot xH_2SO_4$	Sigma-Aldrich
Paraformaldehyde (PFA)	$HO(CH_2O)_nH$	Sigma-Aldrich
poly-D-Lysine hydrobromide	D-Lys-(D-Lys)n-D-Lys · xHBr	Sigma-Aldrich
Potassium chloride	KCl	Carl Roth
Potassium dihydrogen phosphate	KH_2PO_4	Carl Roth
Potassium hexacyanoferrate (III)	$K_3Fe(CN)_6$	Sigma-Aldrich
Potassium hexacyanoferrate(II) trihydrate	$K_4[Fe(CN)_6] \cdot 3H_2O$	Sigma-Aldrich
Sodium azide	NaN_3	Sigma-Aldrich
Sodium chloride	NaCl	Fluka
Sodium hydroxide	NaOH	Carl Roth
Trypan Blue	$C_{34}H_{24}N_6O_{14}S_4Na_4$	Sigma-Aldrich
Tryptone	-	Millipore
Yeast extract	-	Carl Roth

3.1.4. Reagents

Name	**Provider**
Ampicillin	Sigma-Aldrich
anti-CD19 × CD3 bispecific antibody	Absolute Antibody
anti-CD20 × CD3 bispecific antibody	Absolute Antibody
anti-CD20 antibody	Absolute Antibody
anti-CD20 antibody Fc-silent	Absolute Antibody
anti-fluorescein × CD3 bispecific antibody (isotype control)	Absolute Antibody
Blasticidin	InvivoGen
Bovine serum albumin fraction V	Roth
Carbenicillin	Sigma-Aldrich
CellTrace™ Far Red Cell Proliferation Kit, for flow cytometry	Invitrogen™

DMED medium (high glucose)	Gibco™
Dynabeads™ Mouse T-Activator CD3/CD28 for T-Cell Expansion and Activation	Thermo Fischer Scientific
Fetal bovine serum (FBS)	PAN Biotech
Fluorescence mounting medium	Dako
G418 (Geneticin)	InvivoGen
Ghost Dye™ (Violet 450, Red 780)	Tonbo biosciences
Guava® ViaCount™ Reagent	Luminex
IMDM medium	Gibco™
Insulin-Transferrin-Selenium (ITS -G) (100×)	Gibco™
Interleukin-2, mouse (mIL-2)	Sigma-Aldrich
L-Glutamine (200 mM)	Biochrom
Mafosfamide cyclohexylamine	Niomech
MEM non-essential amino acid solution (100×)	Sigma-Aldrich
Penicillin-streptomycin (100 ×)	Biochrom
Polybrene	Sigma-Aldrich
Purified Rat Anti-Mouse CD16/CD32 (Mouse BD Fc Block™)	BD Pharmingen
Puromycin	InvivoGen
Red blood cell lysis buffer	Sigma-Aldrich
Saponin solution (10×)	Thermo Scientific
Sheath Fluid	BD Biosciences
Sodium pyruvate solution	Sigma-Aldrich
Trypsin/EDTA solution (10×)	Biochrom

3.1.5. Antibodies for flow cytometry

Name	**Clone**	**Host**	**Fluorescent conjugate**	**Dilution**	**Provider**
anti-mouse B220/CD45R	RA3-6B2	Rat	PE	1 : 500	BD Biosciences
anti-mouse Bcl2	REA356	Human	APC	1 : 50	Miltenyi Biotec
anti-mouse CD19	6D5	Rat	Alexa Fluor® 647	1 : 800	Biolegend
anti-mouse CD20	SA275A11	Rat	APC, PE	1 : 100	Biolegend
anti-mouse CD25	PC61	Rat	PE	1 : 200	BD Biosciences
anti-mouse CD273 (PD-L2)	MIH37	Rat	APC	1 : 20	Miltenyi Biotec
anti-mouse CD274/PD-L1	MIH5	Rat	APC	1 : 100	BD Biosciences
anti-mouse CD279/PD-1	J43	Armenian hamster	APC	1 : 100	eBioscience
anti-mouse CD3	145-2C11	Armenian hamster	PE	1 : 50	eBioscience
anti-mouse CD4	GK1.5	Rat	PE	1 : 600	BD Biosciences
anti-mouse CD4	GK1.5	Rat	APC	1 : 1200	eBioscience

anti-mouse CD69	H1.2F3	Armenian hamster	APC, APC-Cy7	1 : 200	Biolegend
anti-mouse CD80 (B7-1)	16-10A1	Armenian hamster	APC	1 : 200	eBioscience
anti-mouse CD86 (B7-2)	IT2.2	Mouse	PE	1 : 50	eBioscience
anti-mouse CD86 (B7-2)	GL-1	Rat	APC	1 : 200	eBioscience
anti-mouse CD8a	53.6.7	Rat	FITC, PE, APC	1 : 100	BD Biosciences
anti- mouse IgG2a, λ	B39-4	Rat	APC	1 : 100	BD Biosciences
anti-mouse MHC-I (H-2Db)	28-14-8	Mouse	APC	1 : 400	eBioscience
anti-mouse MHC-II (I-A/I-E)	M5/114.15.2	Rat	APC	1 : 3000	eBioscience
anti-human IgG1, κ	X40	Mouse	APC	1 : 100	BD Biosciences
anti-human PD-L1	MIH1 (RUO)	Mouse	APC	1 : 100	BD Biosciences

3.1.6. Lab consumables

Consumables	**Format**	**Provider**
Cell culture plate	Sterile cell culture plate, 6l/12/24/48-well plates, and 96-well flat-bottom/round-bottom plates	TPP
Cell stainer	Nylon mesh 40 mm	BD Falcon
Counting slides	Luna Cell Counting slides	BioCat
Cryotubes	2mL	Roth
Filters	Spritzenfilter ROTILABO® PVDF, 0.22 µm and 0.45 µm	Roth
Forceps	-	Germany Stainless
Gloves	S, M, L	Roth
MACS tubes	gentleMACS™ C Tubes	Miltenyi Biotec
Magnetic column	MS, LS	Miltenyi Biotec
Needles	25 G 5/8", 26 G 1/2", 27 G 1/2"	BD Microlance™ 3
Petri dish	10cm	Fisher Scientific
Pipette tips	SafeSeal-Tips Professional, sterile (10 mL, 100 mL and 1mL)	Biozym
Scalpels	-	B. Braun
Scissors	-	Germany Stainless
Syringes	sterile syringes (1mL, 10mL and 30mL)	BD Syringe
Tubes	eppendorf tubes (1.5mL, 2.0mL and 5.0 mL)	Sarstedt
	Falcon tubes (15mL and 50mL)	Life Science Corning

3.1.7. Formulas of buffers and solutions

Buffer	Formula
0.5M EDTA	186.1g EDTA in 1L double distilled water (ddH_2O)
1× PBS (pH=7.4)	8g NaCl + 201.3mg KCl + 1.4g Na_2HPO_4 + 272.2mg KH_2PO_4 in 1L MilliQ H_2O
1× X-Gal solution for SA-β-gal staining	0.5mL 20× KC solution + 0.25mL 40× X-Gal gel in 9.25mL PBS solution (pH=5.5 for murine cells, and pH=6 for human cells)
1M MgCl2	101.6g $MgCl_2 \cdot 6H_2O$ in 500mL MilliQ H_2O
2× HBS solution	298mg HEPES, 409mg NaCl, 6.7mg Na_2HPO_4 in 25mL MilliQ H_20 (pH=7.05)
20× KC solution	820mg $K_3Fe(CN)_6$ + 1050mg $K_4Fe(CN)_6 \cdot 3H_2O$ in 25ml 1× PBS
40× X-Gal gel	40mg X-Gal in 1mL N,N-dimethylformamide
Calcium phosphate-based transfection buffer	20ug target DNA + 15ug Helper DNA + 62.5uL 2M $CaCl_2$ solution + Sterile H_2O to a total volume of 500uL
Cell isolation buffer	0.5% BSA + 2mM EDTA in 1× PBS solution
Fixative solution for SA-β-gal staining	0.25% glutaraldehyde + 2% PFA in 1× PBS solution (pH=5.5 for murine cells, and pH=6 for human cells)
Flow cytometry (FCM) staining buffer	0.5% BSA + 0.04% sodium azide in 1× PBS solution
LB Agar	10g tryptone + 5g yeast extract + 10g NaCl + 15g Agar in 1L H_2O
LB medium	10g tryptone + 5g yeast extract + 10g NaCl in 1L H_2O

3.1.8. Kits

Name	Provider
CD19 MicroBeads, mouse	Miltenyi Biotec
Dead Cell Removal Kit	Miltenyi Biotec
HiPure Plasmid Filter Maxiprep Kit (25 Preps)	Thermo Fisher Scientific
Pan T Cell Isolation Kit II, mouse	Miltenyi Biotec
PureLink™ HiPure Plasmid Maxiprep Kit	Thermo Fisher Scientific

3.1.9. Software

Software	Provider
BioRender	BioRender
EndNote	Thomson Reuters
FlowJo_v10.8.1	FlowJo
GraphPad Prism 8	GraphPad

ImageJ	National Institutes of Health
IncuCyte® Live-Cell Analysis software	Sartorius
Microsoft Excel 2015	Microsoft
Microsoft PowerPoint 2015	Microsoft
Microsoft Word 2015	Microsoft

3.2. Methods

3.2.1. Mouse strains

Experimental mice were housed in a specific pathogen-free (SPF) barrier environment at the Charité Research Facility for Experimental Medicine (FEM) according to the guidelines from governmental health review board (Landesamt für Gesundheit und Soziales (LAGeSo)). Food and drinking water were provided, and the ambient temperature for mice was set as 20 ± 2℃ with 40 - 60% humidity. All mouse experiments were approved by the LAGeSo and conducted accordingly. *Eμ-Myc* transgenic mice and *Eμ-Myc; Suv39h1*$^{Y/-}$ transgenic mice were established as previously reported [130, 131], and the genotyping was confirmed via allele-specific genomic PCR. Female mice aged 6-8 weeks old were used for *in vivo* lymphoma propagation, and those aged 8-12 weeks old were used for spleen harvest and pan T-cell isolation (when otherwise, it is specifically indicated in the figure legends). For lymphoma propagation, mice were transplanted with the isolated primary lymphoma cells from *Eμ-Myc* transgenic mice via tail vein injection (1×10^6 cells in 100μL/mouse). Upon regular monitoring, mice were sacrificed when lymphoma manifested. All mice were humanely sacrificed using CO_2 after anesthesia with isoflurane as scheduled or when lymphoma manifested or sickness appeared in the recipient mice.

3.2.2. Lymphoma cell isolation

The primary lymphoma cells were isolated from the *Eμ-myc* transgenic mice, which was conducted according to a well-established protocol in our lab as previously reported [132]. Briefly, the enlarged lymph nodes (axillary and inguinal lymph nodes) can be dissociated from the mice to obtain single-cell suspension using the gentleMACS dissociator. CD19 microbeads were used to further purify the B cells, the

purity of which was then investigated via flow cytometry.

3.2.3. Primary cells and cell lines

To bypass the apoptosis pathway and induce extensive senescence, the isolated primary lymphoma cells were given *Bcl2-MSCV*-plasmid retroviral transduction (with different selection markers: GFP / puromycin-resistance / blasticidin-resistance), as described in Section 3.2.4. The lymphoma cells were cultured with feeder cells in complete culture medium (20% fetal bovine serum, 40% DMED medium (high glucose) and 40% IMDM medium) supplemented with penicillin-streptomycin (100 Units/ml), L-Glutamine (4 mM) and β-mercaptoethanol (25 μM). The Phoenix^{TM}-Eco retrovirus producer cells and human colorectal cancer cell line (SW480) were cultured in the same medium as the NIH-3T3 cells (10% FBS, 90% DMED medium (high glucose) and 1% penicillin-streptomycin). All the cells were maintained in a humid incubator at 37℃ with 5% CO_2. Cells were frozen in the 10% DMSO-containing fetal bovine serum and stocked in a liquid nitrogen container for long-term storage. Conditioned medium from the cultured cells was regularly tested for mycoplasma contamination.

3.2.4. Feeder cell preparation

NIH-3T3 mouse embryonic fibroblast cells were cultured in the complete medium. Upon reaching an exponential growth phase, NIH-3T3 cells were processed to irradiation for feeder cell preparation as previously reported [133].

3.2.5. Transformation, plasmid purification, transfection and retroviral transduction

The helper plasmids and the *Bcl2*-overexpressing plasmids were constructed based on the murine stem cell retrovirus (MSCV) backbone, which was ordered from Clontech. To prepare plasmids, chemically competent cells (JM109, from Zymo Research) were transformed with 1 μL of the original plasmid stock and inoculated on a carbenicillin-containing LB Agar gel on a petri dish for 12 to 14 hours at 37℃. The next day, 2-3

clones were selected to further expand the target DNA-carrying bacteria in a carbenicillin-containing LB medium at 37°C for 12 to 14 hours. Afterwards, the cultured medium was centrifuged at 10,000g for 30 minutes to collect the pellets, which were then processed to plasmid purification using a filter-based plasmid purification kit in accordance to the provider's instructions. Eventually, the plasmids were dissolved in sterile ultra-pure water, and their concentrations were determined via a spectrophotometer. Afterwards, the plasmids were aliquoted and stored in a -20°C freezer.

Phoenix^{TM}-Eco retrovirus producer cells were transiently transfected with MSCV-based plasmids using the calcium phosphate method. The retroviral supernatant was collected after 48 hours and 72 hours upon transfection, and then used for transducing the freshly thawed primary *Eμ-Myc* lymphoma cells. Consequently, *Bcl2; Eμ-Myc* lymphoma cells (*Bcl2*-protected Control LCs) and *Bcl2; Suv39h1$^{Y/-}$; Eμ-Myc* lymphoma cells (*Bcl2*-protected Suv39h1$^{Y/-}$ LCs) were established and used in this project.

3.2.6. Establishment of therapy-induced senescence (TIS)

The *Bcl2*-protected lymphoma cells were treated with MAF (mafosfamide, 10 μg/mL), a cyclophosphamide (CTX) analog that is broadly used to treat tumor cells *in* vitro due to its active properties and spontaneous degradation into 4-hydroxy- cyclophosphamide. After being exposed to MAF for 3 days, cells were proceeded to CellTrace^{TM} dye staining according to the provider's protocol. CellTrace^{TM} dye is one of the commonly used cell-tracing amine-binding dyes that yield strong fluorescence once cleaved by intracellular esterases. The fluorescent signal of CellTrace^{TM} dye-labeled parental cells can be separated and passed to their daughter cells, thereby helping to investigate the division of cells based on the reduced fluorescence intensity of the labeled cells. Therefore, the undivided cells (e.g., TIS cells)retained the dye and displayed intense fluorescence after returning to normal culture conditions for a certain period of time. To enrich TIS cells, the MAF-treated cells werecollected on day 3 post treatment and

stained with CellTrace™ dye working solution (1:1000 in 1× PBS) for 20 minutes at room temperature, followed by the addition of fresh medium for another 5 minutes to terminate the staining. After that, cells were washed twice with fresh medium and proceeded to another 2-day regular culture. Afterwards, cells that retained high-level CellTrace™ dye were positively sorted, sincethey were considered to be viable non-proliferating cells. These cells were collected for SA-β-Gal staining (**see Section 3.2.13**) to further confirm their senescence status. Afterthe SA-β-Gal staining, which marks senescent cells by a blue perinuclear reaction, samples with more than 95% of blue cells were considered senescent, indicating a successful establishment of the *in vitro* therapy-induced senescence (TIS) model. Thereafter, these positively sorted cells (TIS cells) were processed for the subsequent experiments.

3.2.7. Pan T-cell isolation

All the procedures were conducted under a sterile environment, and all buffers and media used were pre-chilled before use. Mouse spleens were harvested and dissociated using a gentleMACS dissociator. The single-cell suspension was then filtered through a 40 μm mesh filter to remove possible cell clumps, and centrifuged at1,500 rpm for 5 minutes at 4°C. Afterwards, the pellet was incubated with red cell lysis buffer for 10 minutes at room temperature. After that, the cell suspension was washed twice with the pre-chilled 1× PBS and proceeded to pan T cell isolation in accordance with the provider's instructions. Briefly, splenocytes were first incubated with an antibody cocktail (10 μL per 1×10^7 cells) in the isolation buffer for 5 minutes at 4°C. Afterwards, the microbeads (20 μL per 1×10^7 cells) were added to the sample for a 10-minute incubation at 4°C. Then, the sample was loaded into a pre-washed MACS column on a magnetic stand, and rinsed with 5 mL isolation buffer to collect the unlabeled cells, which were the pooled pan T cells. After cell counting, the pooled T cells were processed for the subsequent experiments.

3.2.8. Co-culture of T cells and lymphoma cells

The MAF-treated *Bcl2*-protected lymphoma cells (MAF LCs hereafter) were stained with CellTrace™ dye on the third day after mafosfamide treatment, followed by fluorescence-activated cell sorting (FACS) to obtain a purer senescent cell sample. Conversely, the untreated *Bcl2*-protected lymphoma cells (untreated LCs hereafter) were stained with CellTrace™ dye on the same day of co-culture. In the co-culture system, the *Bcl2*-protected lymphoma cells were seeded into a 96-well round-bottom plate (1×10^4 cells/100μL/well). In most settings, the pooled T cells (1×10^5 cells/100μL/well) were then loaded into the same plate as the lymphoma cells to achieve a T cell-lymphoma cell ratio of 10 : 1 (the other ratios that were used are indicated specifically in the corresponding figure legends). Furthermore, the volume for T cells would be adjusted to 50 μL/well in the BsAb-related experiments to achieve a co-culture system with 200μL/well in this project.

The viability of lymphoma cells in the *ex vivo* T-cell killing assays was determined after 24 hours and 48 hours via flow cytometry (The gating strategy is shown below in **Figure 2**). To study the *ex vivo* physical interaction of lymphoma cells and T cells, the pooled T cells were also stained with CellTrace™ dye (a different color from the dye used for lymphoma cells) before co-culture. After 4-hour co-culture, the percentage of coupling cells was determined via flow cytometry (The gating strategy is shown below in **Figure 3**) [134]. The activation of T cells in the co-culture system was monitored after 24 hours, which was indicated by the percentages of $CD69^+CD3^+$ T cells and $CD25^+CD3^+$ T cells. For measuring the proliferation potentials of T cells in the co- culture system, the pooled T cells were stained with CellTrace™ dye before co-culture.After 72 hours, the signals of CellTrace™ dye were measured via flow cytometry and compared between T cells from different settings. Last but not least, the expression of CD274 (PD-1) on T cells was determined on the third day of co-culture.

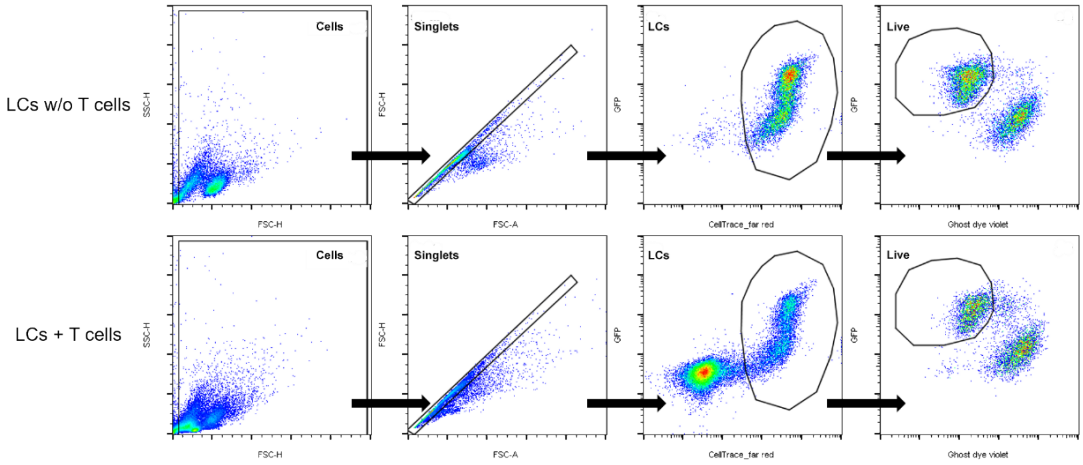

Figure 2. Gating strategy for viability determination of lymphoma cells after co-culture with T cells.

In the FSC_H/SSC_H dot plot, debris was gated out, followed by gating on singlets in the FSC_A/HSC_H dot plot. Then, CellTrace^{TM} dye-labeled lymphoma cells (LCs) were determined as CellTrace_far red^{+} GFP^{+} cells. The viability of these LCs was determined as the percentage of ghost dye_violet-negative GFP^{+} cells (upper panel: LCs without T cells; lower panel: LCs with T cells).

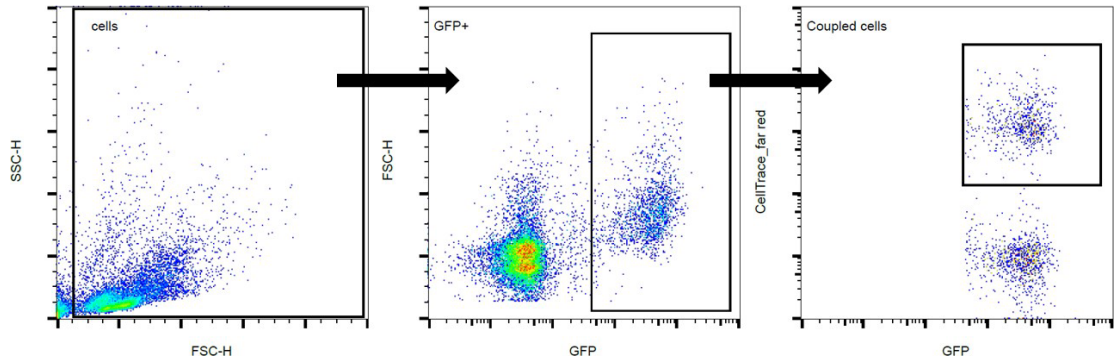

Figure 3. Gating strategy for measuring the interaction of lymphoma cells and T cells in the co-culture.

T cells were labeled with CellTrace^{TM}_far red prior to their co-culture with GFP^{+} LCs. In the FSC_H/SSC_H dot plot, debris was gated out, followed by gating on GFP^{+} cells in the GFP/HSC_H dot plot. Then, the coupling population was determined as the percentage of CellTrace_far red^{+} GFP^{+} among the GFP^{+} cells.

3.2.9. Bispecific antibody treatment

Based on the previous studies [135], four concentrations of the bispecific antibodies (BsAbs hereafter) were investigated for their boosting effects on the *ex vivo* unstimulated T-cell killing assays. Different doses of BsAbs were diluted in fresh culture medium and added into each well (50 μL/well), while BsAb-free culture

medium was added to the control group (50 μL/well).

3.2.10. Fluorescence-activated cell sorting

On the fifth day of mafosfamide treatment, CellTrace™ dye-labeled lymphoma cells were collected for sorting. The gating strategy is shown below (**Figure 4**). The MAF-treated lymphoma cells that remained with a high-level signal of CellTrace™ dye were positively sorted and proceeded to the subsequent experiments.

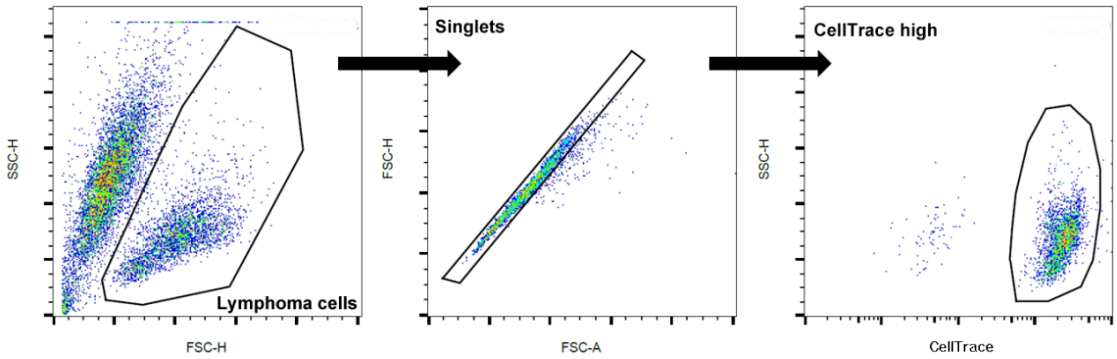

Figure 4. Gating strategy for the fluorescence-activated cell sorting of CellTrace™ dye-labeled lymphoma cells.
In the FSC_H/SSC_H dot plot, debris and dead cells were gated out, followed by gating on singlets in the FSC_A/HSC_H dot plot. Then, CellTrace™ dye-labeled lymphoma cells (LCs) with intense fluorescence were determined as TIS cells in the CellTrace/SSC_H dot plot and positively sorted.

3.2.11. Flow cytometry detection

The fluorescence-conjugated antibodies were first titrated before use. Proper unstained controls, single stained controls, fluorescence minus one (FMO) controls and positive controls were set up for the voltage and compensation adjustment of the flow cytometer to establish the multicolor flow cytometry panels. For sample staining, cells were collected and centrifuged at 1,000 rpm for 5 minutes, followed by washing twice with 1× PBS. Then, the sample was first stained with a viability dye (Ghost Dye™ Violet) according to the provider's protocol. Briefly, cells were incubated with the ghost dye staining solution (1:1000 in 1× PBS) for 30 minutes at 4°C. Afterwards, cells were washed twice with the pre-chilled flow cytometry staining buffer (FCM staining buffer) to terminate the dye staining. For the viability test of lymphoma cells in the *ex vivo* T-cell killing assays, cells were then fixed with 4% PFA solution for 5 minutes at room temperature, followed by washing twice with 1× PBS. Eventually, these cells were resuspended in 1× PBS (200μL/sample) and proceeded to viability measurement using

a flow cytometer. On the other hand, to stain cell surface markers, cells were incubated with the anti-mouse CD16/CD32 antibodies for 5 minutes to block the unspecific antibody-binding of Fc receptors, followed by sample incubation with the fluorescence-conjugated antibodies in the FCM staining buffer for 30 minutes at 4℃. Afterwards, cells were washed twice with the pre-chilled FCM staining buffer, and resuspended in the FCM staining buffer (200μL/sample) for measurement. The acquired data were analyzed using the FlowJo software. The relative viability of lymphoma cells in the *ex vivo* T-cell killing assays was determined as: $Relative\ viability = \frac{Viablity\ of\ LCs\ (+T\ cells)}{Viability\ of\ LCs\ (-T\ cells)} \times 100\%$.

3.2.12. Fluorescence live-cell imaging

To increase the plate adherence of lymphoma cells, poly-D-lysine was used to coat the culture plates as previously described [136]. Briefly, 50μL of the poly-D-lysine solution (50 μg/mL) was loaded onto the well bottom of a 96-well flat-bottom plate, and incubated for 2 hours in the incubator at 37°C. Afterwards, the remaining solution was carefully removed, followed by rinsing the wells twice with sterile Milli-Q water. Then the coated plate was allowed to air dry inside the cell culture hood. The coated plates can be used immediately after drying or stored at 4℃ for up to 4 weeks. The *Bcl2-GFP* lymphoma cells and the CellTrace™ dye-labeled T cells were seeded into the coated plates under the same conditions as described in Section **3.2.8**. Afterwards, the plate was placed into the Live-cell Analysis Instrument (IncuCyte®) for live-cell imaging. The images were captured at 30-minute intervals under a 10× objective magnification for 72 hours. The acquired data were analyzed, and the images were processed via Incucyte® analysis software.

3.2.13. Senescence-associated beta-galactosidase (SA-β-Gal) staining

SA-β-Gal staining was broadly applied for senescence indication in cells and tissues as a conventional assay [137] and performed as previously reported [7]. As non-adherent cells, murine lymphoma cells were collected using centrifugation at 1,000 rpm for 5 minutes, followed by washing twice with 1× PBS. Afterwards, cells were fixed with the

fixative solution for 10 minutes at room temperature, and then washed twice with 1× PBS (pH = 5.5). Then, the cells were resuspended in an appropriate volume of 1× X-Gal solution and incubated with the substrates at 37℃. The incubation time varied between different materials; however, the same incubation time was applied to the paired lymphoma cases (untreated v.s. MAF-treated). After staining, cells were washed twice with 1× PBS. The LCs were eventually resuspended in 1× PBS and transferred to a flat-bottom culture plate. The images were captured under a microscope. With 4 randomly selected fields of each sample, the blue cells were counted through ImageJ. The percentageof blue cells (TIS cells) in each sample was recorded and calculated as mean ± standard deviation (SD).

3.2.14. Bioinformatics analysis

The microarray gene profiling data was generated by our previous colleagues and published in the Gene Expression Omnibus (GEO) repository of the National Center for Biotechnology Information (GSE134753). The microarray gene profiling data of TIS cells [*in vitro* ADR-treated *Suv39h1*-proficient (*Control*) lymphoma cells] andnon-TIS cells [both untreated *Control* and *in vitro* ADR-treated *Suv39h1*-deficient ($Suv39h1^{ER}$) lymphoma cells] was processed to Gene Set Enrichment Analysis (GSEA) using the GSEA v4.2.2 software [138, 139]. Normalized enrichment scores (NES) with *P*-values < 0.05 and false discovery rate (FDR) < 0.25 were regarded as statistically significant. The TIS signature was a composition of significantly changed genes (*P*-value <0.01, and log |FC| > 1) in the TIS cells (*in vitro* ADR-treated *Control* lymphoma cells) compared to the non-TIS cells (both untreated *Control* and *in vitro* ADR-treated $Suv39h1^{ER}$ lymphoma cells). The significantly changed genes were proceeded to gene functional annotation and cluster analysis on an online platform (Database for Annotation, Visualization and Integrated Discovery, DAVID). The visualization of the top 20 enriched Gene Ontology (GO) terms for biological processes was conducted on the online platform Sangerbox 3.0. The research on the subcellular location and protein function of genes was conducted on the online open-access platform UniProt.

3.2.15. Statistical analysis

Graphpad Prism 8 was utilized for statistical analysis in this project. The continuous data were presented as mean ± standard deviation (SD). Following the normality test, comparisons between the two groups were conducted using the unpaired *t*-test for unpaired data or paired *t*-Test for paired data. To analyze the differences between the means of multiple groups, the data were compared and tested using two-way ANOVA. A *P*-value less than 0.05 was considered statistically significant.

4. Results

4.1. Immune response-related signatures were enriched in the TIS lymphoma cells.

4.1.1. TIS lymphoma cells exhibited abundant immune-related genetic signatures.

To explore the potentiality of TIS lymphoma cells in influencing the general immune response, we first mined our previously published microarray-based gene expression profiling data of the *Eμ-myc; Bcl2*-protected lymphoma cells (GSE134753). The samples were categorized into the TIS group (*in vitro* ADR-treated *Control*, n=19)and the non-TIS group (untreated *Control* and *in vitro* ADR-treated $Suv39h1^{ER}$, n=22). Gene set enrichment analysis was conducted to compare the TIS cells and the non-TIS cells, with an emphasis on the immune response-related gene sets (**Figure 5a**). In comparison with the non-TIS group, the TIS group exhibited significant enrichment of multiple gene sets, which was involved in the immune response, T cell activity and peptide/MHC-I/MHC-II processes (**Table 1**). Interestingly, the gene set "*Negative Regulation of Adaptive Immune Response*" was considerably abundant in the TIS cells. A list of genes that were changed significantly in the TIS cells compared to the non-TIS cells was generated by our colleagues after performing the differential gene expression analysis, which has also been published [6]. Genes with log(FC) > 1 (P < 0.01) and log(FC) < 1 (P < 0.01) were regarded as significantly up-regulated and down-regulated in the TIS group, respectively. These significantly changed genes were further analyzed for gene functional annotation and biological theme enrichment. Afterwards, the most enriched GO terms (biological process) were identified (**Figure 5b**), including those relevant to the immune response (marked with stars in **Figure 5b**). The GO terms *Immune Response* and *Immune System Process* were further investigated for their overlapping genes to explore the candidate genes that may affect the immune response towards TIS cells. Interestingly, eight overlapping genes were found (**Figure 5c**). Furthermore, their protein products are mostly localized on the cell membrane where they can engage in the immune response process (**Table 2**). Among these genes,*CD274*

(also known as *PD-L1*) has been well elucidated in terms of its immunosuppressive role in the adaptive T-cell response. In essence, TIS lymphoma cells exhibited abundant genetic signatures involved in regulating the overall immune response.

Table 1. TIS lymphoma cells exhibited enriched gene sets related to the immune response, T cell activity and peptide presentation process.

Gene sets	NES	FDR
GOBP_ACTIVATION_OF_IMMUNE_RESPONSE	1.37	0.045
GOBP_CYTOKINE_PRODUCTION_INVOLVED_IN_IMMUNE_RESPONSE	1.50	0.006
GOBP_ACTIVATION_OF_INNATE_IMMUNE_RESPONSE	1.38	0.065
GOBP_HUMORAL_IMMUNE_RESPONSE	1.31	0.076
GOBP_NEGATIVE_REGULATION_OF_ADAPTIVE_IMMUNE_RESPONSE	1.21	0.180
GOBP_ALPHA_BETA_T_CELL_ACTIVATION	1.37	0.080
GOBP_ALPHA_BETA_T_CELL_DIFFERENTIATION	1.28	0.154
GOBP_ALPHA_BETA_T_CELL_PROLIFERATION	1.50	0.031
REACTOME_PEPTIDE_LIGAND_BINDING_RECEPTORS	1.60	0.008
REACTOME_CLASS_I_MHC_MEDIATED_ANTIGEN_PROCESSING_PRESENTATION	1.34	0.087
GOBP_MHC_CLASS_II_BIOSYNTHETIC_PROCESS	1.28	0.133

Table 2. The subcellular location of the proteins encoded by the overlapped genes in the GO term-*Immune Response* and the GO term-*Immune System Process*.

Gene	Subcellular location
Clec4d: C-Type Lectin Domain Family 4 Member D, CD368	Cell membrane
Clec4e: C-Type Lectin Domain Family 4 Member E	Cell membrane, cell projection, phagocytic cup
Clec4n: C-Type Lectin Domain Family 4 Member N	Plasma membrane
CD274: PD-L1, B7H1	Cell membrane
Lst1: Leukocyte Specific Transcript 1	Cell membrane
Marchf1: Membrane Associated Ring-CH-Type Finger 1	Cell membrane Golgi apparatus, lysosome membrane, cytoplasmic vesicle membrane, endosome membrane
Tlr13: Toll-like receptor 13	Endosome membrane
Tlr2: Toll-like receptor 2	Plasma membrane, phagosome membrane, membrane raft, Golgi apparatus

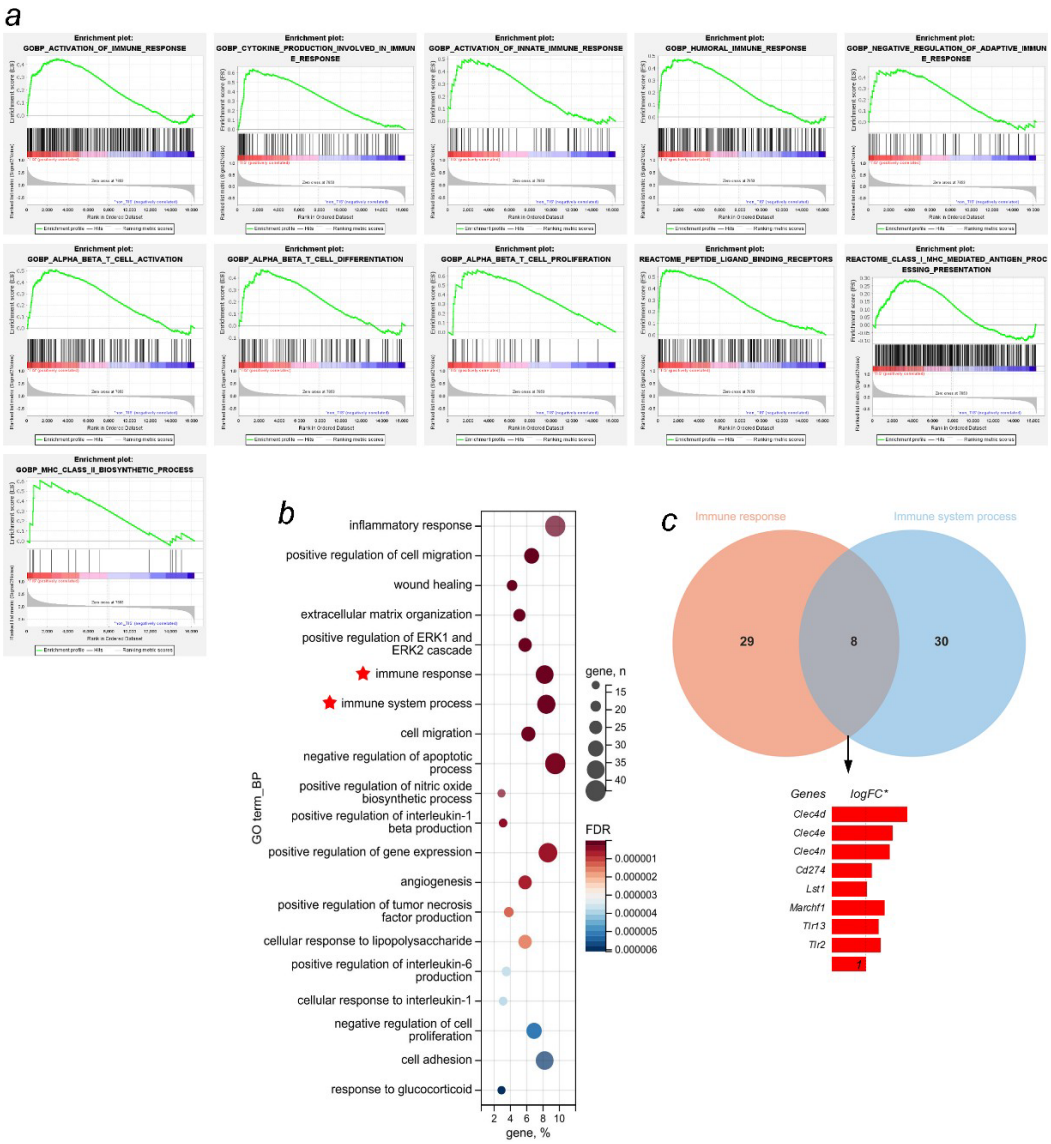

Figure 5. Immune response-related genetic signatures were enriched in the TIS lymphoma cells.

Using our previously published microarray-based gene expression profiling data of the *Eμ-myc; Bcl2*-protected lymphoma samples (GSE134753), we categorized the samples into TIS cells (*in vitro* ADR-treated *Control*, n=19) and non-TIS cells (untreated *Control* and *in vitro* ADR-treated *Suv39h1*^{ER}, n=22). (a) Gene set enrichment analysis was conducted to compare the TIS cells and the non-TIS cells focusing on the immune response-related gene sets. An NES larger than 1 with an FDR q-value less than 0.25 was considered significant up- regulation in the TIS group. (b) Top 20 GO terms (biological process) from the functional annotation of the significantly changed genes (P < 0.01, log|FC| > 1) in the TIS cells compared to the non-TIS cells. The n and % of genes represent the number of genes and their percentagein the overall significantly changed genes. Red stars mark the immune response-related GO terms. (c) Candidate genes that may mediate the immune response towards TIS cells. The number of genes that were involved in the GO term-*Immune Response* and the GO term-*Immune System Process* (Venn diagram) as well as the fold change of these overlapped genes in the TIS cells compared to the non-TIS cells (bar chart). The dotted line marks logFC = 1. *, P < 0.01. NES,

normalized enrichment score; FDR, false discovery rate; GO term_BP, Gene Ontology Term_Biological Process; FC, fold change.

4.1.2. Enhanced expression of co-stimulatory and inhibitory molecules on the TIS lymphoma cell surface.

Given the abundance of immune-regulatory genetic signatures in the TIS lymphoma cells, we decided to investigate the immunological molecules on the TIS cell surfaces. Hence, we used an *in vitro* TIS model by treating the *Eμ-myc; Bcl2-GFP* lymphoma cells (*Bcl2-GFP* lymphoma cells for short) with mafosfamide (MAF). As shown in **Figure 6a**, the lymphoma cells were treated with MAF for three days, followed by a two-day normal culture. After that, the senescence induction was validated using SA-β-gal staining, a conventional assay for detecting the activity of β-galactosidase exclusively in murine senescent cells at pH 5.5 (**Figure 6b**). After MAF treatment, over 90% of the *Bcl2-GFP* lymphoma cells entered senescence (**Figure 6b**). As a histone methyltransferase, Suv39h1 (locations: Xp11.23) mediates the chromatin compaction by trimethylating histone H3-lysine 9 (H3K9) during the senescence induction. The loss of Suv39h1 on the X chromosome leads to senescence incapability. As an additional control, *Suv39h1$^{Y/-}$; Bcl2-GFP* lymphoma cells received MAF treatment in the same way as *Control; Bcl2-GFP* lymphoma cells did. The SA-β-gal staining indicated a reduced senescence induction in the *Suv39h1$^{Y/-}$; Bcl2-GFP* lymphoma cells after chemotherapy (**Figure 6c**).

Upon *in vitro* TIS, the *Bcl2-GFP* lymphoma cells were subjected to the quantification of cell surface proteins using fluorescence-conjugated antibodies, followed by flow cytometry measurement. As compared to the untreated lymphoma cells (proliferating cells), MAF-treated lymphoma cells (TIS lymphoma cells) exhibited a significant up-regulation of surface proteins including CD80, CD86 and MHC-I (**Figure 6d**). The up-regulation of surface MHC-II was also noted in 4 of 6 lymphoma cases, although the extent and direction varied profoundly among the samples (**Figure 6d**). Furthermore, one of the immune checkpoint proteins, PD-L1, was found significantly up-regulated in the TIS lymphoma cells (**Figure 6e**). Likewise, therapy-induced PD-L1 up-regulation

could be observed in a human colorectal cancer cell line (SW480) after 5-FU treatment (**Figure 6f**). Collectively, TIS cells displayed an up-regulation of MHC-I, MHC-II and co-stimulatory factors (CD80, CD86) on their cell surfaces, along with the enhanced presence of PD-L1.

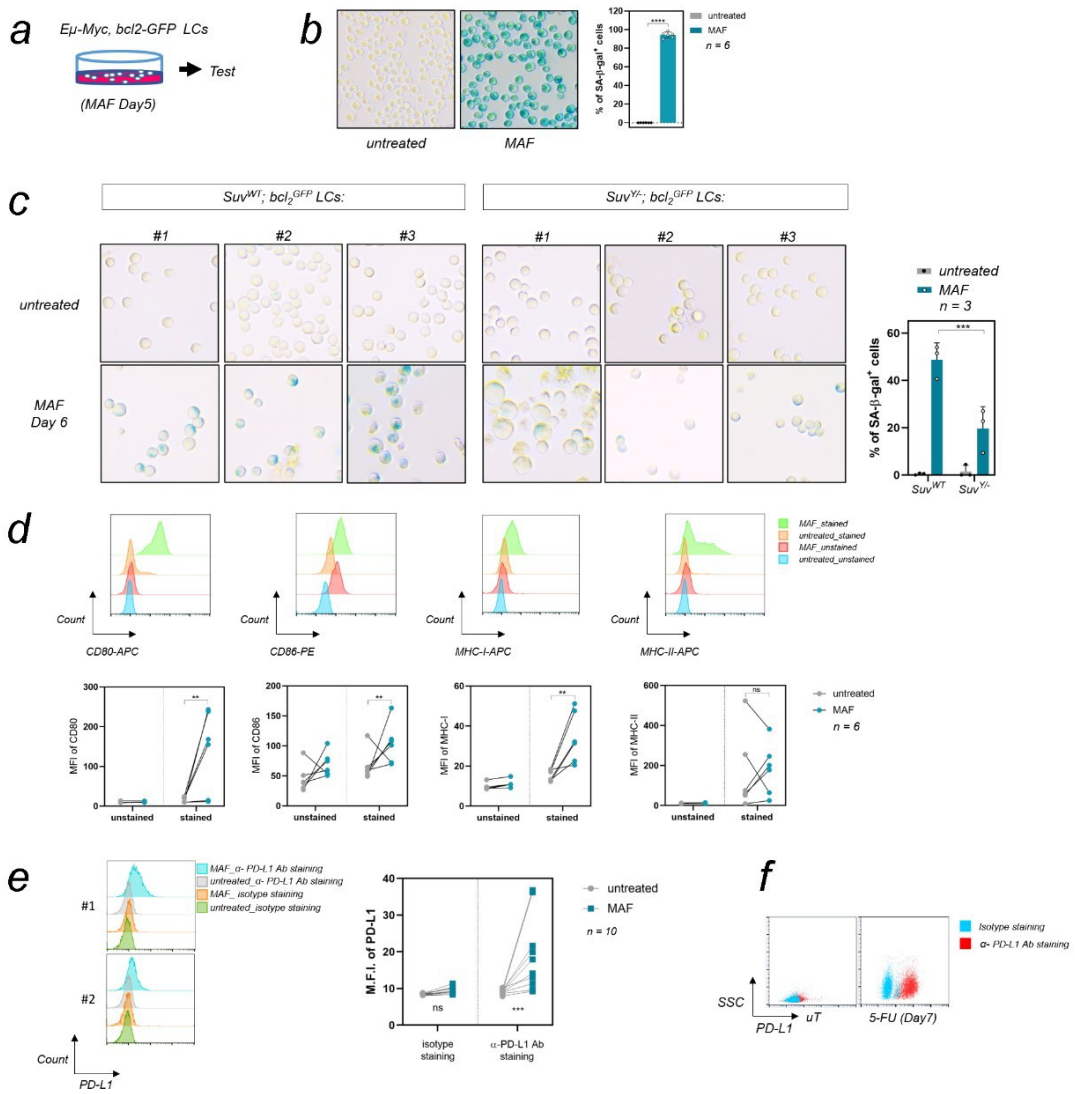

Figure 6. Co-stimulatory and inhibitory molecules were up-regulated in the TIS lymphoma cells.

(a) Schematic diagram of the *in vitro* TIS model using *Eμ-myc; Bcl2*-protected lymphoma cells, which received a 3-day mafosfamide treatment (10μg/mL) and another 2-day regular culture. (b) & (c) Representative images of lymphoma cells (untreated v.s. MAF-treated) in the SA-β-gal staining (6 distinct *Control; Bcl2-GFP* lymphoma cases were used in (b); 3 distinct *Control; Bcl2-GFP* and 3 distinct *Suv39h1*$^{Y/-}$*; Bcl2-GFP* lymphoma cases were usedin (c)). The percentages of senescent cells (blue cells) were summarized and analyzed (b-rightand c-right). On the fifth day of MAF treatment, lymphoma cells were stained with the viability dye (Ghost dye violet) and the fluorescence-conjugated antibodies targeting mouse CD80, CD86, MHC-I, MHC-II and PD-L1. (d) Representative histograms (upper panel) and MFI summaries (lower

panel) of the fluorescence-conjugated antibody staining to quantify the surface expression of CD80, CD86, MHC-I and MHC-II on the viable lymphoma cells. (e) Two representative histograms (left) and the MFI summary (right) of the anti-PD-L1 antibody staining of the viable lymphoma cells. (f) Representative histogram of the colorectal cancercell line SW480 receiving the anti-human PD-L1 antibody staining on the seventh day of 5-FU treatment. MAF, mafosfamide; MFI, median fluorescence intensity; 5-FU, 5-Fluoruracil; Ab, antibody. **, $P < 0.01$; ****, $P < 0.0001$; ns, not significant.

4.2. Primary T-cell surveillance of TIS lymphoma cells.

4.2.1. Establishment of an *ex vivo* T-cell killing assay.

Given the enhanced surface expression of the immune-promoting molecules (MHC-I, MHC-II, CD80 and CD86) as well as the immunosuppressive protein (PD-L1) on the TIS cells, we decided to investigate the T-cell surveillance of TIS cells *ex vivo* in order to exclude the detrimental effects of chemotherapy on the mouse immune system. Therefore, we established an *ex vivo* T-cell killing assay (**Figure 7a**). Briefly, pan T cells were isolated from the spleens of healthy wild-type C57Bl/6N mice, which were lymphoma-naïve strain-matched donors. The isolation efficiency was monitored by anti-CD3-PE staining. Through flow cytometry analysis, the percentages of viable $CD3^+$ cells in the purified samples were compared before and after isolation (**Figure 7b**). Freshly isolated pan T cells with a purity of more than 95% viable $CD3^+$ cells were pooled and co-cultured separately with untreated and MAF-treated *Bcl2-GFP* lymphoma cells. The co-culture system was maintained for 4 to 72 hours depending on the experimental purposes.

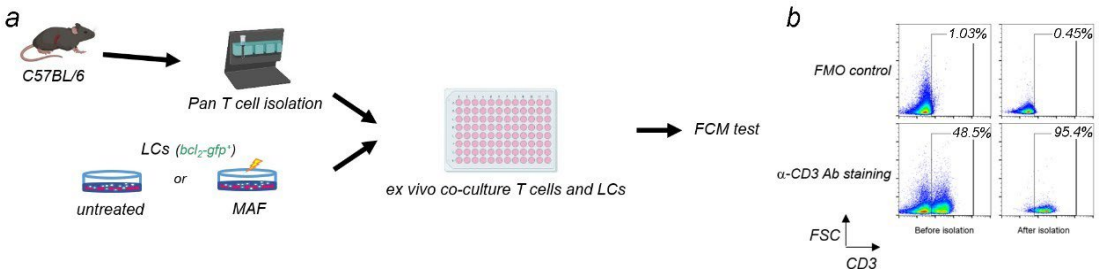

Figure 7. Establishment of the *ex vivo* T cell and lymphoma cell co-culture system.
(a) Schematic diagram of the *ex vivo* co-culture system using the *Eμ-myc; Bcl2*-protected lymphoma cells and the unstimulated pan T cells isolated from the wild-type lymphoma-naïve strain-matched C57BL/6N mice. (b) Representative dot plot of the isolated T cells after the anti-

CD3 antibody staining. FCM, flow cytometry; FMO control, fluorescence minus one control; Ab, antibody.

4.2.2. Unstimulated T cells preferentially killed TIS lymphoma cells.

Based on the workflow described in **Section 4.2.1.**, the pooled T cells without pre-stimulation were co-cultured with *Bcl2-GFP; Control* lymphoma cells (untreated or pre-treated with MAF) at two T cell-LC ratios and for different co-culture durations. After that, the viability of lymphoma cells was determined by flow cytometry. The relative viability was computed with the viability of lymphoma cells alone as the baseline. After 24-hour co-culture, the relative viability of TIS lymphoma cells was significantly decreased compared to that of untreated lymphoma cells at a T cell-LCratio of 10:1 (**Figure 8a**). When the co-culture duration was prolonged to 48 and 72 hours, the tendency of relative viability was comparatively consistent in the untreated and MAF-treated lymphoma cells upon co-culture with T cells at a T cell-LC ratio of 10:1 (**Figure 8b**). Therefore, the T cell-LC ratio in the co-culture system was set at 10:1, and the co-culture duration was set to 24 hours (or 48 hours additionally) in the subsequent experiments.

To assess the potential sublethal damage conferred by chemotherapy in TIS lymphoma cells prior to their exposure to unstimulated T cells, equally chemo-treated *Bcl2-GFP; Suv39h1*$^{Y/-}$ lymphoma cells were utilized as a senescence-incapable control. The pooled T cells from male wild-type lymphoma-naïve C57BL/6N mice were used for the *ex vivo* T-cell killing assay. Compared to the MAF-treated *Bcl2-GFP; Control* lymphoma cells (TIS cells), the MAF-treated *Bcl2-GFP; Suv39h1*$^{Y/-}$ lymphoma cells (non-TIS cells after treatment) exhibited comparable relative viabilities to their untreated controls (**Figure 8c**). Therefore, senescence status - but not chemotherapy exposure - plays a predominant role in determining the vulnerability of TIS lymphoma cells towards the T-cell killing *ex vivo*.

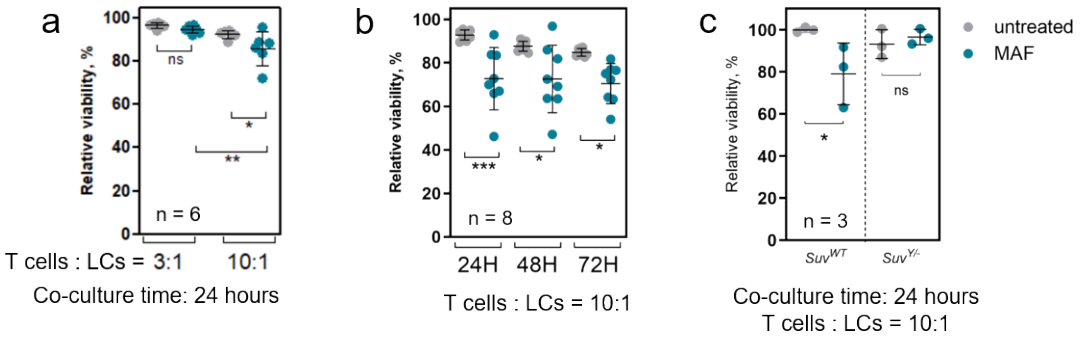

Figure 8. Unstimulated T cells preferentially killed the TIS lymphoma cells.
In the *ex vivo* T-cell killing assay, the spleens of female wild-type (lymphoma-naïve strain-matched) C57BL/6N mice were used to pool pan T cells. Without pre-stimulation, the pooled T cells were co-cultured with the *Bcl2-GFP; Control* LCs (untreated or pre-treated with MAF) at different T cell-LC ratios (a) and for different co-culture durations (b). In the vulnerability comparison of the *Bcl2-GFP; Control* LCs to the *Bcl2-GFP; Suv39h1*$^{Y/-}$ LCs (c) in the pan T-cell killing assay, the pooled T cells were isolated from male wild-type (lymphoma-naïve strain-matched) C57BL/6N mice. The viability of LCs after co-culture was determined by Ghost dye (violet) staining through flow cytometry. After data analysis using the Flowjo software, the relative viability of LCs was determined as $= \frac{Viability\ of\ LCs\ (+T\ cells)}{Viability\ of\ LCs\ (-T\ cells)} \times 100\%$. *, $P < 0.05$; **, $P < 0.01$; ***, $P < 0.001$; ns, not significant.

4.2.3. TIS lymphoma cells were prone to interact with and activate unstimulated T cells *ex vivo*.

Given the increased vulnerability of TIS cells towards T-cell cytotoxicity *ex vivo*, we decided to investigate the impacts of TIS cells on the primary T-cell response. We first quantified the interaction effectiveness of lymphoma cells to the unstimulated T cells. CellTrace^{TM} pre-labeled T cells (Red^{+}) and *Bcl2-GFP; Control* lymphoma cells (GFP^{+}) were used in this assay. After a 4-hour co-culture, a significantly higher percentage of coupled cells (Red^{+}GFP^{+}/GFP^{+}%) was recorded in the TIS lymphoma cell and T cell co-culture system than in the untreated lymphoma cell and T cell co-culture system, implying that more TIS lymphoma cells can interact with T cells following a short-term encounter (**Figure 9a-left**). Since the T cells were labeled with CellTrace^{TM}dye before co-culture and aliquoted equally into the co-culture system, the fluorescence intensity of the CellTrace^{TM} dye on the coupled lymphoma cells could indicate an approximate number of T cells on the target cells. Stronger mean fluorescence intensity (MFI) was found in the TIS lymphoma cell and T cell co-culture system than in the untreated

lymphoma cell and T cell co-culture system, suggesting that more T cells were interacting with TIS lymphoma cells (**Figure 9a-right**).

CD69, also known as an early T-cell activation marker [140], was shown to be more abundant on the T cells that were co-cultured with TIS lymphoma cells, while remaining at their basal level on those co-cultured with untreated lymphoma cells (**Figure 9b**). CD25 (α-chain of the IL-2 receptor), is constitutively expressed in regulatory T cells (Tregs) [141]. Moreover, the activated T cells can express CD25 in response to IL-2 [142]. Here, T cells co-cultured with TIS lymphoma cells also exhibited an enhanced expression of CD25 (**Figure 9c**). Collectively, these results showed that TIS lymphoma cells were prone to interact with the unstimulated T cells *ex vivo*, and enhanced the subsequent T-cell activation.

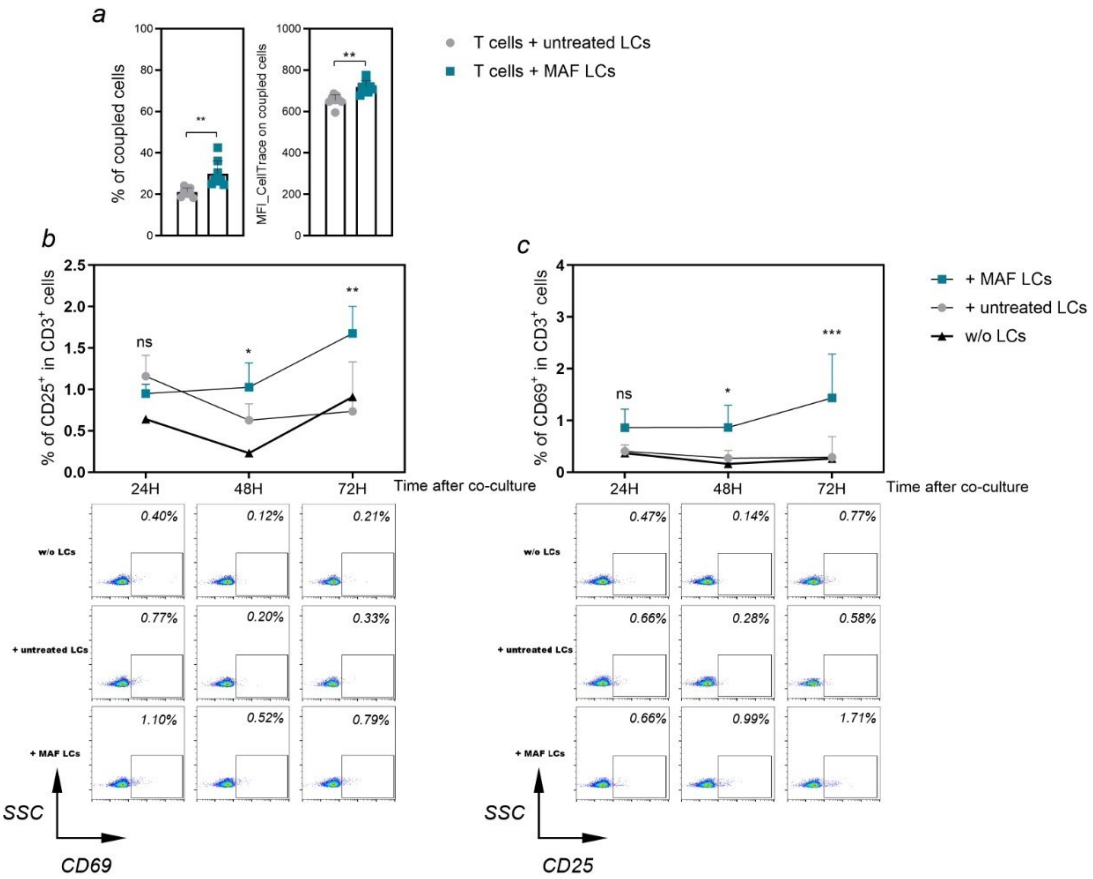

Figure 9. TIS lymphoma cells were prone to interact with unstimulated T cells and trigger their activation.

(a) The pooled T cells, without pre-stimulation, were stained with CellTrace^{TM} dye (far red) and then co-cultured with *Bcl2-GFP; Control* LCs for 4 hours, followed by flow cytometry measurement. The percentage of coupled cells was determined as the percentage of CellTrace dye^{+} GFP^{+} cells among the whole GFP^{+} cell population (left). The MFI of CellTrace^{TM} dye on the coupled cell population was analyzed (right). (b) Upon co-culture with *Bcl2-GFP; Control*

LCs, the activation status of T cells was determined after 24, 48 and 72 hours by anti-CD3 + anti-CD69 (b) and anti-CD25 (c) antibody-based staining. Below the bar chart are the representative dot plots for the T-cell phenotyping from the flow cytometry measurement. Eight distinct lymphoma cases were included in the T-cell phenotyping analysis. MFI, median fluorescence intensity; *, $P < 0.05$; **, $P < 0.01$; ***, $P < 0.001$; ns, not significant.

For measuring their proliferation potential, the pooled T cells were initially labeled with CellTrace™ dye before being co-cultured with either untreated or MAF-treated lymphoma cells. After 3-day co-culture, the fluorescence dilution of CellTrace™ dye was determined via flow cytometry. Unexpectedly, an obvious fluorescence dilution of the CellTrace™ dye could not be observed on T cells in either co-culture system (**Figure 10**), indicating a generally limited T-cell proliferation in this setting.

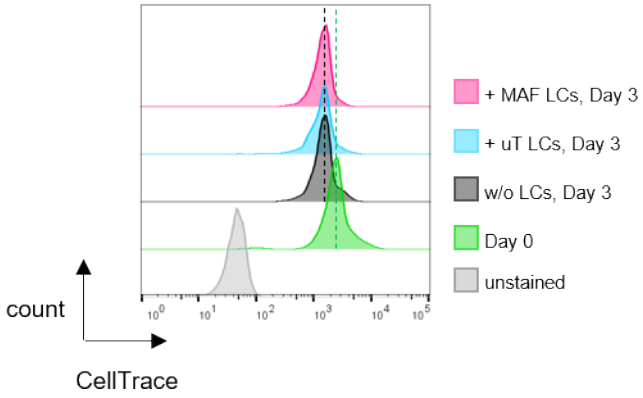

Figure 10. T cells co-cultured with TIS lymphoma cells exhibited a limited proliferation tendency.
The pooled T cells were first stained with CellTrace™ dye and then co-cultured with the untreated or MAF-treated *Bcl2-GFP; Control* LCs for 3 days. The dilution of the CellTrace™ dye signal in the viable $CD3^+$ T cells (as shown in the histograms) was determined by anti-CD3-PE staining through flow cytometry. Eight distinct lymphoma cases were included in the T-cell phenotyping analysis.

4.3. Anti-CD19/CD20 × CD3 BsAbs boosted T-cell surveillance of TIS lymphoma cells.

4.3.1. Anti-CD19/CD20 × CD3 BsAbs facilitated the killing capability of T cells *ex vivo*.

Proliferating (without MAF pre-treatment) lymphoma cells were comparatively more resistant to the *ex vivo* T-cell killing, while TIS lymphoma cells exhibited a vulnerability tendency towards the T-cell surveillance *ex vivo*. This might be a result of the enhanced immunogenicity of TIS cells and their SASP-inducing immunostimulatory microenvironment that favored lymphoma cells interacting with T cells and the subsequent activation of the lymphoma-specific T-cell clones. The general underresponsiveness of lymphoma cells to T-cell surveillance suggested the need for alternative immunotherapies that can boost the T-cell cytotoxicity towards malignant B cells. For example, T-cell redirecting BsAbs can be used to simultaneously target CD3 molecules on T cells and CD19/CD20 on lymphoma cells, thereby bridging T cells to the malignant B cells and enabling T cells to execute tumor lysis effect. This approach with off-the-shelf BsAbs (as described in **Section 2**) was therefore investigated in this project regarding their T-cell boosting efficacy towards either proliferating or TIS lymphomacells.

Serial doses of anti-CD19 × CD3 and anti-CD20 × CD3 BsAbs (hereafter referred to as CD19-BsAb and CD20-BsAb, respectively) were tested using our *ex vivo* T-cell killing assay to investigate the BsAb efficacies in influencing the cytotoxic potentiality of the unstimulated T cells towards lymphoma cells, and especially TIS lymphoma cells. When targeting untreated lymphoma cells, CD19-BsAb enabled T cells to achieve approximately 40% killing effectiveness (relative viability ≈ 60%) at a dose as low as 0.005 nmol/mL after 24 hours of co-culture (**Figure 11a**). Even though the co-culture was extended to 48 hours, further reduction of the relative viabilities was not recorded in the CD19-BsAb group (**Figure 11b**). The continuous proliferation of the surviving lymphoma cells (without MAF pre-treatment) might cover the viability reduction

resulting from T-cell killing. To visualize and measure the proliferation capability of untreated lymphoma cells under the T-cell surveillance, live-cell imaging was conducted using four representative *Bcl2-GFP; Control* lymphoma clones. The number of GFP^+ lymphoma cells was quantified and analyzed using the IncuCyte® software. Consistently with the viability measurement from flow cytometry, untreated lymphoma cells (GFP^+) outgrew in a considerably slower manner in the CD19-BsAb group compared to those in other groups (**Figure 11e, f**), implying a death-proliferation imbalance of lymphoma cells under the CD19-BsAb-enhanced T-cell surveillance. On the other hand, CD20-BsAb failed to further boost the T-cell cytotoxicity towards untreated lymphoma cells, and exhibited a comparable T-cell boosting efficacy as the isotype control BsAb (**Figure 11e, f**).

When being applied to the TIS lymphoma cells, both CD19-BsAb and CD20-BsAb significantly enhanced the lymphoma-targeting T-cell cytotoxicity (**Figure 11c, d**). Specifically, T cells achieved over 95% efficiency in killing TIS lymphoma cells with the addition of CD19-BsAb (relative viability less than 5%) at a dose as low as 0.005 nmol/mL, while achieving approximately 80% killing efficacy in the presence of CD20-BsAb (relative viability less than 20%) at a dose of 0.01 nmol/mL at 24 and 48 hours after co-culture. Thereafter, 0.01 nmol/mL was set as the standard therapeutic dose of BsAbs for the subsequent experiments. During the live-cell imaging, the cellnumber of TIS lymphoma cells (GFP^+) was rather steady in the T-cell co-culture systemwithout BsAbs or with isotype control BsAb (**Figure 11g, h**). The addition of CD19- BsAb and CD20-BsAb to the T-cell co-culture system drastically reduced the amount of GFP^+ TIS lymphoma cells (**Figure 11g, h**), the GFP signal of which can barely be detected after 72 hours. It suggested a tremendous enhancement of CD19-BsAb and CD20-BsAb in helping T cells (without pre-stimulation) kill the TIS lymphoma cells *ex vivo*.

Collectively, CD19-BsAb boosted T-cell cytotoxicity towards the proliferating lymphoma cells to some extent, while massively inducing the T-cell cytotoxicity towards the TIS lymphoma cells. However, CD20-BsAb preferentially enhanced the T-cell cytotoxicity towards the TIS but not the proliferating lymphoma cells.

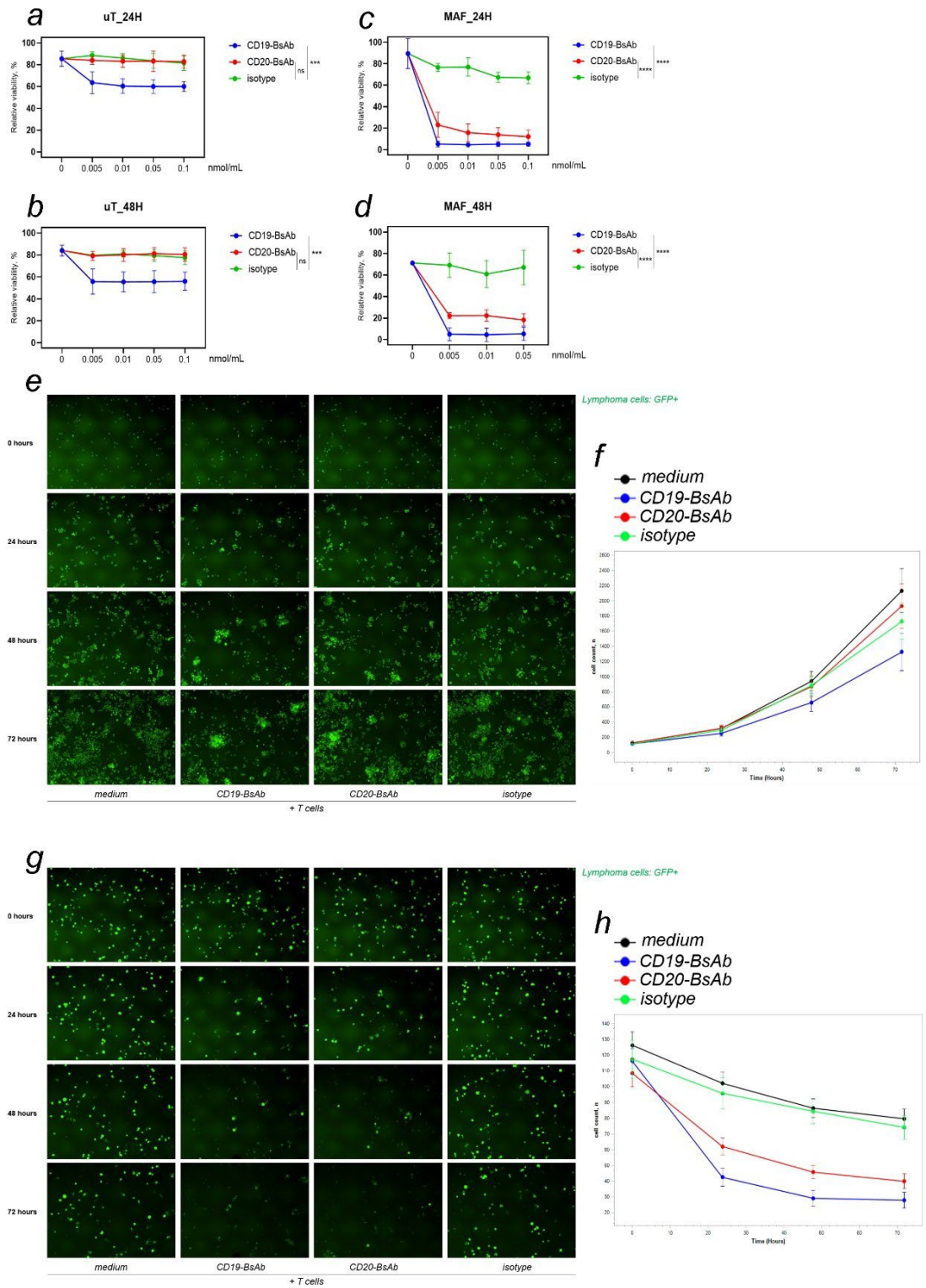

Figure 11. CD19-BsAb and CD20-BsAb boosted the killing potentiality of the unstimulated T cells towards TIS lymphoma cells.

The *Bcl2-GFP; Control* LCs received a 3-day MAF treatment and 2-day normal culture sequentially. The viable senescent LCs were positively sorted and co-cultured with the pooled unstimulated T cells from female wild-type lymphoma-naïve strain-matched C57BL/6N mice for 24 hours (a, untreated LCs; c, MAF-treated LCs) and 48 hours (b, untreated LCs; d, MAF-treated LCs) in the presence of CD19-BsAb, CD20-BsAb and isotype control BsAb at different

doses. The viability of LCs was determined by Ghost dye (violet) staining through flow cytometry measurement. Three distinct lymphoma cases were included in the *ex vivo* T-cell killing assays. Live-cell imaging of T cell and LC co-culture was conducted using four *Bcl2-GFP; Control* lymphoma clones for real-time analysis; images of one representative clone (e, untreated LCs; g, MAF-treated LCs) and summarized quantitative analysis of GFP^+ cells from 4 representative lymphoma clones in each setting (f, untreated LCs; h, MAF-treated LCs).The LCs were co-cultured with the pooled unstimulated T cells in (at) the T cell-LC ratio of 10:1 in a poly-D-lysine coated plate. Here the CD19-BsAb, CD20-BsAb and isotype control BsAb (isotype for short) were used at the dose of 0.01 nmol/mL. The images were consecutively captured every 30 minutes for 72 hours. LCs, lymphoma cells; *, $P < 0.05$; ***, $P < 0.001$; ****, $P < 0.0001$; ns, not significant.

Additionally, the *Bcl2-GFP; Suv39h1*$^{Y/-}$ lymphoma cells were used as the senescence-incapable controls in the *ex vivo* T-cell killing assay. As shown in **Figure 12 a** and **b**, the MAF-treated *Bcl2-GFP; Suv39h1*$^{Y/-}$ lymphoma cells exhibited comparable T-cell vulnerability to their untreated controls in the absence of BsAbs. However, T cells were still boosted to kill these MAF-treated non-TIS cells with the addition of CD19-BsAb, which functioned less efficiently compared to its efficacy in boosting the T-cell cytotoxicity against the MAF-treated TIS lymphoma cells. Meanwhile, the number of viable proliferating lymphoma cells that survived the CD19-BsAb-enhanced T-cell cytotoxicity was significantly reduced in the untreated *Bcl2-GFP; Control* lymphoma cells as well as the untreated *Bcl2-GFP; Suv39h1*$^{Y/-}$ lymphoma cells (**Figure12c**). This suggested a consistent efficacy of CD19-BsAb in boosting the T-cell surveillance of proliferating lymphoma cells regardless of the *Suv39h1* gene, although to a much higher extent if CD19-BsAb was added to the Suv39h1-proficient TIS lymphoma cells. Nonetheless, CD20-BsAb failed to significantly enhance the killing potential of T cells towards MAF-treated non-TIS cells (**Figure 12**). Overall, the results in this section implied that T cells without pre-stimulation were less efficient in killing the MAF-treated senescence-incapable lymphoma cells than the MAF-treated TIS lymphoma cells even in the presence of CD19-BsAb and CD20-BsAb.

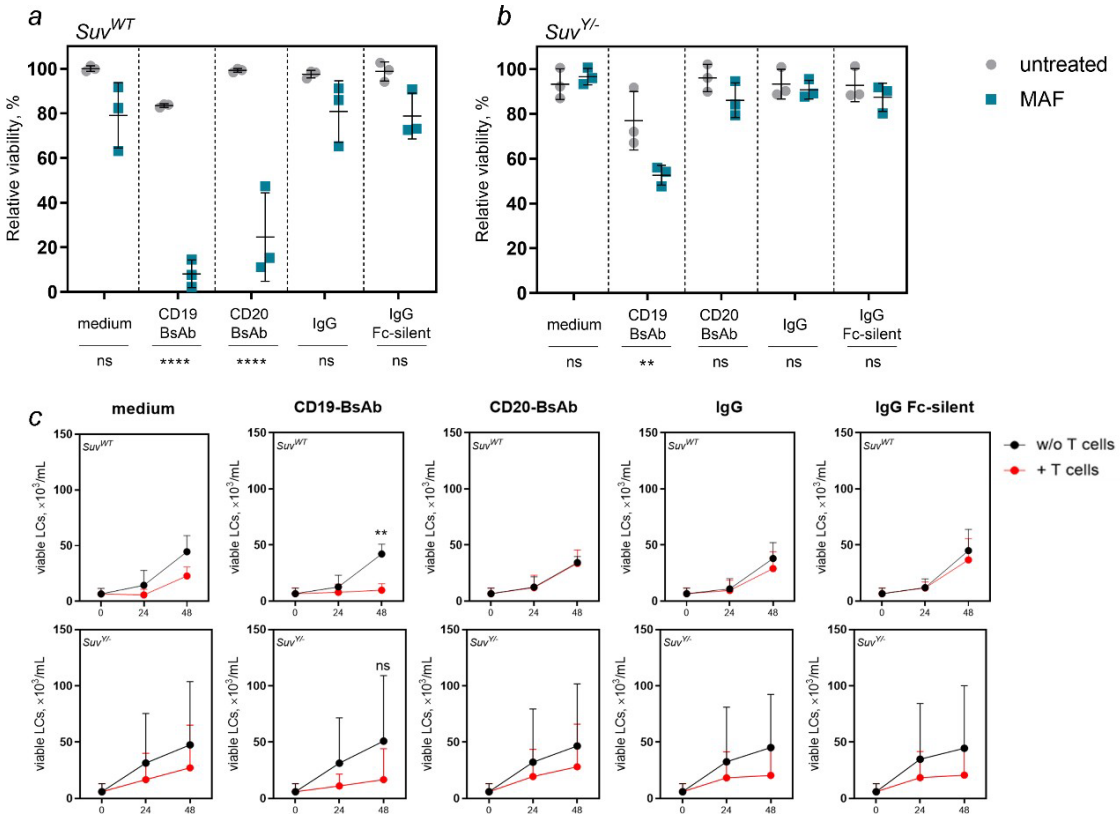

Figure 12. Senescence-incapable lymphoma cells were less vulnerable to the T-cell cytotoxicity in the presence of CD19-BsAb and CD20-BsAb.

The *Bcl2*-protected *Control* LCs (a) and *Suv39h1*$^{Y/-}$ LCs (b) received a 3-day MAF treatment and a sequential 2-day normal culture. Afterwards, the viable LCs were enriched by FACS and co-cultured with the pooled T cells from the male wild-type C57BL/6N mice (lymphoma-naïve strain-matched). The co-culture system (T cells: LCs = 10: 1) was added with the CD19-BsAb, CD20-BsAb, anti-CD20 IgG (IgG) and Fc-silent IgG control (IgG Fc-silent) antibodies (all at a dose of 0.01 nmol/mL), respectively. The viability test was conducted after 24 hours upon co-culture. An additional time point, 48 hours, was set for the untreated LCs. The viability of LCs was determined by Ghost dye (violet) staining through flow cytometry. The concentrations of viable LCs after co-culture were calculated with 1 $\times 10^5$ cells/mL as the initial cell concentration for the untreated LCs in each setting (c). The X axis marks three time points: 0, 24, and 48 hours upon co-culture. In the *ex vivo* T-cell killing assays, three distinct *Bcl2-GFP; Control* lymphoma cases and three distinct *Bcl2-GFP; Suv39h1*$^{Y/-}$ lymphoma cases were included. **, $P < 0.01$; ****, $P < 0.0001$; ns, not significant.

4.3.2. CD19-BsAb and CD20-BsAb promoted T cells to interact with lymphoma cells as well as enhancing T-cell activation and proliferation.

To examine the effectiveness of lymphoma cells interacting with T cells, CellTrace^{TM} dye pre-labeled T cells (Red$^+$) and *Bcl2-GFP; Control* lymphoma cells (GFP$^+$) were co-cultured as was done in the *ex vivo* T-cell killing assay. After a 4-hour incubation, the

TIS lymphoma cell and T-cell co-culture systems showed higher percentages of coupled cells (Red^+GFP^+/GFP^+%) than the untreated lymphoma cell and T-cell co-culture systems (**Figure 13a, b**). In particular, CD19-BsAb exhibited the strongest efficiency in boosting T cells to interact not only with TIS lymphoma cells, but also with untreated lymphoma cells. Nevertheless, CD20-BsAb exclusively enhanced T cells to interact with TIS but not untreated lymphoma cells. Furthermore, the MFI of CellTrace^{TM} dye on the coupled cells was found to be stronger in the TIS lymphoma cell and T-cell co-culture systems compared to the untreated lymphoma cell and T-cell co-culture systems, indicating that more T cells were coupling with TIS lymphoma cells in the presence of CD19-BsAb and CD20-BsAb (**Figure 13a, b**). Surprisingly, a comparable MFI of CellTrace^{TM} dye on the coupled cells was observed in all the untreated lymphoma cell and T-cell co-culture systems, including those with the addition of CD19-BsAb. This suggested that CD19-BsAb increased the chance of T cells interacting with more untreated lymphoma cells, while failing to increase the amount of T cells adhering to these untreated lymphoma cells. Similar results were also obtained from the live-cell imaging. As shown in **Figure 13c**, single lymphoma cells (GFP^+) were surrounded closely by T cells (Red^+). On average, more T cells adhered to the TIS lymphoma cells compared to the untreated lymphoma cells, and especially in the presence of CD19-BsAb and CD20-BsAb. The visualization of lymphoma cell and T cell co-culture in a live-cell imager further validated the flow cytometry analysis of their interaction patterns. Collectively, TIS lymphoma cells interacted with more T cells in a higher frequency compared to the proliferating lymphoma cells.

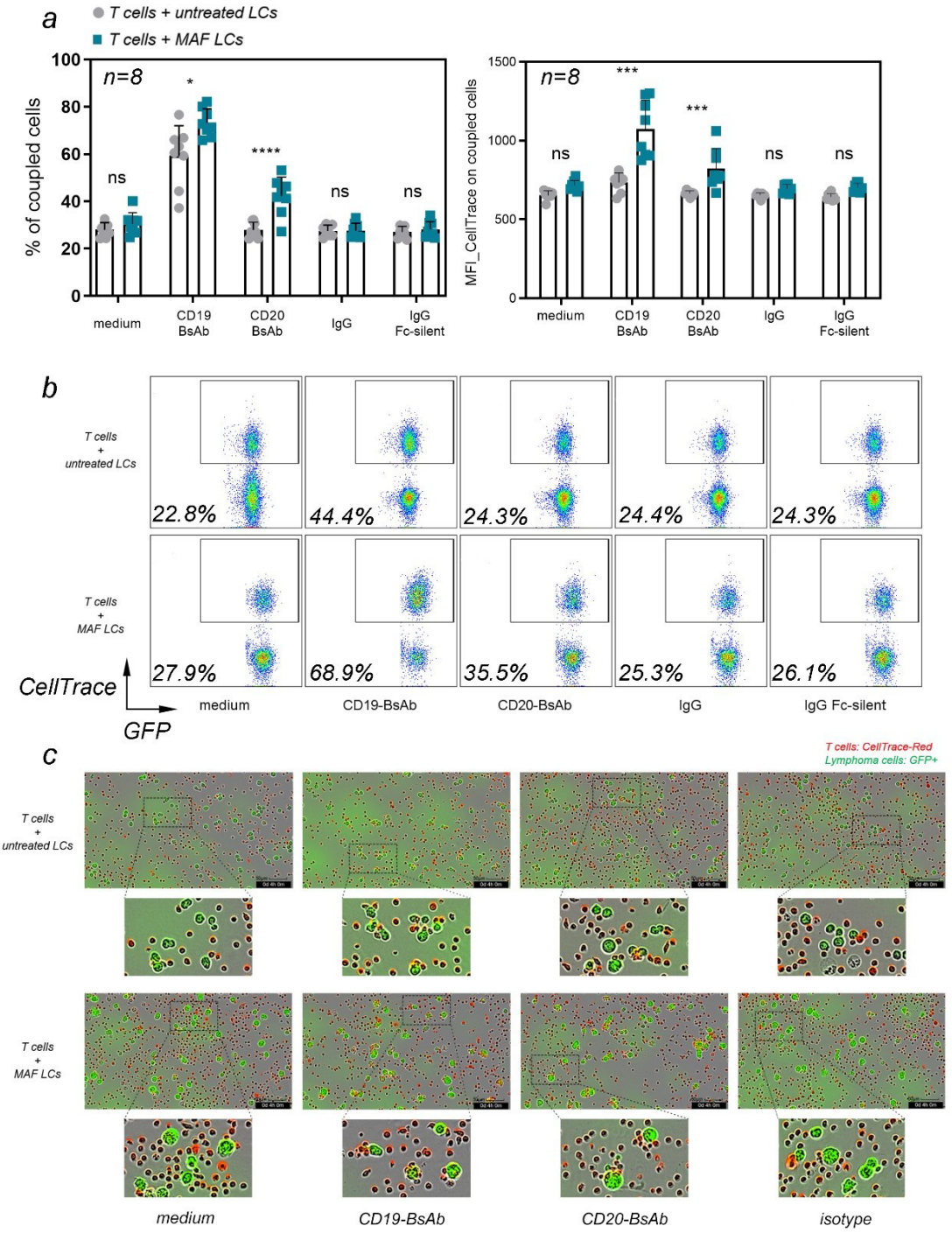

Figure 13. CD19-BsAb and CD20-BsAb enhanced lymphoma cells interacting with the unstimulated T cells.

The pooled T cells were stained with CellTrace^{TM} dye (red) and co-cultured with *Bcl2-GFP; Control* LCs at a T cell-LC ratio of 10:1 for 4 hours in the absence or presence of CD19-BsAb, CD20-BsAb, anti-CD20 IgG (IgG) and its Fc-silent IgG control (IgG Fc-silent) antibodies (all at the dose of 0.01 nmol/mL), followed by the flow cytometry measurement for quantifying the coupled cells among the overall GFP$^+$ cell population (a, left). The MFI of CellTrace^{TM} dye in the coupled cells was analyzed (a, right). (b) Representative dot-plots of the coupled cell population (CellTrace$^+$ GFP$^+$) among the overall GFP$^+$ cells (upper panel for untreated LCs, lower panel for MAF-treated LCs). Eight distinct lymphoma cases were included in the T cell-

LC interaction assay. (c) Live-cell imaging of T cell-LC co-culture using one representative *Bcl2-GFP; Control* lymphoma clone. The LCs were co-cultured with the pooled unstimulated T cells in a T cell-LC ratio of 10:1 in a poly-D-lysine coated plate. Here, the CD19-BsAb, CD20-BsAb, and isotype control BsAb were used at the dose of 0.01 nmol/mL. The images were captured after the 4-hour co-culture (upper panel for untreatedLCs, lower panel for MAF-treated LCs). MFI, median fluorescence intensity; *, $P < 0.05$;
***, $P < 0.001$; ****, $P < 0.0001$; ns, not significant.

Following the interaction with target cells, T cells can be activated specifically via matched TCR-pMHC (peptide-MHC complex) recognition or nonspecifically by activating the CD3/CD28 pathway. Therefore, the activation of T cells in the presence of CD19-BsAb and CD20-BsAb was also studied. After 24 hours of incubation, T cells co-cultured with TIS lymphoma cells showed an increased proportion of $CD69^+$ cells in the overall $CD3^+$ T-cell population (**Figure 14**). CD19-BsAb, in particular, exhibited the strongest efficacy in boosting T-cell activation in the co-culture systems with either the untreated or TIS lymphoma cells, with no significant difference between these two co-culture systems. Nonetheless, CD20-BsAb induced a significantly stronger T-cell activation when T cells were co-cultured with the TIS lymphoma cells rather than with the untreated lymphoma cells. Additionally, anti-CD19/CD20 × CD3 BsAbs alone were unable to activate T cells in the absence of lymphoma cells. The varied effects of CD19-BsAb and CD20-BsAb on T-cell activation were in line with their differences in stimulating T cells to interact with lymphoma cells.

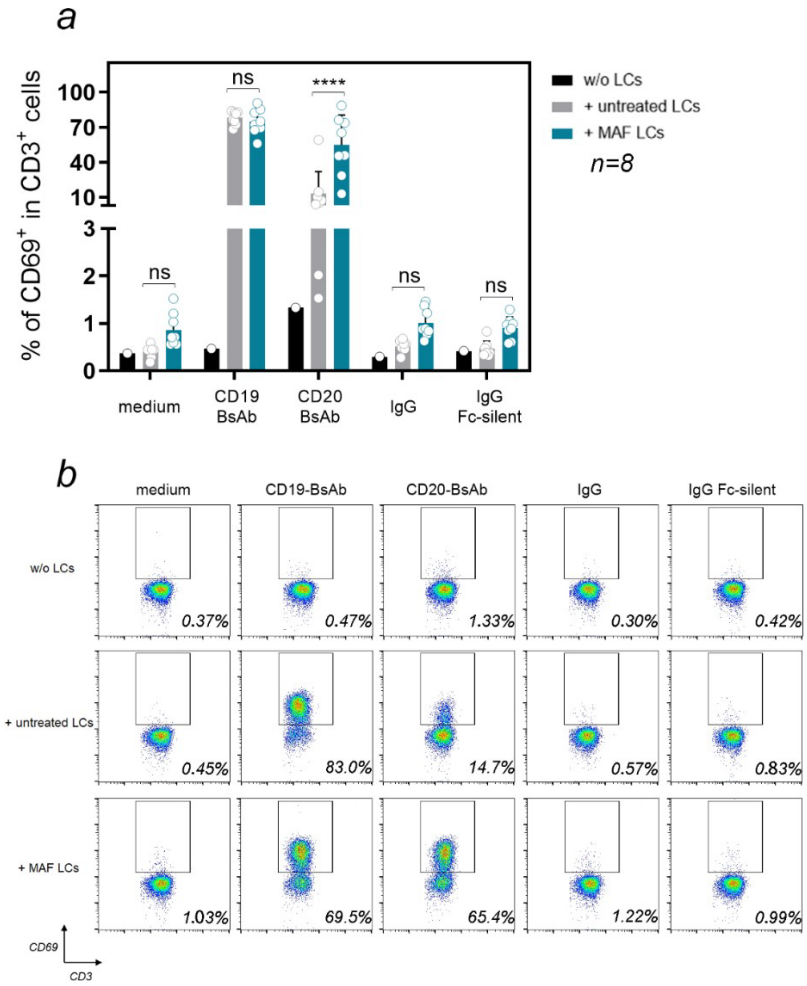

Figure 14. CD19-BsAb and CD20-BsAb facilitated the unstimulated T cells to activate upon encountering lymphoma cells.

(a) The pooled T cells were co-cultured with *Bcl2-GFP; Control* LCs in a T cell-LC ratio of 10:1 in the presence of CD19-BsAb, CD20-BsAb, anti-CD20 IgG (IgG) and its Fc-silent IgG control (IgG Fc-silent) antibodies (all at the dose of 0.01 nmol/mL) for 24 hours, followed by Ghost dye (violet) staining and anti-CD3-PE + anti-CD69-APC antibody staining. The flow cytometry measurement was conducted to quantify the proportion of $CD69^+$ cells among the viable $CD3^+$ T-cell population. (b) Representative dot-plots of the anti-CD3 + anti-CD69 antibody staining in the 24-hour co-culture system. The population was gated on the viable GFP^-CD3^+ cells (T cells). ****, $P < 0.0001$; ns, not significant.

Additionally, the proliferation potentiality of co-cultured T cells was investigated in the presence of CD19-BsAb and CD20-BsAb, as reflected by progressive reduction in the fluorescence intensity of CellTrace™ dye on T cells upon cell division. After three days of incubation, significant reduction of fluorescence intensity of CellTrace™ dye was observed on the T cells co-cultured with TIS lymphoma cells in the presence of either CD19-BsAb or CD20-BsAb, as well as the T cells co-cultured with the untreated

lymphoma cells exclusively in the CD20-BsAb setting (**Figure 15**).

Overall, CD19-BsAb and CD20-BsAb effectively boosted T cells to interact with TIS lymphoma cells, leading to T cell activation and proliferation. In addition to targeting TIS cells, CD19-BsAb fostered T cells to interact with the untreated lymphoma cells ("proliferating cells"), which also resulted in the subsequent T-cell activation and proliferation.

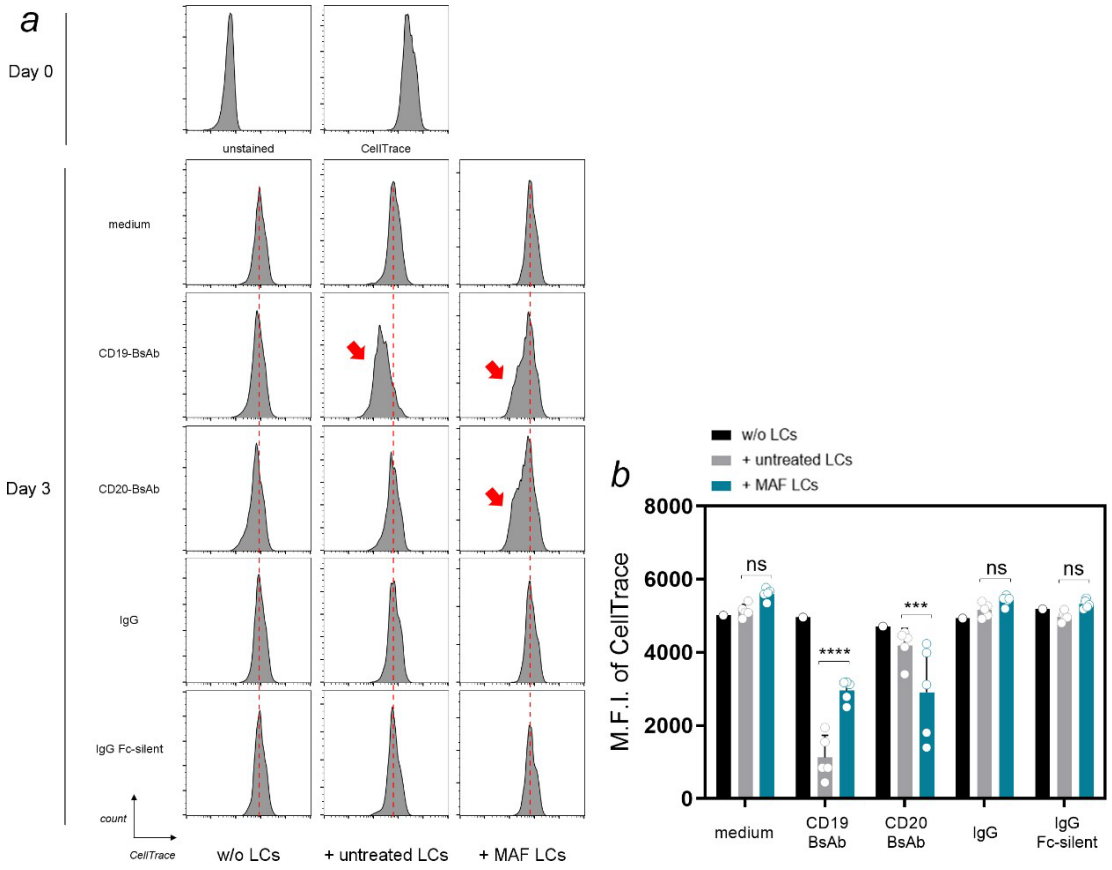

Figure 15. CD19-BsAb and CD20-BsAb promoted the unstimulated T cells to proliferate upon encountering lymphoma cells.

The pooled T cells were stained with CellTrace™ dye (far red) and co-cultured with *Bcl2-GFP; Control* LCs in a T cell-LC ratio of 10:1 in the presence of CD19-BsAb, CD20-BsAb, anti-CD20 IgG (IgG) and its Fc-silent IgG control (IgG Fc-silent) antibodies (all at the dose of 0.01 nmol/mL) for 3 days, followed by Ghost dye (violet) and anti-CD3-PE antibody staining. The flow cytometry measurement was conducted to detect the signal reduction of the CellTrace™ dye on the viable $CD3^+$ T cells. (a) The dashed lines mark the peaks and red arrows mark the diluting fluorescence intensity of the CellTrace™ dye on the T cells that were co-cultured with LCs in the absence of BsAbs. (b) MFI of CellTrace™ dye on the viable $CD3^+$ T cells. Five distinct *Bcl2-GFP; Control* lymphomas were used in the T-cell proliferation assay. MFI, median fluorescence intensity; ***, $P < 0.001$; ****, $P < 0.0001$; ns, not significant.

4.4. PD-L1 potentially interfered with the T-cell surveillance of TIS lymphoma cells.

4.4.1. PD-L1^{high} lymphoma cells were less vulnerable to the T-cell killing *ex vivo*.

Given the therapy-induced PD-L1 expression on the TIS cells, and to understand the potential impact of PD-L1 on the *ex vivo* T-cell killing of *E*μ-*myc; Bcl2*-protected lymphoma cells, we divided the lymphoma cases into the PD-L1^{high} and PD-L1^{low} groups according to their PD-L1 up-regulation levels after TIS induction. TIS lymphoma cells in the PD-L1^{low} group tended to be more vulnerable to the T-cell killing compared to their untreated controls (**Figure 16a**), with a significant difference in their relative viabilities. Moreover, the relative viabilities of the PD-L1^{high} TIS lymphoma cells tended to be higher than the PD-L1^{low} TIS lymphoma cells in the *ex vivo* T-cell killing assay. Further analysis of the surviving lymphoma cells after their co-culture with T cells revealed that therapy-induced PD-L1 expression was enhanced under the T-cell surveillance (**Figure 16b**), implying that PD-L1 up-regulation may act as a protective shield for TIS lymphoma cells when encountering T cells. Moreover, PD-1^{+} T cells were found at a higher frequency when co-cultured with the TIS lymphoma cells compared to those co-cultured with the untreated lymphoma cells (**Figure 16c**).

4.4.2. PD-L1 was a possible protector for TIS lymphoma cells in the CD20-BsAb-enhanced T-cell surveillance.

Interestingly, when investigating the lymphoma cells that survived T-cell killing in the presence of CD20-BsAb, we found that PD-L1 expression remained at its basal level in the untreated lymphoma cells with or without T cells in the co-culture. However, TIS lymphoma cells, particularly those from the PD-L1^{high} group, had significantly stronger PD-L1 expression on the surviving cells (**Figure 16d**). Furthermore, T cells treated with CD20-BsAb in the co-culture system had a higher frequency of PD-1^{+} T cells and a stronger PD-1 level on their cell surfaces, with no significant difference in the T cells co-cultured with either the TIS lymphoma cells or the untreated lymphoma cells (**Figure**

16e). This gave us a hint that therapy-induced PD-L1 expression potentially serves as a safeguard for TIS lymphoma cells under the CD20-BsAb-enhanced T-cell surveillance.

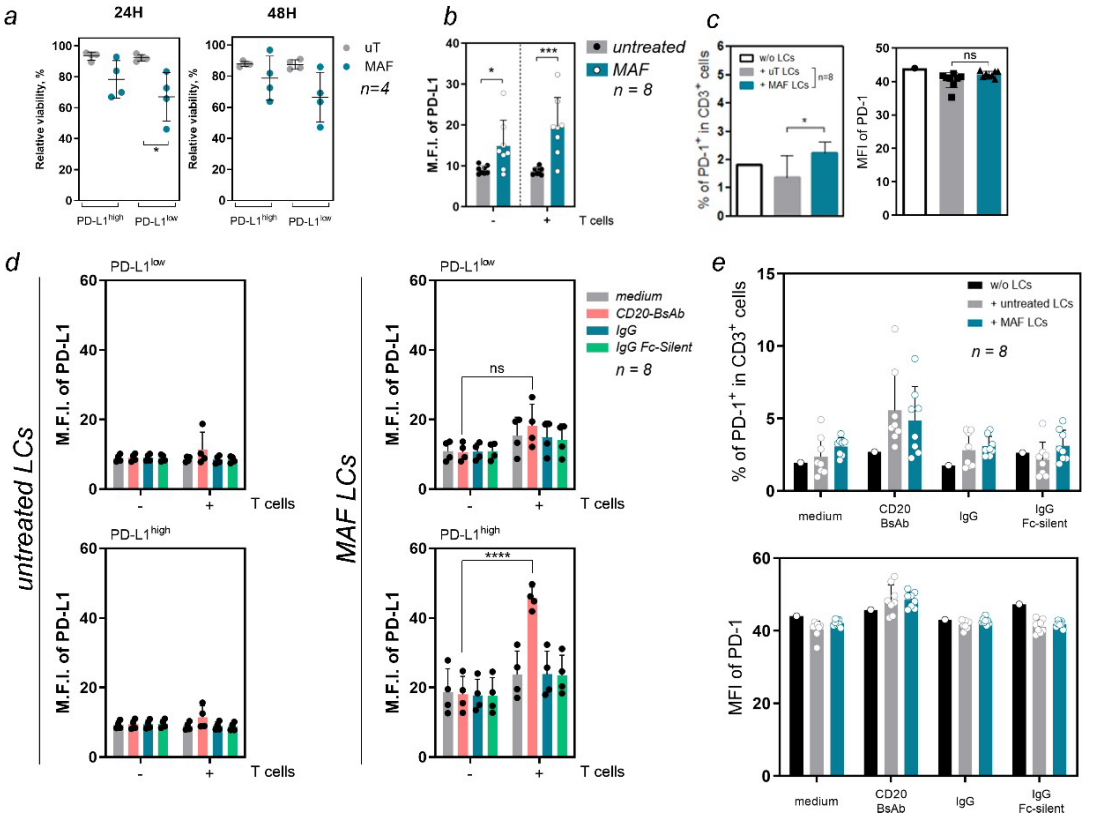

Figure 16. PD-L1^{high} TIS lymphoma cells exhibited resistance to the T-cell killing *ex vivo*. The *Bcl2*-protected *Control* LCs were divided into the PD-L1^{high} and PD-L1^{low} groups basedon their therapy-induced PD-L1 expression after MAF treatment (4 distinct lymphoma cases in each group). (a) Survival tendency of the PD-L1^{high} and PD-L1^{low} *Bcl2*-protected *Control* LCs in the *ex vivo* T-cell killing assay. LCs were co-cultured with the pooled T cells in a T cell-LC ratio of 10: 1 for 24 (left) and 48 hours (right). The viability of LCs was determined by Ghost dye (violet) staining through flow cytometry. (b) & (d) PD-L1 expression on the surviving LCs in the *ex vivo* T-cell killing assay. After being co-cultured with the pooled unstimulated T cells for 48 hours without BsAb (b) or with CD20-BsAb (d), LCs were stained with Ghost dye (violet) + anti-PD-L1-APC antibody, and proceeded for the flow cytometry measurement. The MFI of PD-L1 antibody staining was analyzed among the viable LCs. (c) & (e) PD-1 expression on the viable CD3$^+$ T cells in the *ex vivo* T-cell killing assay. After being co-cultured with the LCs for 72 hours in the absence (c) or presence (e) of CD20-BsAb, cells were stained with Ghost dye (violet) + anti-CD3-PE + anti-PD-1-APC antibodies, and proceeded for the flow cytometry measurement. The MFI of PD-1 antibody staining was analyzed among the viable CD3$^+$ T cells. MFI, median fluorescence intensity; *, $P < 0.05$; ***,$P < 0.001$.

5. Discussion

Molecular heterogeneity and variable treatment sensitivity account for a large proportion of patients failing the curative Rituximab-CHOP immune-chemotherapy standard of care. Despite novel next-line options, most patients with refractory/relapsed diffused large B-cell lymphoma (R/R DLBCL) experience dismal outcome [143]. Investigating the immunoediting strategies that lymphoma cells exploit to survive immune-chemotherapy is of great importance for better distinguishing the subgroup of patients who could potentially benefit from novel immunotherapies [144]. Moreover, therapy-induced state switches such as cellular senescence appear to impact on the long-term outcomes of DLBCL patients but remain understudied. The epigenetic signature of therapy-induced senescence (TIS) can be a predictor for the treatment outcome of DLBCL patients [6, 23]. TIS can be marked a double-edged sword, as it is beneficial as a stable arrest program but detrimental due to a senescence-associated pro-inflammatory secretome and stem-like reprogramming [145]. In particular, the T-cell surveillance of and T-cell utilization against senescent B-cell lymphoma deserve further investigation. Therefore, this study aimed to explore how T-cell activity can be harnessed to eliminate TIS lymphoma cells, with a specific view on the immunostimulatory capacity of anti-CD19/CD20 × CD3 bispecific antibodies (CD19-BsAb and CD20-BsAb, respectively) that currently enter lymphoma treatment in the clinic in this process.

First of all, we investigated the intrinsically altered gene expression patterns in TIS based on our previously published gene profile of the senescence-capable (*Control*) and senescence-incapable (*Suv39h1*^{ER}) *E*μ-*myc; Bcl2*-protected lymphoma cells underthe Adriamycin chemotherapy scenario. The TIS lymphoma cells displayed enriched immune response-related gene sets, including *Immune Response*, *T Cell Activity* and *Peptide/MHC-I/MHC-II antigen processing*. This insight was compatible with the findings of up-regulated MHC-I/MHC-II molecules upon oncogene-induced senescence (OIS) [32, 33], which indicated that senescence was actively involved in regulating immune response, specifically in terms of senescence immunosurveillance.

Interestingly, the gene set "*Negative Regulation of Adaptive Immune Response*" was considerably abundant in the TIS cells, which is also consistent with our previous findings using an OIS model. We found that OIS exhibited several enriched genetic signatures involved in the negative regulation of immune response and T-cell activation [23]. Further analysis of the differentially expressed genes in the TIS cells revealed that a considerable proportion of these significantly changed genes were involved in the biological processes of *Immune Response* and *Immune System Process*. Moreover, a narrow-down tracing of these two genetic signatures uncovered a group of overlapping genes, including one of the immune checkpoint protein-encoding genes, *CD274* (*PD-L1*). In 2021, we reported that the enhanced PD-L1/PD-L2 expression on the cell surfaces of senescence-prone *MyD88-/CARD11*-mutant lymphomas could execute as an immune-evading strategy for the malignant B cells [23]. To date, the "good" (immunostimulation) and "bad" (immune evasion) sides of senescent tumor cells in the disease control of B-cell lymphomas require further investigation.

To examine the immunoediting features of TIS cells, we transduced the primary *Eμ-myc* lymphoma cells with *Bcl2*-overexpressing plasmids and established an *in vitro* TIS model which triggers senescence in lymphoma cells while reducing their apoptotic activities upon mafosfamide (MAF) chemotherapy, as described in our previous study [26]. A striking senescence induction was confirmed in the MAF-treated *Bcl2; Control* lymphoma cells (hereafter, TIS lymphoma cells for short) from the SA-β- gal staining. The TIS lymphoma cells exhibited a significant up-regulation of MHC-I molecules and co-stimulatory factors (CD80, CD86) on the cell surfaces. Moreover, the up-regulation of surface MHC-II molecules was noted in 4 of 6 lymphoma cases, although the extent and direction varied profoundly among the samples. The results here are in line with previous studies: apart from the findings of up-regulated MHC-I/II in OIS [32, 33], Busse et al. discovered an enhanced expression of HLA-DR (a human MHC-II molecule), CD80 and CD86 on the monocytes from aging individuals [146]. Consistently with the differential gene expression analysis, the immune checkpoint protein PD-L1 was up-regulated significantly in the TIS lymphoma cells. Likewise, we also noted a therapy-induced PD-L1 up-regulation in a human colorectal cancer cell line (SW480) after 5-FU

treatment, suggesting that TIS-induced PD-L1 might be a general phenotype in tumor cells, which required further study on more cancer cell types. These results suggested that TIS lymphoma cells gained enhanced immunogenicity compared to their proliferating controls, which increased the possibility for TIS lymphoma cells to be identified by, and interact with, immune cells. As a selective countermeasure, the senescence-triggered immune response might be limited by the senescence-induced PD-L1 expression. Whether or not these immunoediting characteristics of TIS cells are senescence-specific requires further investigation on the MAF-treated *Suv39h1*$^{Y/-}$*; Bcl2*-protected lymphoma cells. So far, the immunoenhancing features (MHC-I, MHC-II, CD80 and CD86) and immunotolerant molecule (CD274) were up-regulated in the TIS lymphoma cells, which encouraged us to continue studying their survival under T-cell surveillance.

To mimic the endogenous interaction of T cells and lymphoma cells *ex vivo*, we isolated syngeneic T cells and co-cultured them with un-pretreated or MAF-pretreated (TIS) *Suv39h1*-proficient *Bcl2*-protected lymphoma cells *ex vivo*. The results showed that TIS lymphoma cells were more vulnerable to the co-cultured T cells compared to their proliferating controls, while the senescence-incapable lymphoma cells exhibited comparable T-cell vulnerabilities between the MAF-treated and untreated lymphoma cells. This implied that senescence might render lymphoma cells more vulnerable to the unstimulated T cells, which mimics the primary T-cell response, or influence the recognition and activation of T cells during the immunosurveillance of cancer cells. To investigate the difference in T-cell response towards proliferating and senescent lymphoma cells, we first examined the physical interaction efficiency of T cells to lymphoma cells. The results indicated a higher frequency of TIS lymphoma cells interacting with the co-cultured T cells, and more T cells engaging with TIS lymphoma cells on average compared to the proliferating lymphoma cells. Furthermore, with the antigen-processing function of the malignant B cells, T cells might be activated after recognizing and interacting with the lymphoma cells. Therefore, we analyzed two T-cell activation markers (CD69 and CD25) on T cells in the co-culture system. $CD69^+$ T cells and $CD25^+$ T cells were more abundant in the co-culture system with TIS

lymphoma cells compared to the proliferating lymphoma cells. Normally, T-cell activation requires signal 1 (upon TCR-pMHC complex interaction) and signal 2 (upon the interaction of co-stimulatory factors and their corresponding receptors, e.g., CD28-CD80/CD86), after which the fully activated T cells enter a highly proliferative state and differentiate into effector T cells and memory T cells [147]. We used a live-cell dye (CellTrace™) to trace the proliferation of T cells in the *ex vivo* co-culture. Unfortunately, a generally limited T-cell proliferation was observed in the co-culture system with either the TIS or proliferating lymphoma cells. Here, we studied the "primary" T-cell surveillance of lymphoma cells *ex vivo* using the unstimulated T cells, the majority of which were naïve T cells that had never encountered lymphoma cells before. Stronger co-stimulatory signals are required to activate naïve T cells compared to antigen-specific memory T cells [147]. Therefore, only moderate cytotoxic effects were observed in these unstimulated T cells when targeting TIS lymphoma cells. Consistently with this finding, the co-cultured T cells showed modest levels of activation, proliferation and cytotoxicity against TIS lymphoma cells. The general underresponsiveness of lymphoma cells to T-cell surveillance requires alternative immunotherapies that can boost the T-cell cytotoxicity towards malignant B cells. For example, CAR T-cell therapy can be generated to target CD19 or CD20 on the lymphoma cell surfaces without requiring the specificity match between the TCRs on the CAR-T cells and the peptide-MHC-I complexes on the lymphoma cells, thereby bypassing the MHC-restricted antigen recognition [85]. The virus-based or virus-free transduction of T cells to express CD19-or CD20-CARs requires weeks or days of manufacture, which is a time-consuming and costly therapy. Another possible approach to activate T cells and boost their cytotoxicity is using T-cell redirecting BsAbs to simultaneously target CD3 on T cells and CD19/CD20 on lymphoma cells, thereby bridging T cells with the malignant B cells to initiate the T-cell cytotoxicity against their engaging tumor cells. This approach with off-the-shelf BsAbs was therefore investigated in this project regarding their T-cell boosting efficacy towards lymphoma cells. The B-cell-targeting T-cell redirecting BsAbs showed certain promising efficacies in R/R DLBCL patients [95, 97, 98] as well as in elderly DLBCL patients without any

pre- treatment [99], which suggests a potential for T-cell-redirecting BsAbs in disease control when in combination with conventional chemotherapy. In the current study, the *ex vivo* T-cell killing assays with CD19-BsAb and CD20-BsAb showed that CD19-BsAb enabled T cells to achieve approximately 40% to 50% effectiveness in killing proliferating lymphoma cells. Conversely, CD20-BsAb failed in boosting T cells to kill more proliferating lymphoma cells. However, both CD19-BsAb and CD20-BsAb significantly enhanced the cytotoxicity of T cells against TIS lymphoma cells. More specifically, when compared to CD20-BsAb, CD19-BsAb exhibited a higher efficacy in boosting T cells (without pre-stimulation) to kill TIS lymphoma cells *ex* vivo. However, the immunostimulatory effects of CD19-BsAb and CD20-BsAb were notably less pronounced in the T cells targeting the MAF-treated senescence-incapable lymphomas, implying that senescence might act as a BsAb-sensitizer for treating B-cell lymphomas. Further analysis of T cell and lymphoma cell interaction revealed that CD19-BsAb dramatically encouraged T cells to interact with either proliferating or TIS lymphoma cells. Conversely, a higher proportion of TIS lymphoma cells tended to interact with T cells compared to their proliferating controls, especially in the presence of CD20-BsAb, which exclusively encouraged T cells to interact with TIS lymphoma cells but not proliferating lymphoma cells. In parallel, CD19-BsAb exhibited comparably strong effects on boosting T-cell activation in the co-culture systems with either proliferating or TIS lymphoma cells. However, CD20-BsAb only induced a noteworthy activation of T cells when they were co-cultured with TIS lymphoma cells but not with their proliferating controls. A similar pattern was also noted in the T-cell proliferation tests. A robust proliferation of T cells was found in those co-cultured with TIS lymphoma cells in the presence of either CD19-BsAb or CD20-BsAb, and in those co-cultured with proliferating lymphoma cells only with the addition of CD19-BsAb. Overall, CD19-BsAb and CD20-BsAb can effectively boost T cells to interact with TIS lymphoma cells, leading to T-cell activation, proliferation and functional cytotoxicity performance. In addition to targeting TIS lymphoma cells, CD19-BsAb can also foster T cells to interact with the proliferating lymphoma cells, resulting in subsequent T-cell activation, proliferation and cytotoxicity execution. So far,

we have learned that CD19-BsAb can promote the unstimulated syngeneic T cells to perform immunosurveillance of the proliferating lymphoma cells to some extent, while both CD19-BsAb and CD20-BsAb can dramatically boost these T cells to eliminate TIS lymphoma cells *ex vivo*.

The immune checkpoint protein PD-L1 is a critical regulator in limiting T-cell activation and in leading to T-cell exhaustion by binding to its receptor PD-1 on the activated T cells. Due to the up-regulated PD-L1 on the cell surfaces of TIS lymphomas, we examined the impacts of PD-L1 on the T-cell surveillance of B-cell lymphomas *ex vivo*. The subgroup of PD-L1^{high} TIS lymphoma cells were less vulnerable to T-cell cytotoxicity compared to the PD-L1^{low} TIS lymphoma cells in a short-term exposure to primary T-cell surveillance. However, the difference of these two groups of lymphoma cells in surviving under T-cell pressure was not striking, which might be a result of the various up-regulation levels of PD-L1 on lymphomas and the huge intrinsic heterogenicity of lymphomas. Moreover, the surviving TIS lymphoma cells expressed more PD-L1 under the cytotoxic pressure from T cells in the absence or presence of CD20-BsAb, suggesting that PD-L1 could be a protector for TIS lymphoma cells in the CD20-BsAb-enhanced T-cell surveillance. These results suggested that the PD-L1/PD-1 axis might play a role in restricting the cytotoxicity of T cells towards TIS lymphoma cells *ex vivo*, even in the presence of CD20-BsAb, which implied a therapeutic application of the PD-L1/PD-1 immune checkpoint blockade to enhance T-cell killing against TIS lymphoma cells in combination with CD20-BsAb. For example, one clinical report on a patient with refractory B-cell-precursor acute lymphoblastic leukemia (ALL) revealed that the PD-L1 expression on malignant cells could contribute to blinatumomab resistance [148]. Another study on pediatric acute ALL revealed that blinatumomab-resistant ALL lesions exhibited a stronger PD-L1 expression, and a promising efficacy of blinatumomab combined with pembrolizumab (an anti-PD-1 blocking antibody) was shown in a young patient with refractory ALL [149]. Similarly, a phase I clinical trial of blinatumomab combined with immune checkpoint blockades (PD-1 blocking antibody Nivolumab + CTLA-4 blocking antibody Ipilimumab) showed that this treatment modality achieved an 80% CR rate in the adult R/R ALL patients, with

tolerable side effects [150]. Furthermore, other immune checkpoint proteins were found to be increased in T cells (PD-1, Tim3 and TIGIT) and the paired tumor cells (PD-L1/L2, CD155 and Galectin-9) from the R/R B-cell- precursor ALL patients who were refractory to blinatumomab [151]. These findings suggested that blockade of the PD-L1/PD-1 axis might further de-repress the T-cell surveillance of TIS lymphoma cells with enhanced PD-L1 expression after chemotherapy. Therefore, the CD20-BsAb-enhanced T-cell surveillance of senescent lymphoma cells shed a light on preventing the disease relapse of DLBCLs, which requires caution to be taken regarding the immune checkpoint proteins in the treatment processes.

Certain limitations also exist in this study. For example, the TIS lymphoma model was established by treating *Bcl2*-overexpressing *Eμ-myc* lymphoma cells with mafosfamide, which causes DNA damage, cell division suspension and mitotic catastrophe, leading to apoptotic, necrotic and autophagic cell death [152, 153]. Other genotoxic agent- or irradiation-induced senescence models, or less genotoxic pro-senescent agents such as the CDK4/6-inhibitor (Palbociclib), were not investigated, which limits our findings to be generalized as a pan-senescence scenario. Therefore, the coherence of T-cell surveillance of senescent cancer cells requires studies considering the cancer cell types, senescence-inducing strategies, and BsAb formats, among others. Secondly, we focused on the "primary" T-cell surveillance of senescent cells *ex vivo* that mimics the endogenous recognition and interaction of syngeneic T cells to lymphoma cells. However, an *in vivo* setting is necessary to elucidate the senescence surveillance under a complex immune network. Accordingly, both immunocompetent mice with T-cell depletion and immunocompromised mice can be used to study the immunosurveillance of healthy syngeneic T cells towards senescent lymphoma cells *in vivo*. Furthermore, otherimmune checkpoint proteins need to be explored in the TIS lymphoma model to generate an overview of the immune landscape of senescent lymphomas. Lastly, the genetic and epigenetic mechanisms of PD-L1 up-regulation in TIS lymphoma cells need to be further addressed in a follow-up study.

In conclusion, the current study depicts the immune response-related signature of TIS lymphoma cells, which exhibit an immunostimulatory and immunoinhibitory landscape

of TIS lymphomas, leading to primary T-cell surveillance *ex vivo*. The T-cell-redirecting CD19-BsAb and CD20-BsAb boosted T cells to kill the TIS lymphoma cells,which was co-restricted by their up-regulated PD-L1 as a countermeasure.

6. References

[1] Sapkota S, Shaikh H. Non-Hodgkin Lymphoma [M]. StatPearls. Treasure Island (FL). 2022.
[2] Padala S A, Kallam A. Diffuse Large B Cell Lymphoma [M]. StatPearls. Treasure Island (FL). 2022.
[3] Tilly H, Gomes da Silva M, Vitolo U, Jack A, Meignan M, Lopez-Guillermo A, Walewski J, Andre M, Johnson P W, Pfreundschuh M, Ladetto M, Committee E G. Diffuse large B-cell lymphoma (DLBCL): ESMO Clinical Practice Guidelines for diagnosis, treatment and follow-up [J]. Annals of oncology : official journal of the European Society for Medical Oncology, 2015, 26 Suppl 5(v116-125.
[4] Sehn L H, Herrera A F, Flowers C R, Kamdar M K, McMillan A, Hertzberg M, Assouline S, Kim T M, Kim W S, Ozcan M, Hirata J, Penuel E, Paulson J N, Cheng J, Ku G, Matasar M J. Polatuzumab Vedotin in Relapsed or Refractory Diffuse Large B-Cell Lymphoma [J]. Journal of clinical oncology : official journal of the American Society of Clinical Oncology, 2020, 38(2): 155-165.
[5] Liu E, Marin D, Banerjee P, Macapinlac H A, Thompson P, Basar R, Nassif Kerbauy L, Overman B, Thall P, Kaplan M, Nandivada V, Kaur I, Nunez Cortes A, Cao K, Daher M, Hosing C, Cohen E N, Kebriaei P, Mehta R, Neelapu S, Nieto Y, Wang M, Wierda W, Keating M, Champlin R, Shpall E J, Rezvani K. Use of CAR-Transduced Natural Killer Cells in CD19-Positive Lymphoid Tumors [J]. The New England journal of medicine, 2020, 382(6): 545-553.
[6] Schleich K, Kase J, Dorr J R, Trescher S, Bhattacharya A, Yu Y, Wailes E M, Fan D N Y, Lohneis P, Milanovic M, Lau A, Lenze D, Hummel M, Chapuy B, Leser U, Reimann M, Lee S, Schmitt C A. H3K9me3-mediated epigenetic regulation of senescence in mice predicts outcome of lymphoma patients [J]. Nature communications, 2020, 11(1): 3651.
[7] Braig M, Lee S, Loddenkemper C, Rudolph C, Peters A H, Schlegelberger B, Stein H, Dorken B, Jenuwein T, Schmitt C A. Oncogene-induced senescence as an initial barrier in lymphoma development [J]. Nature, 2005, 436(7051): 660-665.
[8] Hayflick L. The Limited in Vitro Lifetime of Human Diploid Cell Strains [J]. Experimental cell research, 1965, 37(614-636.
[9] Shay J W. Role of Telomeres and Telomerase in Aging and Cancer [J]. Cancer discovery, 2016, 6(6): 584-593.
[10] Serrano M, Lin A W, McCurrach M E, Beach D, Lowe S W. Oncogenic ras provokes premature cell senescence associated with accumulation of p53 and p16INK4a [J]. Cell, 1997, 88(5): 593-602.
[11] Perez-Mancera P A, Young A R, Narita M. Inside and out: the activities of senescence in cancer [J]. Nature reviews Cancer, 2014, 14(8): 547-558.
[12] Lin A W, Barradas M, Stone J C, van Aelst L, Serrano M, Lowe S W. Premature senescence involving p53 and p16 is activated in response to constitutive MEK/MAPK mitogenic signaling [J]. Genes & development, 1998, 12(19): 3008-3019.
[13] Bartkova J, Rezaei N, Liontos M, Karakaidos P, Kletsas D, Issaeva N, Vassiliou L V, Kolettas E, Niforou K, Zoumpourlis V C, Takaoka M, Nakagawa H, Tort F, Fugger K, Johansson F, Sehested M, Andersen C L, Dyrskjot L, Orntoft T, Lukas J, Kittas C, Helleday T,

Halazonetis T D, Bartek J, Gorgoulis V G. Oncogene-induced senescence is part of the tumorigenesis barrier imposed by DNA damage checkpoints [J]. Nature, 2006, 444(7119): 633-637.
[14] Rai T S, Cole J J, Nelson D M, Dikovskaya D, Faller W J, Vizioli M G, Hewitt R N, Anannya O, McBryan T, Manoharan I, van Tuyn J, Morrice N, Pchelintsev N A, Ivanov A, Brock C, Drotar M E, Nixon C, Clark W, Sansom O J, Anderson K I, King A, Blyth K, Adams P D. HIRA orchestrates a dynamic chromatin landscape in senescence and is required for suppression of neoplasia [J]. Genes & development, 2014, 28(24): 2712-2725.
[15] Chandra T, Kirschner K, Thuret J Y, Pope B D, Ryba T, Newman S, Ahmed K, Samarajiwa S A, Salama R, Carroll T, Stark R, Janky R, Narita M, Xue L, Chicas A, Nunez S, Janknecht R, Hayashi-Takanaka Y, Wilson M D, Marshall A, Odom D T, Babu M M, Bazett-Jones D P, Tavare S, Edwards P A, Lowe S W, Kimura H, Gilbert D M, Narita M. Independence of repressive histone marks and chromatin compaction during senescent heterochromatic layer formation [J]. Molecular cell, 2012, 47(2): 203-214.
[16] Narita M, Nunez S, Heard E, Narita M, Lin A W, Hearn S A, Spector D L, Hannon G J, Lowe S W. Rb-mediated heterochromatin formation and silencing of E2F target genes during cellular senescence [J]. Cell, 2003, 113(6): 703-716.
[17] Lee S, Schmitt C A. The dynamic nature of senescence in cancer [J]. Nature cell biology, 2019, 21(1): 94-101.
[18] Coppe J P, Desprez P Y, Krtolica A, Campisi J. The senescence-associated secretory phenotype: the dark side of tumor suppression [J]. Annual review of pathology, 2010, 5(99-118.
[19] Ito Y, Hoare M, Narita M. Spatial and Temporal Control of Senescence [J]. Trends in cell biology, 2017, 27(11): 820-832.
[20] Chibaya L, Snyder J, Ruscetti M. Senescence and the tumor-immune landscape: Implications for cancer immunotherapy [J]. Seminars in cancer biology, 2022,
[21] Biran A, Perelmutter M, Gal H, Burton D G, Ovadya Y, Vadai E, Geiger T, Krizhanovsky V. Senescent cells communicate via intercellular protein transfer [J]. Genes & development, 2015, 29(8): 791-802.
[22] Triana-Martinez F, Loza M I, Dominguez E. Beyond Tumor Suppression: Senescence in Cancer Stemness and Tumor Dormancy [J]. Cells, 2020, 9(2):
[23] Reimann M, Schrezenmeier J, Richter-Pechanska P, Dolnik A, Hick T P, Schleich K, Cai X, Fan D N Y, Lohneis P, Masswig S, Denker S, Busse A, Knittel G, Flumann R, Childs D, Childs L, Gatjens-Sanchez A M, Bullinger L, Rosenwald A, Reinhardt H C, Schmitt C A. Adaptive T-cell immunity controls senescence-prone MyD88- or CARD11-mutant B-cell lymphomas [J]. Blood, 2021, 137(20): 2785-2799.
[24] Dorr J R, Yu Y, Milanovic M, Beuster G, Zasada C, Dabritz J H, Lisec J, Lenze D, Gerhardt A, Schleicher K, Kratzat S, Purfurst B, Walenta S, Mueller-Klieser W, Graler M, Hummel M, Keller U, Buck A K, Dorken B, Willmitzer L, Reimann M, Kempa S, Lee S, Schmitt C A. Synthetic lethal metabolic targeting of cellular senescence in cancer therapy [J]. Nature, 2013, 501(7467): 421-425.
[25] Reimann M, Lee S, Loddenkemper C, Dorr J R, Tabor V, Aichele P, Stein H, Dorken B, Jenuwein T, Schmitt C A. Tumor stroma-derived TGF-beta limits myc-driven lymphomagenesis via Suv39h1-dependent senescence [J]. Cancer cell, 2010, 17(3): 262-272.
[26] Milanovic M, Fan D N Y, Belenki D, Dabritz J H M, Zhao Z, Yu Y, Dorr J R, Dimitrova

L, Lenze D, Monteiro Barbosa I A, Mendoza-Parra M A, Kanashova T, Metzner M, Pardon K, Reimann M, Trumpp A, Dorken B, Zuber J, Gronemeyer H, Hummel M, Dittmar G, Lee S, Schmitt C A. Senescence-associated reprogramming promotes cancer stemness [J]. Nature, 2018, 553(7686): 96-100.
[27] Yu Y, Schleich K, Yue B, Ji S, Lohneis P, Kemper K, Silvis M R, Qutob N, van Rooijen E, Werner-Klein M, Li L, Dhawan D, Meierjohann S, Reimann M, Elkahloun A, Treitschke S, Dorken B, Speck C, Mallette F A, Zon L I, Holmen S L, Peeper D S, Samuels Y, Schmitt C A, Lee S. Targeting the Senescence-Overriding Cooperative Activity of Structurally Unrelated H3K9 Demethylases in Melanoma [J]. Cancer cell, 2018, 33(2): 322-336 e328.
[28] Xue W, Zender L, Miething C, Dickins R A, Hernando E, Krizhanovsky V, Cordon-Cardo C, Lowe S W. Senescence and tumour clearance is triggered by p53 restoration in murine liver carcinomas [J]. Nature, 2007, 445(7128): 656-660.
[29] Ruscetti M, Leibold J, Bott M J, Fennell M, Kulick A, Salgado N R, Chen C C, Ho Y J, Sanchez-Rivera F J, Feucht J, Baslan T, Tian S, Chen H A, Romesser P B, Poirier J T, Rudin C M, de Stanchina E, Manchado E, Sherr C J, Lowe S W. NK cell-mediated cytotoxicity contributes to tumor control by a cytostatic drug combination [J]. Science, 2018, 362(6421): 1416-1422.
[30] Iannello A, Thompson T W, Ardolino M, Lowe S W, Raulet D H. p53-dependent chemokine production by senescent tumor cells supports NKG2D-dependent tumor elimination by natural killer cells [J]. The Journal of experimental medicine, 2013, 210(10): 2057-2069.
[31] Lujambio A, Akkari L, Simon J, Grace D, Tschaharganeh D F, Bolden J E, Zhao Z, Thapar V, Joyce J A, Krizhanovsky V, Lowe S W. Non-cell-autonomous tumor suppression by p53 [J]. Cell, 2013, 153(2): 449-460.
[32] Petti C, Molla A, Vegetti C, Ferrone S, Anichini A, Sensi M. Coexpression of NRASQ61R and BRAFV600E in human melanoma cells activates senescence and increases susceptibility to cell-mediated cytotoxicity [J]. Cancer Res, 2006, 66(13): 6503-6511.
[33] van Tuyn J, Jaber-Hijazi F, MacKenzie D, Cole J J, Mann E, Pawlikowski J S, Rai T S, Nelson D M, McBryan T, Ivanov A, Blyth K, Wu H, Milling S, Adams P D. Oncogene-Expressing Senescent Melanocytes Up-Regulate MHC Class II, a Candidate Melanoma Suppressor Function [J]. The Journal of investigative dermatology, 2017, 137(10): 2197-2207.
[34] Sturmlechner I, Zhang C, Sine C C, van Deursen E J, Jeganathan K B, Hamada N, Grasic J, Friedman D, Stutchman J T, Can I, Hamada M, Lim D Y, Lee J H, Ordog T, Laberge R M, Shapiro V, Baker D J, Li H, van Deursen J M. p21 produces a bioactive secretome that places stressed cells under immunosurveillance [J]. Science, 2021, 374(6567): eabb3420.
[35] Lasry A, Ben-Neriah Y. Senescence-associated inflammatory responses: aging and cancer perspectives [J]. Trends in immunology, 2015, 36(4): 217-228.
[36] Kang T W, Yevsa T, Woller N, Hoenicke L, Wuestefeld T, Dauch D, Hohmeyer A, Gereke M, Rudalska R, Potapova A, Iken M, Vucur M, Weiss S, Heikenwalder M, Khan S, Gil J, Bruder D, Manns M, Schirmacher P, Tacke F, Ott M, Luedde T, Longerich T, Kubicka S, Zender L. Senescence surveillance of pre-malignant hepatocytes limits liver cancer development [J]. Nature, 2011, 479(7374): 547-551.
[37] Eggert T, Wolter K, Ji J, Ma C, Yevsa T, Klotz S, Medina-Echeverz J, Longerich T, Forgues M, Reisinger F, Heikenwalder M, Wang X W, Zender L, Greten T F. Distinct Functions of Senescence-Associated Immune Responses in Liver Tumor Surveillance and Tumor

Progression [J]. Cancer cell, 2016, 30(4): 533-547.
[38] Goncalves S, Yin K, Ito Y, Chan A, Olan I, Gough S, Cassidy L, Serrao E, Smith S, Young A, Narita M, Hoare M. COX2 regulates senescence secretome composition and senescence surveillance through PGE2 [J]. Cell reports, 2021, 34(11): 108860.
[39] Mazzoni M, Mauro G, Erreni M, Romeo P, Minna E, Vizioli M G, Belgiovine C, Rizzetti M G, Pagliardini S, Avigni R, Anania M C, Allavena P, Borrello M G, Greco A. Senescent thyrocytes and thyroid tumor cells induce M2-like macrophage polarization of human monocytes via a PGE2-dependent mechanism [J]. Journal of experimental & clinical cancer research : CR, 2019, 38(1): 208.
[40] Pereira B I, Devine O P, Vukmanovic-Stejic M, Chambers E S, Subramanian P, Patel N, Virasami A, Sebire N J, Kinsler V, Valdovinos A, LeSaux C J, Passos J F, Antoniou A, Rustin M H A, Campisi J, Akbar A N. Senescent cells evade immune clearance via HLA-E-mediated NK and CD8(+) T cell inhibition [J]. Nature communications, 2019, 10(1): 2387.
[41] Munoz D P, Yannone S M, Daemen A, Sun Y, Vakar-Lopez F, Kawahara M, Freund A M, Rodier F, Wu J D, Desprez P Y, Raulet D H, Nelson P S, van 't Veer L J, Campisi J, Coppe J P. Targetable mechanisms driving immunoevasion of persistent senescent cells link chemotherapy-resistant cancer to aging [J]. JCI insight, 2019, 5(
[42] Paver E C, Cooper W A, Colebatch A J, Ferguson P M, Hill S K, Lum T, Shin J S, O'Toole S, Anderson L, Scolyer R A, Gupta R. Programmed death ligand-1 (PD-L1) as a predictive marker for immunotherapy in solid tumours: a guide to immunohistochemistry implementation and interpretation [J]. Pathology, 2021, 53(2): 141-156.
[43] Toso A, Revandkar A, Di Mitri D, Guccini I, Proietti M, Sarti M, Pinton S, Zhang J, Kalathur M, Civenni G, Jarrossay D, Montani E, Marini C, Garcia-Escudero R, Scanziani E, Grassi F, Pandolfi P P, Catapano C V, Alimonti A. Enhancing chemotherapy efficacy in Pten-deficient prostate tumors by activating the senescence-associated antitumor immunity [J]. Cell reports, 2014, 9(1): 75-89.
[44] Ruhland M K, Loza A J, Capietto A H, Luo X, Knolhoff B L, Flanagan K C, Belt B A, Alspach E, Leahy K, Luo J, Schaffer A, Edwards J R, Longmore G, Faccio R, DeNardo D G, Stewart S A. Stromal senescence establishes an immunosuppressive microenvironment that drives tumorigenesis [J]. Nature communications, 2016, 7(11762.
[45] Garcia A J, Ruscetti M, Arenzana T L, Tran L M, Bianci-Frias D, Sybert E, Priceman S J, Wu L, Nelson P S, Smale S T, Wu H. Pten null prostate epithelium promotes localized myeloid-derived suppressor cell expansion and immune suppression during tumor initiation and progression [J]. Molecular and cellular biology, 2014, 34(11): 2017-2028.
[46] Zhu Y, Tchkonia T, Pirtskhalava T, Gower A C, Ding H, Giorgadze N, Palmer A K, Ikeno Y, Hubbard G B, Lenburg M, O'Hara S P, LaRusso N F, Miller J D, Roos C M, Verzosa G C, LeBrasseur N K, Wren J D, Farr J N, Khosla S, Stout M B, McGowan S J, Fuhrmann-Stroissnigg H, Gurkar A U, Zhao J, Colangelo D, Dorronsoro A, Ling Y Y, Barghouthy A S, Navarro D C, Sano T, Robbins P D, Niedernhofer L J, Kirkland J L. The Achilles' heel of senescent cells: from transcriptome to senolytic drugs [J]. Aging cell, 2015, 14(4): 644-658.
[47] Wang L, Bernards R. Taking advantage of drug resistance, a new approach in the war on cancer [J]. Frontiers of medicine, 2018, 12(4): 490-495.
[48] Kirkland J L, Tchkonia T. Senolytic drugs: from discovery to translation [J]. Journal of internal medicine, 2020, 288(5): 518-536.

[49] Wu H, Schiff D S, Lin Y, Neboori H J, Goyal S, Feng Z, Haffty B G. Ionizing radiation sensitizes breast cancer cells to Bcl-2 inhibitor, ABT-737, through regulating Mcl-1 [J]. Radiation research, 2014, 182(6): 618-625.
[50] Wang L, Leite de Oliveira R, Wang C, Fernandes Neto J M, Mainardi S, Evers B, Lieftink C, Morris B, Jochems F, Willemsen L, Beijersbergen R L, Bernards R. High-Throughput Functional Genetic and Compound Screens Identify Targets for Senescence Induction in Cancer [J]. Cell reports, 2017, 21(3): 773-783.
[51] Fleury H, Malaquin N, Tu V, Gilbert S, Martinez A, Olivier M A, Sauriol A, Communal L, Leclerc-Desaulniers K, Carmona E, Provencher D, Mes-Masson A M, Rodier F. Exploiting interconnected synthetic lethal interactions between PARP inhibition and cancer cell reversible senescence [J]. Nature communications, 2019, 10(1): 2556.
[52] Galiana I, Lozano-Torres B, Sancho M, Alfonso M, Bernardos A, Bisbal V, Serrano M, Martinez-Manez R, Orzaez M. Preclinical antitumor efficacy of senescence-inducing chemotherapy combined with a nanoSenolytic [J]. Journal of controlled release : official journal of the Controlled Release Society, 2020, 323(624-634.
[53] Saleh T, Carpenter V J, Tyutyunyk-Massey L, Murray G, Leverson J D, Souers A J, Alotaibi M R, Faber A C, Reed J, Harada H, Gewirtz D A. Clearance of therapy-induced senescent tumor cells by the senolytic ABT-263 via interference with BCL-XL -BAX interaction [J]. Molecular oncology, 2020, 14(10): 2504-2519.
[54] Shahbandi A, Rao S G, Anderson A Y, Frey W D, Olayiwola J O, Ungerleider N A, Jackson J G. BH3 mimetics selectively eliminate chemotherapy-induced senescent cells and improve response in TP53 wild-type breast cancer [J]. Cell death and differentiation, 2020, 27(11): 3097-3116.
[55] Whittle J R, Vaillant F, Surgenor E, Policheni A N, Giner G, Capaldo B D, Chen H R, Liu H K, Dekkers J F, Sachs N, Clevers H, Fellowes A, Green T, Xu H, Fox S B, Herold M J, Smyth G K, Gray D H D, Visvader J E, Lindeman G J. Dual Targeting of CDK4/6 and BCL2 Pathways Augments Tumor Response in Estrogen Receptor-Positive Breast Cancer [J]. Clinical cancer research : an official journal of the American Association for Cancer Research, 2020, 26(15): 4120-4134.
[56] Vilgelm A E, Pawlikowski J S, Liu Y, Hawkins O E, Davis T A, Smith J, Weller K P, Horton L W, McClain C M, Ayers G D, Turner D C, Essaka D C, Stewart C F, Sosman J A, Kelley M C, Ecsedy J A, Johnston J N, Richmond A. Mdm2 and aurora kinase a inhibitors synergize to block melanoma growth by driving apoptosis and immune clearance of tumor cells [J]. Cancer Res, 2015, 75(1): 181-193.
[57] Kaefer A, Yang J, Noertersheuser P, Mensing S, Humerickhouse R, Awni W, Xiong H. Mechanism-based pharmacokinetic/pharmacodynamic meta-analysis of navitoclax (ABT-263) induced thrombocytopenia [J]. Cancer chemotherapy and pharmacology, 2014, 74(3): 593-602.
[58] Pi L, Rooprai J, Allan D S, Atkins H, Bredeson C, Fulcher A J, Ito C, Ramsay T, Shorr, Stanford W L, Sabloff M, Christou G. Evaluating dose-limiting toxicities of MDM2 inhibitors in patients with solid organ and hematologic malignancies: A systematic review of the literature [J]. Leuk Res, 2019, 86(106222.
[59]Di Micco R, Krizhanovsky V, Baker D, d'Adda di Fagagna F. Cellular senescence in ageing: from mechanisms to therapeutic opportunities [J]. Nature reviews Molecular cell biology, 2021, 22(2): 75-95.

[60] Herranz N, Gallage S, Mellone M, Wuestefeld T, Klotz S, Hanley C J, Raguz S, Acosta J C, Innes A J, Banito A, Georgilis A, Montoya A, Wolter K, Dharmalingam G, Faull P, Carroll T, Martinez-Barbera J P, Cutillas P, Reisinger F, Heikenwalder M, Miller R A, Withers D, Zender L, Thomas G J, Gil J. mTOR regulates MAPKAPK2 translation to control the senescence-associated secretory phenotype [J]. Nature cell biology, 2015, 17(9): 1205-1217.
[61] Laberge R M, Sun Y, Orjalo A V, Patil C K, Freund A, Zhou L, Curran S C, Davalos A R, Wilson-Edell K A, Liu S, Limbad C, Demaria M, Li P, Hubbard G B, Ikeno Y, Javors M, Desprez P Y, Benz C C, Kapahi P, Nelson P S, Campisi J. MTOR regulates the pro-tumorigenic senescence-associated secretory phenotype by promoting IL1A translation [J]. Nature cell biology, 2015, 17(8): 1049-1061.
[62] Alimbetov D, Davis T, Brook A J, Cox L S, Faragher R G, Nurgozhin T, Zhumadilov Z, Kipling D. Suppression of the senescence-associated secretory phenotype (SASP) in human fibroblasts using small molecule inhibitors of p38 MAP kinase and MK2 [J]. Biogerontology, 2016, 17(2): 305-315.
[63] Mosteiro L, Pantoja C, Alcazar N, Marion R M, Chondronasiou D, Rovira M, Fernandez-Marcos P J, Munoz-Martin M, Blanco-Aparicio C, Pastor J, Gomez-Lopez G, De Martino A, Blasco M A, Abad M, Serrano M. Tissue damage and senescence provide critical signals for cellular reprogramming in vivo [J]. Science, 2016, 354(6315):
[64] Xu M, Tchkonia T, Ding H, Ogrodnik M, Lubbers E R, Pirtskhalava T, White T A, Johnson K O, Stout M B, Mezera V, Giorgadze N, Jensen M D, LeBrasseur N K, Kirkland J L. JAK inhibition alleviates the cellular senescence-associated secretory phenotype and frailty in old age [J]. Proceedings of the National Academy of Sciences of the United States of America, 2015, 112(46): E6301-6310.
[65] Dijkgraaf E M, Santegoets S J, Reyners A K, Goedemans R, Wouters M C, Kenter G G, van Erkel A R, van Poelgeest M I, Nijman H W, van der Hoeven J J, Welters M J, van der Burg S H, Kroep J R. A phase I trial combining carboplatin/doxorubicin with tocilizumab, an anti-IL-6R monoclonal antibody, and interferon-alpha2b in patients with recurrent epithelial ovarian cancer [J]. Annals of oncology : official journal of the European Society for Medical Oncology, 2015, 26(10): 2141-2149.
[66] Merritt W M, Lin Y G, Spannuth W A, Fletcher M S, Kamat A A, Han L Y, Landen C N, Jennings N, De Geest K, Langley R R, Villares G, Sanguino A, Lutgendorf S K, Lopez-Berestein G, Bar-Eli M M, Sood A K. Effect of interleukin-8 gene silencing with liposome-encapsulated small interfering RNA on ovarian cancer cell growth [J]. Journal of the National Cancer Institute, 2008, 100(5): 359-372.
[67] Schott A F, Goldstein L J, Cristofanilli M, Ruffini P A, McCanna S, Reuben J M, Perez R P, Kato G, Wicha M. Phase Ib Pilot Study to Evaluate Reparixin in Combination with Weekly Paclitaxel in Patients with HER-2-Negative Metastatic Breast Cancer [J]. Clinical cancer research : an official journal of the American Association for Cancer Research, 2017, 23(18): 5358-5365.
[68] Lee S, Yu Y, Trimpert J, Benthani F, Mairhofer M, Richter-Pechanska P, Wyler E, Belenki D, Kaltenbrunner S, Pammer M, Kausche L, Firsching T C, Dietert K, Schotsaert M, Martinez-Romero C, Singh G, Kunz S, Niemeyer D, Ghanem R, Salzer H J F, Paar C, Mulleder M, Uccellini M, Michaelis E G, Khan A, Lau A, Schonlein M, Habringer A, Tomasits J, Adler J M, Kimeswenger S, Gruber A D, Hoetzenecker W, Steinkellner H, Purfurst B, Motz R, Di Pierro

F, Lamprecht B, Osterrieder N, Landthaler M, Drosten C, Garcia-Sastre A, Langer R, Ralser M, Eils R, Reimann M, Fan D N Y, Schmitt C A. Virus-induced senescence is a driver and therapeutic target in COVID-19 [J]. Nature, 2021, 599(7884): 283-289.
[69] Kim B G, Malek E, Choi S H, Ignatz-Hoover J J, Driscoll J J. Novel therapies emerging in oncology to target the TGF-beta pathway [J]. Journal of hematology & oncology, 2021, 14(1): 55.
[70] Moore G, Annett S, McClements L, Robson T. Top Notch Targeting Strategies in Cancer: A Detailed Overview of Recent Insights and Current Perspectives [J]. Cells, 2020, 9(6):
[71] Le Naour J, Zitvogel L, Galluzzi L, Vacchelli E, Kroemer G. Trial watch: STING agonists in cancer therapy [J]. Oncoimmunology, 2020, 9(1): 1777624.
[72] Andre P, Denis C, Soulas C, Bourbon-Caillet C, Lopez J, Arnoux T, Blery M, Bonnafous C, Gauthier L, Morel A, Rossi B, Remark R, Breso V, Bonnet E, Habif G, Guia S, Lalanne A I, Hoffmann C, Lantz O, Fayette J, Boyer-Chammard A, Zerbib R, Dodion P, Ghadially H, Jure-Kunkel M, Morel Y, Herbst R, Narni-Mancinelli E, Cohen R B, Vivier E. Anti-NKG2A mAb Is a Checkpoint Inhibitor that Promotes Anti-tumor Immunity by Unleashing Both T and NK Cells [J]. Cell, 2018, 175(7): 1731-1743 e1713.
[73] Ferrari de Andrade L, Tay R E, Pan D, Luoma A M, Ito Y, Badrinath S, Tsoucas D, Franz B, May K F, Jr., Harvey C J, Kobold S, Pyrdol J W, Yoon C, Yuan G C, Hodi F S, Dranoff G, Wucherpfennig K W. Antibody-mediated inhibition of MICA and MICB shedding promotes NK cell-driven tumor immunity [J]. Science, 2018, 359(6383): 1537-1542.
[74] Jerby-Arnon L, Shah P, Cuoco M S, Rodman C, Su M J, Melms J C, Leeson R, Kanodia A, Mei S, Lin J R, Wang S, Rabasha B, Liu D, Zhang G, Margolais C, Ashenberg O, Ott P A, Buchbinder E I, Haq R, Hodi F S, Boland G M, Sullivan R J, Frederick D T, Miao B, Moll T, Flaherty K T, Herlyn M, Jenkins R W, Thummalapalli R, Kowalczyk M S, Canadas I, Schilling B, Cartwright A N R, Luoma A M, Malu S, Hwu P, Bernatchez C, Forget M A, Barbie D A, Shalek A K, Tirosh I, Sorger P K, Wucherpfennig K, Van Allen E M, Schadendorf D, Johnson B E, Rotem A, Rozenblatt-Rosen O, Garraway L A, Yoon C H, Izar B, Regev A. A Cancer Cell Program Promotes T Cell Exclusion and Resistance to Checkpoint Blockade [J]. Cell, 2018, 175(4): 984-997 e924.
[75] Guan X, LaPak K M, Hennessey R C, Yu C Y, Shakya R, Zhang J, Burd C E. Stromal Senescence By Prolonged CDK4/6 Inhibition Potentiates Tumor Growth [J]. Molecular cancer research : MCR, 2017, 15(3): 237-249.
[76] Deng J, Wang E S, Jenkins R W, Li S, Dries R, Yates K, Chhabra S, Huang W, Liu H, Aref A R, Ivanova E, Paweletz C P, Bowden M, Zhou C W, Herter-Sprie G S, Sorrentino J A, Bisi J E, Lizotte P H, Merlino A A, Quinn M M, Bufe L E, Yang A, Zhang Y, Zhang H, Gao P, Chen T, Cavanaugh M E, Rode A J, Haines E, Roberts P J, Strum J C, Richards W G, Lorch J H, Parangi S, Gunda V, Boland G M, Bueno R, Palakurthi S, Freeman G J, Ritz J, Haining W N, Sharpless N E, Arthanari H, Shapiro G I, Barbie D A, Gray N S, Wong K K. CDK4/6 Inhibition Augments Antitumor Immunity by Enhancing T-cell Activation [J]. Cancer discovery, 2018, 8(2): 216-233.
[77] Knudsen E S, Kumarasamy V, Chung S, Ruiz A, Vail P, Tzetzo S, Wu J, Nambiar R, Sivinski J, Chauhan S S, Seshadri M, Abrams S I, Wang J, Witkiewicz A K. Targeting dual signalling pathways in concert with immune checkpoints for the treatment of pancreatic cancer [J]. Gut, 2021, 70(1): 127-138.

[78] Kim K M, Noh J H, Bodogai M, Martindale J L, Yang X, Indig F E, Basu S K, Ohnuma K, Morimoto C, Johnson P F, Biragyn A, Abdelmohsen K, Gorospe M. Identification of senescent cell surface targetable protein DPP4 [J]. Genes & development, 2017, 31(15): 1529-1534.
[79] Amor C, Feucht J, Leibold J, Ho Y J, Zhu C, Alonso-Curbelo D, Mansilla-Soto J, Boyer J A, Li X, Giavridis T, Kulick A, Houlihan S, Peerschke E, Friedman S L, Ponomarev V, Piersigilli A, Sadelain M, Lowe S W. Senolytic CAR T cells reverse senescence-associated pathologies [J]. Nature, 2020, 583(7814): 127-132.
[80] Jurtz V I, Jessen L E, Bentzen A K, Jespersen M C, Mahajan S, Vita R, Jensen K K, Marcatili P, Hadrup S R, Peters B, Nielsen M. NetTCR: sequence-based prediction of TCR binding to peptide-MHC complexes using convolutional neural networks [J]. bioRxiv : the preprint server for biology, 2018, 433706.
[81] Nisonoff A, Rivers M M. Recombination of a mixture of univalent antibody fragments of different specificity [J]. Archives of biochemistry and biophysics, 1961, 93(460-462.
[82]Brinkmann U, Kontermann R E. The making of bispecific antibodies [J]. mAbs, 2017, 9(2): 182-212.
[83] Blanco B, Dominguez-Alonso C, Alvarez-Vallina L. Bispecific Immunomodulatory Antibodies for Cancer Immunotherapy [J]. Clinical cancer research : an official journal of the American Association for Cancer Research, 2021, 27(20): 5457-5464.
[84] Trabolsi A, Arumov A, Schatz J H. T Cell-Activating Bispecific Antibodies in Cancer Therapy [J]. J Immunol, 2019, 203(3): 585-592.
[85] Strohl W R, Naso M. Bispecific T-Cell Redirection versus Chimeric Antigen Receptor (CAR)-T Cells as Approaches to Kill Cancer Cells [J]. Antibodies, 2019, 8(3):
[86] Garrido F. HLA Class-I Expression and Cancer Immunotherapy [J]. Advances in experimental medicine and biology, 2019, 1151(79-90.
[87] Cheadle E J. MT-103 Micromet/MedImmune [J]. Current opinion in molecular therapeutics, 2006, 8(1): 62-68.
[88] Klinger M, Brandl C, Zugmaier G, Hijazi Y, Bargou R C, Topp M S, Gokbuget N, Neumann S, Goebeler M, Viardot A, Stelljes M, Bruggemann M, Hoelzer D, Degenhard E, Nagorsen D, Baeuerle P A, Wolf A, Kufer P. Immunopharmacologic response of patients with B-lineage acute lymphoblastic leukemia to continuous infusion of T cell-engaging CD19/CD3-bispecific BiTE antibody blinatumomab [J]. Blood, 2012, 119(26): 6226-6233.
[89] Topp M S, Gokbuget N, Stein A S, Zugmaier G, O'Brien S, Bargou R C, Dombret H, Fielding A K, Heffner L, Larson R A, Neumann S, Foa R, Litzow M, Ribera J M, Rambaldi A, Schiller G, Bruggemann M, Horst H A, Holland C, Jia C, Maniar T, Huber B, Nagorsen D, Forman S J, Kantarjian H M. Safety and activity of blinatumomab for adult patients with relapsed or refractory B-precursor acute lymphoblastic leukaemia: a multicentre, single-arm, phase 2 study [J]. The Lancet Oncology, 2015, 16(1): 57-66.
[90] Goebeler M E, Knop S, Viardot A, Kufer P, Topp M S, Einsele H, Noppeney R, Hess G, Kallert S, Mackensen A, Rupertus K, Kanz L, Libicher M, Nagorsen D, Zugmaier G, Klinger M, Wolf A, Dorsch B, Quednau B D, Schmidt M, Scheele J, Baeuerle P A, Leo E, Bargou R C. Bispecific T-Cell Engager (BiTE) Antibody Construct Blinatumomab for the Treatment of Patients With Relapsed/Refractory Non-Hodgkin Lymphoma: Final Results From a Phase I Study [J]. Journal of clinical oncology : official journal of the American Society of Clinical

Oncology, 2016, 34(10): 1104-1111.
[91] Viardot A, Goebeler M E, Hess G, Neumann S, Pfreundschuh M, Adrian N, Zettl F, Libicher M, Sayehli C, Stieglmaier J, Zhang A, Nagorsen D, Bargou R C. Phase 2 study of the bispecific T-cell engager (BiTE) antibody blinatumomab in relapsed/refractory diffuse large B-cell lymphoma [J]. Blood, 2016, 127(11): 1410-1416.
[92] Dufner V, Sayehli C M, Chatterjee M, Hummel H D, Gelbrich G, Bargou R C, Goebeler M E. Long-term outcome of patients with relapsed/refractory B-cell non-Hodgkin lymphoma treated with blinatumomab [J]. Blood advances, 2019, 3(16): 2491-2498.
[93] Coyle L, Morley N J, Rambaldi A, Mason K D, Verhoef G, Furness C L, Zhang A, Jung A S, Cohan D, Franklin J L. Open-Label, phase 2 study of blinatumomab as second salvage therapy in adults with relapsed/refractory aggressive B-cell non-Hodgkin lymphoma [J]. Leukemia & lymphoma, 2020, 61(9): 2103-2112.
[94] Messeant O, Houot R, Manson G. T-cell Redirecting Therapies for the Treatment of B-cell Lymphomas: Recent Advances [J]. Cancers, 2021, 13(17):
[95] Schuster S J, Bartlett N L, Assouline S, Yoon S-S, Bosch F, Sehn L H, Cheah C Y, Shadman M, Gregory G P, Ku M, Wei M C, Yin S, Kwan A, Yousefi K, Hernandez G, Li C-C, O'Hear C, Budde L E. Mosunetuzumab Induces Complete Remissions in Poor Prognosis Non-Hodgkin Lymphoma Patients, Including Those Who Are Resistant to or Relapsing After Chimeric Antigen Receptor T-Cell (CAR-T) Therapies, and Is Active in Treatment through Multiple Lines [J]. Blood, 2019, 134(Supplement_1): 6-6.
[96] Hutchings M, Mous R, Clausen M R, Johnson P, Linton K M, Chamuleau M E D, Lewis D J, Sureda Balari A, Cunningham D, Oliveri R S, Elliott B, DeMarco D, Azaryan A, Chiu C, Li T, Chen K M, Ahmadi T, Lugtenburg P J. Dose escalation of subcutaneous epcoritamab in patients with relapsed or refractory B-cell non-Hodgkin lymphoma: an open-label, phase 1/2 study [J]. Lancet, 2021, 398(10306): 1157-1169.
[97] Bannerji R, Allan J N, Arnason J E, Brown J R, Advani R, Ansell S M, O'Brien S M, Duell J, Martin P, Joyce R M, Li J, Flink D M, Zhu M, Weinreich D M, Yancopoulos G D, Sirulnik A, Chaudhry A, Ambati S R, Topp M S. Odronextamab (REGN1979), a Human CD20 x CD3 Bispecific Antibody, Induces Durable, Complete Responses in Patients with Highly Refractory B-Cell Non-Hodgkin Lymphoma, Including Patients Refractory to CAR T Therapy [J]. Blood, 2020, 136(Supplement 1): 42-43.
[98] Hutchings M, Morschhauser F, Iacoboni G, Carlo-Stella C, Offner F C, Sureda A, Salles G, Martinez-Lopez J, Crump M, Thomas D N, Morcos P N, Ferlini C, Broske A E, Belousov A, Bacac M, Dimier N, Carlile D J, Lundberg L, Perez-Callejo D, Umana P, Moore T, Weisser M, Dickinson M J. Glofitamab, a Novel, Bivalent CD20-Targeting T-Cell-Engaging Bispecific Antibody, Induces Durable Complete Remissions in Relapsed or Refractory B-Cell Lymphoma: A Phase I Trial [J]. Journal of clinical oncology : official journal of the American Society of Clinical Oncology, 2021, 39(18): 1959-1970.
[99] Olszewski A J, Avigdor A, Babu S, Levi I, Abadi U, Holmes H, McKinney M, McCord R, Xie Y, Chen C, Sarouei K, Qayum N, O'Hear C, Sellam G, Eradat H. Single-Agent Mosunetuzumab Is a Promising Safe and Efficacious Chemotherapy-Free Regimen for Elderly/Unfit Patients with Previously Untreated Diffuse Large B-Cell Lymphoma [J]. Blood, 2020, 136(Supplement 1): 43-45.
[100] Hutchings M, Mous R, Clausen M R, Johnson P, Linton K M, Chamuleau M E D,

Lewis D J, Sureda Balari A, Cunningham D, Oliveri R S, DeMarco D, Elliott B, Chen K-m, Lugtenburg P J. Subcutaneous Epcoritamab Induces Complete Responses with an Encouraging Safety Profile across Relapsed/Refractory B-Cell Non-Hodgkin Lymphoma Subtypes, Including Patients with Prior CAR-T Therapy: Updated Dose Escalation Data [J]. Blood, 2020, 136(Supplement 1): 45-46.

[101] de Charette M, Marabelle A, Houot R. Turning tumour cells into antigen presenting cells: The next step to improve cancer immunotherapy? [J]. Eur J Cancer, 2016, 68(134-147.

[102] de Charette M, Houot R. Hide or defend, the two strategies of lymphoma immune evasion: potential implications for immunotherapy [J]. Haematologica, 2018, 103(8): 1256-1268.

[103] Dustin M L. The immunological synapse [J]. Cancer immunology research, 2014, 2(11): 1023-1033.

[104] Challa-Malladi M, Lieu Y K, Califano O, Holmes A B, Bhagat G, Murty V V, Dominguez-Sola D, Pasqualucci L, Dalla-Favera R. Combined genetic inactivation of beta2-Microglobulin and CD58 reveals frequent escape from immune recognition in diffuse large B cell lymphoma [J]. Cancer cell, 2011, 20(6): 728-740.

[105] Fangazio M, Ladewig E, Gomez K, Garcia-Ibanez L, Kumar R, Teruya-Feldstein J, Rossi D, Filip I, Pan-Hammarstrom Q, Inghirami G, Boldorini R, Ott G, Staiger A M, Chapuy B, Gaidano G, Bhagat G, Basso K, Rabadan R, Pasqualucci L, Dalla-Favera R. Genetic mechanisms of HLA-I loss and immune escape in diffuse large B cell lymphoma [J]. Proceedings of the National Academy of Sciences of the United States of America, 2021, 118(22):

[106] Tada K, Maeshima A M, Hiraoka N, Yamauchi N, Maruyama D, Kim S W, Watanabe T, Katayama N, Heike Y, Tobinai K, Kobayashi Y. Prognostic significance of HLA class I and II expression in patients with diffuse large B cell lymphoma treated with standard chemoimmunotherapy [J]. Cancer immunology, immunotherapy : CII, 2016, 65(10): 1213-1222.

[107] Hashwah H, Schmid C A, Kasser S, Bertram K, Stelling A, Manz M G, Muller A. Inactivation of CREBBP expands the germinal center B cell compartment, down-regulates MHCII expression and promotes DLBCL growth [J]. Proceedings of the National Academy of Sciences of the United States of America, 2017, 114(36): 9701-9706.

[108] Kendrick S, Rimsza L M, Scott D W, Slack G W, Farinha P, Tan K L, Persky D, Puvvada S, Connors J M, Sehn L, Gascoyne R D, Schmelz M. Aberrant cytoplasmic expression of MHCII confers worse progression free survival in diffuse large B-cell lymphoma [J]. Virchows Archiv : an international journal of pathology, 2017, 470(1): 113-117.

[109] Razzaghi R, Agarwal S, Kotlov N, Plotnikova O, Nomie K, Huang D W, Wright G W, Smith G A, Li M, Takata K, Yamadi M, Yao C, O'Shea J J, Phelan J D, Pittaluga S, Scott D W, Muppidi J R. Compromised counterselection by FAS creates an aggressive subtype of germinal center lymphoma [J]. The Journal of experimental medicine, 2021, 218(3):

[110] Wohlfart S, Sebinger D, Gruber P, Buch J, Polgar D, Krupitza G, Rosner M, Hengstschlager M, Raderer M, Chott A, Mullauer L. FAS (CD95) mutations are rare in gastric MALT lymphoma but occur more frequently in primary gastric diffuse large B-cell lymphoma [J]. The American journal of pathology, 2004, 164(3): 1081-1089.

[111] Chatzitolios A, Venizelos I, Tripsiannis G, Anastassopoulos G, Papadopoulos N.

Prognostic significance of CD95, P53, and BCL2 expression in extranodal non-Hodgkin's lymphoma [J]. Annals of hematology, 2010, 89(9): 889-896.
[112] Iqbal J, Sanger W G, Horsman D E, Rosenwald A, Pickering D L, Dave B, Dave S, Xiao L, Cao K, Zhu Q, Sherman S, Hans C P, Weisenburger D D, Greiner T C, Gascoyne R D, Ott G, Muller-Hermelink H K, Delabie J, Braziel R M, Jaffe E S, Campo E, Lynch J C, Connors J M, Vose J M, Armitage J O, Grogan T M, Staudt L M, Chan W C. BCL2 translocation defines a unique tumor subset within the germinal center B-cell-like diffuse large B-cell lymphoma [J]. The American journal of pathology, 2004, 165(1): 159-166.
[113] Schmitz R, Wright G W, Huang D W, Johnson C A, Phelan J D, Wang J Q, Roulland S, Kasbekar M, Young R M, Shaffer A L, Hodson D J, Xiao W, Yu X, Yang Y, Zhao H, Xu W, Liu X, Zhou B, Du W, Chan W C, Jaffe E S, Gascoyne R D, Connors J M, Campo E, Lopez-Guillermo A, Rosenwald A, Ott G, Delabie J, Rimsza L M, Tay Kuang Wei K, Zelenetz A D, Leonard J P, Bartlett N L, Tran B, Shetty J, Zhao Y, Soppet D R, Pittaluga S, Wilson W H, Staudt L M. Genetics and Pathogenesis of Diffuse Large B-Cell Lymphoma [J]. The New England journal of medicine, 2018, 378(15): 1396-1407.
[114] Laurent C, Charmpi K, Gravelle P, Tosolini M, Franchet C, Ysebaert L, Brousset P, Bidaut A, Ycart B, Fournie J J. Several immune escape patterns in non-Hodgkin's lymphomas [J]. Oncoimmunology, 2015, 4(8): e1026530.
[115] Kiyasu J, Miyoshi H, Hirata A, Arakawa F, Ichikawa A, Niino D, Sugita Y, Yufu Y, Choi I, Abe Y, Uike N, Nagafuji K, Okamura T, Akashi K, Takayanagi R, Shiratsuchi M, Ohshima K. Expression of programmed cell death ligand 1 is associated with poor overall survival in patients with diffuse large B-cell lymphoma [J]. Blood, 2015, 126(19): 2193-2201.
[116] Rossille D, Gressier M, Damotte D, Maucort-Boulch D, Pangault C, Semana G, Le Gouill S, Haioun C, Tarte K, Lamy T, Milpied N, Fest T, Groupe Ouest-Est des Leucemies et Autres Maladies du S, Groupe Ouest-Est des Leucemies et Autres Maladies du S. High level of soluble programmed cell death ligand 1 in blood impacts overall survival in aggressive diffuse large B-Cell lymphoma: results from a French multicenter clinical trial [J]. Leukemia, 2014, 28(12): 2367-2375.
[117] Krittikarux S, Wudhikarn K, Tangnuntachai N, Assanasen T, Sukswai N, Asawapanumas T, Chanswangphuwana C. The influence of programmed cell death ligand 2 (PD-L2) expression on survival outcome and tumor microenvironment in diffuse large B cell lymphoma [J]. Leukemia & lymphoma, 2020, 61(14): 3395-3403.
[118] Rossille D, Azzaoui I, Feldman A L, Maurer M J, Laboure G, Parrens M, Pangault C, Habermann T M, Ansell S M, Link B K, Tarte K, Witzig T E, Lamy T, Slager S L, Roussel M, Milpied N, Cerhan J R, Fest T. Soluble programmed death-ligand 1 as a prognostic biomarker for overall survival in patients with diffuse large B-cell lymphoma: a replication study and combined analysis of 508 patients [J]. Leukemia, 2017, 31(4): 988-991.
[119] Chao M P, Alizadeh A A, Tang C, Myklebust J H, Varghese B, Gill S, Jan M, Cha A C, Chan C K, Tan B T, Park C Y, Zhao F, Kohrt H E, Malumbres R, Briones J, Gascoyne R D, Lossos I S, Levy R, Weissman I L, Majeti R. Anti-CD47 antibody synergizes with rituximab to promote phagocytosis and eradicate non-Hodgkin lymphoma [J]. Cell, 2010, 142(5): 699-713.
[120] Kazama R, Miyoshi H, Takeuchi M, Miyawaki K, Nakashima K, Yoshida N, Kawamoto K, Yanagida E, Yamada K, Umeno T, Suzuki T, Kato K, Takizawa J, Seto M, Akashi K, Ohshima K. Combination of CD47 and signal-regulatory protein-alpha constituting the

"don't eat me signal" is a prognostic factor in diffuse large B-cell lymphoma [J]. Cancer science, 2020, 111(7): 2608-2619.
[121] Mullauer L, Mosberger I, Chott A. Fas ligand expression in nodal non-Hodgkin's lymphoma [J]. Modern pathology : an official journal of the United States and Canadian Academy of Pathology, Inc, 1998, 11(4): 369-375.
[122] Lech-Maranda E, Bienvenu J, Broussais-Guillaumot F, Warzocha K, Michallet A S, Robak T, Coiffier B, Salles G. Plasma TNF-alpha and IL-10 level-based prognostic model predicts outcome of patients with diffuse large B-Cell lymphoma in different risk groups defined by the International Prognostic Index [J]. Archivum immunologiae et therapiae experimentalis, 2010, 58(2): 131-141.
[123] Liu X Q, Lu K, Feng L L, Ding M, Gao J M, Ge X L, Wang X. Up-regulated expression of indoleamine 2,3-dioxygenase 1 in non-Hodgkin lymphoma correlates with increased regulatory T-cell infiltration [J]. Leukemia & lymphoma, 2014, 55(2): 405-414.
[124] El Hussein S, Shaw K R M, Vega F. Evolving insights into the genomic complexity and immune landscape of diffuse large B-cell lymphoma: opportunities for novel biomarkers [J]. Modern pathology : an official journal of the United States and Canadian Academy of Pathology, Inc, 2020, 33(12): 2422-2436.
[125] Steen C B, Luca B A, Esfahani M S, Azizi A, Sworder B J, Nabet B Y, Kurtz D M, Liu C L, Khameneh F, Advani R H, Natkunam Y, Myklebust J H, Diehn M, Gentles A J, Newman A M, Alizadeh A A. The landscape of tumor cell states and ecosystems in diffuse large B cell lymphoma [J]. Cancer cell, 2021, 39(10): 1422-1437 e1410.
[126] Zhukovsky E A, Morse R J, Maus M V. Bispecific antibodies and CARs: generalized immunotherapeutics harnessing T cell redirection [J]. Current opinion in immunology, 2016, 40(24-35.
[127] Ahuja A, Shupe J, Dunn R, Kashgarian M, Kehry M R, Shlomchik M J. Depletion of B cells in murine lupus: efficacy and resistance [J]. J Immunol, 2007, 179(5): 3351-3361.
[128] Krop I, de Fougerolles A R, Hardy R R, Allison M, Schlissel M S, Fearon D T. Self-renewal of B-1 lymphocytes is dependent on CD19 [J]. European journal of immunology, 1996, 26(1): 238-242.
[129] Ridgway J B, Presta L G, Carter P. 'Knobs-into-holes' engineering of antibody CH3 domains for heavy chain heterodimerization [J]. Protein engineering, 1996, 9(7): 617-621.
[130] Adams J M, Harris A W, Pinkert C A, Corcoran L M, Alexander W S, Cory S, Palmiter R D, Brinster R L. The c-myc oncogene driven by immunoglobulin enhancers induceslymphoid malignancy in transgenic mice [J]. Nature, 1985, 318(6046): 533-538.
[131] Peters A H, O'Carroll D, Scherthan H, Mechtler K, Sauer S, Schofer C, Weipoltshammer K, Pagani M, Lachner M, Kohlmaier A, Opravil S, Doyle M, Sibilia M, Jenuwein T. Loss of the Suv39h histone methyltransferases impairs mammalian heterochromatin and genome stability [J]. Cell, 2001, 107(3): 323-337.
[132] Schmitt C A, Fridman J S, Yang M, Baranov E, Hoffman R M, Lowe S W. Dissecting p53 tumor suppressor functions in vivo [J]. Cancer cell, 2002, 1(3): 289-298.
[133] Schmitt C A, McCurrach M E, de Stanchina E, Wallace-Brodeur R R, Lowe S W. INK4a/ARF mutations accelerate lymphomagenesis and promote chemoresistance by disabling p53 [J]. Genes & development, 1999, 13(20): 2670-2677.
[134] Gérard A. In vitro T Cell–DC and T Cell–T Cell Clustering Assays [J]. Bio-protocol,

2013, 3(20): e933.
[135] Sun L L, Ellerman D, Mathieu M, Hristopoulos M, Chen X, Li Y, Yan X, Clark R, Reyes A, Stefanich E, Mai E, Young J, Johnson C, Huseni M, Wang X, Chen Y, Wang P, Wang H, Dybdal N, Chu Y W, Chiorazzi N, Scheer J M, Junttila T, Totpal K, Dennis M S, Ebens A J. Anti-CD20/CD3 T cell-dependent bispecific antibody for the treatment of B cell malignancies [J]. Science translational medicine, 2015, 7(287): 287ra270.
[136] Wesalo J S, Deiters A. Chapter Ten - Fast phosphine-activated control of protein function using unnatural lysine analogues [M]//CHENOWETH D M. Methods in enzymology. Academic Press. 2020: 191-217.
[137] Dimri G P, Lee X, Basile G, Acosta M, Scott G, Roskelley C, Medrano E E, Linskens M, Rubelj I, Pereira-Smith O, et al. A biomarker that identifies senescent human cells in culture and in aging skin in vivo [J]. Proceedings of the National Academy of Sciences of the United States of America, 1995, 92(20): 9363-9367.
[138] Subramanian A, Tamayo P, Mootha V K, Mukherjee S, Ebert B L, Gillette M A, Paulovich A, Pomeroy S L, Golub T R, Lander E S, Mesirov J P. Gene set enrichment analysis: a knowledge-based approach for interpreting genome-wide expression profiles [J]. Proceedings of the National Academy of Sciences of the United States of America, 2005, 102(43): 15545-15550.
[139] Mootha V K, Lindgren C M, Eriksson K F, Subramanian A, Sihag S, Lehar J, Puigserver P, Carlsson E, Ridderstrale M, Laurila E, Houstis N, Daly M J, Patterson N, Mesirov J P, Golub T R, Tamayo P, Spiegelman B, Lander E S, Hirschhorn J N, Altshuler D, Groop L C. PGC-1alpha-responsive genes involved in oxidative phosphorylation are coordinately downregulated in human diabetes [J]. Nature genetics, 2003, 34(3): 267-273.
[140] Ziegler S F, Ramsdell F, Alderson M R. The activation antigen CD69 [J]. Stem Cells, 1994, 12(5): 456-465.
[141] Verbsky J W, Routes J R. 41 - Recurrent Fever, Infections, Immune Disorders, and Autoinflammatory Diseases [M]//KLIEGMAN R M, LYE P S, BORDINI B J, et al. Nelson Pediatric Symptom-Based Diagnosis. Elsevier. 2018: 746-773.e741.
[142] Brusko T M, Wasserfall C H, Hulme M A, Cabrera R, Schatz D, Atkinson M A. Influence of membrane CD25 stability on T lymphocyte activity: implications for immunoregulation [J]. PLoS One, 2009, 4(11): e7980.
[143] He M Y, Kridel R. Treatment resistance in diffuse large B-cell lymphoma [J]. Leukemia, 2021, 35(8): 2151-2165.
[144] Nesic M, El-Galaly T C, Bogsted M, Pedersen I S, Dybkaer K. Mutational landscape of immune surveillance genes in diffuse large B-cell lymphoma [J]. Expert review of hematology, 2020, 13(6): 655-668.
[145] Childs B G, Baker D J, Kirkland J L, Campisi J, van Deursen J M. Senescence and apoptosis: dueling or complementary cell fates? [J]. EMBO reports, 2014, 15(11): 1139-1153.
[146] Busse S, Steiner J, Alter J, Dobrowolny H, Mawrin C, Bogerts B, Hartig R, Busse M. Expression of HLA-DR, CD80, and CD86 in Healthy Aging and Alzheimer's Disease [J]. Journal of Alzheimer's disease : JAD, 2015, 47(1): 177-184.
[147] Fulop T, Le Page A, Garneau H, Azimi N, Baehl S, Dupuis G, Pawelec G, Larbi A. Aging, immunosenescence and membrane rafts: the lipid connection [J]. Longevity & healthspan, 2012, 1(6.

[148] Kohnke T, Krupka C, Tischer J, Knosel T, Subklewe M. Increase of PD-L1 expressing B-precursor ALL cells in a patient resistant to the CD19/CD3-bispecific T cell engager antibody blinatumomab [J]. Journal of hematology & oncology, 2015, 8(111.
[149] Feucht J, Kayser S, Gorodezki D, Hamieh M, Doring M, Blaeschke F, Schlegel P, Bosmuller H, Quintanilla-Fend L, Ebinger M, Lang P, Handgretinger R, Feuchtinger T. T-cell responses against CD19+ pediatric acute lymphoblastic leukemia mediated by bispecific T-cell engager (BiTE) are regulated contrarily by PD-L1 and CD80/CD86 on leukemic blasts [J]. Oncotarget, 2016, 7(47): 76902-76919.
[150] Webster J, Luskin M R, Prince G T, DeZern A E, DeAngelo D J, Levis M J, Blackford A, Sharon E, Streicher H, Luznik L, Gojo I. Blinatumomab in Combination with Immune Checkpoint Inhibitors of PD-1 and CTLA-4 in Adult Patients with Relapsed/Refractory (R/R) CD19 Positive B-Cell Acute Lymphoblastic Leukemia (ALL): Preliminary Results of a Phase I Study [J]. Blood, 2018, 132(Supplement 1): 557-557.
[151] Kobayashi T, Ubukawa K, Fujishima M, Takahashi N. Correlation between increased immune checkpoint molecule expression and refractoriness to blinatumomab evaluated by longitudinal T cell analysis [J]. Int J Hematol, 2021, 113(4): 600-605.
[152] Goldstein M, Roos W P, Kaina B. Apoptotic death induced by the cyclophosphamide analogue mafosfamide in human lymphoblastoid cells: contribution of DNA replication, transcription inhibition and Chk/p53 signaling [J]. Toxicology and applied pharmacology, 2008, 229(1): 20-32.
[153] Fan D N Y, Schmitt C A. Genotoxic Stress-Induced Senescence [J]. Methods Mol Biol, 2019, 1896(93-105.

7. Statutory Declaration

"I, Xiurong Cai, by personally signing this document in lieu of an oath, hereby affirm that I prepared the submitted dissertation on the topic [T-cell surveillance of therapy-induced senescent lymphoma cells in the presence of anti-CD19/CD20×CD3 bispecific antibodies (T-Zell-Überwachung von therapieinduzierten seneszenten Lymphomzellen in Gegenwart von Anti-CD19/CD20×CD3 bispezifischen Antikörpern)], independently and without the support of third parties, and that I used no other sources and aids than those stated.

All parts which are based on the publications or presentations of other authors, either in letter or in spirit, are specified as such in accordance with the citing guidelines. The sections on methodology (in particular regarding practical work, laboratory regulations, statistical processing) and results (in particular regarding figures, charts and tables) are exclusively my responsibility.

Furthermore, I declare that I have correctly marked all of the data, the analyses, and the conclusions generated from data obtained in collaboration with other persons, and that I have correctly marked my own contribution and the contributions of other persons (cf. declaration of contribution). I have correctly marked all texts or parts of texts that were generated in collaboration with other persons.

My contributions to any publications to this dissertation correspond to those stated in the below joint declaration made together with the supervisor. All publications created within the scope of the dissertation comply with the guidelines of the ICMJE (International Committee of Medical Journal Editors; www.icmje.org) on authorship. In addition, I declare that I shall comply with the regulations of Charité – Universitätsmedizin Berlin on ensuring good scientific practice.

I declare that I have not yet submitted this dissertation in identical or similar form to another Faculty.
The significance of this statutory declaration and the consequences of a false statutory declaration under criminal law (Sections 156, 161 of the German Criminal Code) are known to me."

Date	Signature

8. Curriculum Vitae

My curriculum vitae does not appear in the electronic version of my paper for reasons of data protection.

9. List of publications

1. The macrophage-associated microRNA-4715-3p/Gasdermin D axis potentially indicates fibrosis progression in nonalcoholic fatty liver disease: evidence from transcriptome and biological data. Shuai Chen, **Xiurong Cai**, Yu Liu, Yu Shen, Adrien Guillot, Frank Tacke, Liming Tang, Hanyang Liu. Bioengineered. 2022 May;13(5):11740-11751.
2. Adaptive T-cell immunity controls senescence-prone MyD88- or CARD11-mutant B-cell lymphomas. Maurice Reimann, Jens Schrezenmeier, Paulina Richter-Pechanska, Anna Dolnik, Timon Pablo Hick, Kolja Schleich, **Xiurong Cai**, Dorothy N Y Fan, Philipp Lohneis, Sven Maßwig, Sophy Denker, Antonia Busse, Gero Knittel, Ruth Flümann, Dorothee Childs, Liam Childs, Ana-Maria Gätjens-Sanchez, Lars Bullinger, Andreas Rosenwald, Hans Christian Reinhardt, Clemens A Schmitt. Blood. 2021 May 20; 137(20): 2785-2799.
3. circNFATC3 sponges miR-548I acts as a ceRNA to protect NFATC3 itself and suppressed hepatocellular carcinoma progression. Changchang Jia, Zhicheng Yao, Zexiao Lin, Liyun Zhao, **Xiurong Cai**, Shaohong Chen, Meihai Deng, Qi Zhang. J Cell Physiol. 2021 Feb;236(2):1252-1269.
4. Efficacy of cytokine-induced killer cell-based immunotherapy for hepatocellular carcinoma. Chang-Chang Jia, Yun-Hao Chen, **Xiu-Rong Cai**, Yang Li, Xiao-Fang Zheng, Zhi-Cheng Yao, Li-Yun Zhao, Dong-Bo Qiu, Shu-Juan Xie, Wen-Jie Chen, Chang Liu, Qiu-Li Liu, Xiang-Yuan Wu, Tian-Tian Wang, Qi Zhang. Am J Cancer Res. 2019 Jun 1;9(6):1254-1265.
5. Endoplasmic reticulum stress induced Lox-1+ CD15+ polymorphonuclear myeloid-derived suppressor cells in hepatocellular carcinoma. Jiang Nan, Yan-FangXing, Bo Hu, Jian-Xin Tang, Hui-Min Dong, Yu-Mei He, Dan-Yun Ruan, Qing- Jian Ye, Jia-Rong Cai, Xiao-Kun Ma, Jie Chen, **Xiu-Rong Cai**, Ze-Xiao Lin, Xiang-Yuan Wu, Xing Li. Immunology. 2018 May;154(1):144-155.
6. Modified CLIP score with albumin-bilirubin grade retains prognostic prediction in

patients who had undergone trans-catheter arterial chemoembolization therapy for HBV-related hepatocellular carcinoma. **Xiu-Rong Cai,** Zhan-Hong Chen, Meng-Meng Liu, Jin-Xiang Lin, Xiao-Ping Zhang, Jie Chen, Qu Lin, Xiao-Kun Ma, Jing-Yun Wen, Si-Dong Xie, Xiang-Yuan Wu, Min Dong. J Cancer. 2018 Jun 14;9(13):2380-2388.

7. Albumin-to-Alkaline Phosphatase Ratio as An Independent Prognostic Factor for Overall Survival of Advanced Hepatocellular Carcinoma Patients Without Receiving Standard Anti-Cancer Therapies. **Xiurong Cai,** Zhanhong Chen, Jie Chen, Xiaokun Ma, Mingjun Bai, Tiantian Wang, Xiangwei Chen, Donghao Wu, Li Wei, Xing Li, Qu Lin, Jingyun Wen, Danyun Ruan, Zexiao Lin, Min Dong, Xiangyuan Wu. J Cancer 2018; 9(1):189-197.
8. The Predictive Value of Albumin-to-Alkaline Phosphatase Ratio for Overall Survival of Hepatocellular Carcinoma Patients Treated with Trans-Catheter Arterial Chemoembolization Therapy. Zhan-Hong Chen, Xiao-Ping Zhang, **Xiu-Rong Cai**, Si-Dong Xie, Meng-Meng Liu, Jin-Xiang Lin, Xiao-Kun Ma, Jie Chen, Qu Lin, Min Dong, Xiang-Yuan Wu, Jing-Yun Wen, Rui-Hua Xu. J Cancer. 2018 Sep 8;9(19):3467-3478.
9. Autologous transplantation of cytokine-induced killer cells as an adjuvant therapy for hepatocellular carcinoma in Asia: an update meta-analysis and systematic review. **Xiu-Rong Cai,** Xing Li, Jin-Xiang Lin, Tian-Tian Wang, Min Dong, Zhan-Hong Chen, Chang-Chang Jia, Ying-Fen Hong, Qu Lin, Xiang-Yuan Wu. Oncotarget, 2017, Vol. 8, (No. 19): 31318-31328.
10. Identification of the prognostic value of lymphocyte-to-monocyte ratio in patients with HBV-associated advanced hepatocellular carcinoma. Ying-Fen Hong, Zhan-Hong Chen, Li Wei, Xiao-Kun Ma, Xing Li, Jing-Yun Wen, Tian-Tian Wang, **Xiu-Rong Cai**, Dong-Hao Wu, Jie Chen, Dan-Yun Ruan, Ze-Xiao Lin, Qu Lin, Min Dong, Xiang-Yuan Wu. Oncol Lett. 2017 Aug;14(2):2089-2096.

10. Acknowledgements

Words cannot express my gratitude to Prof. Dr. med. Clemens Schmitt for his insightful guidance and invaluable feedback during my study in Berlin, Germany. Thank you for inviting me as a doctoral student to complete a scientific project in the Department of Hematology, Oncology and Cancer Immunology at Charité - Universitätsmedizin Berlin. With the support of my second supervisor Prof. Dr. rer. nat. Gerald Willimsky, I can properly start this incredible project. Moreover, I could not have undertaken this journey successfully without my lab supervisor Dr. rer. nat. Dorothy Ngo Yin Fan, who generously provided professional knowledge and expertise to me for my research work. I would like to express my sincere acknowledgement to Dr Fan not only for her academic suggestions for my project, but also for her kind heart in my life after work. I would like to thank Prof. Dr. rer. nat. Soyoung Lee for her support in the conduction of my project. Additionally, this endeavor would not have been possible without the support from the Chinese Scholarship Council (CSC), which financed my 4-year doctoral study in Germany. I am also grateful to be a doctoral student at the Berlin School of Integrative Oncology (BSIO), which gave me lots of opportunities to be involved in a young scientist community and take part in various academic or leisure activities.

I am also grateful to my colleagues from AG Schmitt (Dr. rer. nat. Maurice Reimann, Dr. rer. nat. Animesh Bhattacharya, Dr. rer. nat. Dimitri Belenki, Ana Maria Gätjens-Sanchez, Dr. med. Jan Rafael Dörr, Dr. rer. nat. Yong Yu, Dr. med. Aitomi Bittner, Andrea Lau, Nadine Burbach, Sven Maßwig, Philipp Schulz, Gregor Kandler and Sabine Kaltenbrunner) and Nazli Güllü from AG Ulrike Stein, for their professional advice and technical support.

Lastly, I would be remiss in not mentioning my family. Their belief in me has kept my spirits and motivation high during my study in Berlin. I would also like to thank my friends for all the entertainment and emotional support.

11. Statistician's certificate

CHARITÉ

CharitéCentrum für Human- und Gesundheitswissenschaften

Charité | Campus Charité Mitte | 10117 Berlin

Name, Vorname: Cai, Xiurong
Email adresse: xiurong.cai@charite.de
Matrikelnummer: 226747
PromotionsbetreuerIn: Prof. Dr. med. Clemens Schmitt
Promotionsinstitution / Klinik: Medizinische Klinik mit Schwerpunkt Hämatologie, Onkologie und Tumorimmunologie

Institut für Biometrie und klinische Epidemiologie (iBikE)
Direktor: Prof. Dr. Frank Konietschke
Postanschrift:
Charitéplatz 1 | 10117 Berlin
Besucheranschrift:
Reinhardtstr. 58 | 10117 Berlin
Tel. +49 (0)30 450 562171
frank.konietschke@charite.de
https://biometrie.charite.de/

Bescheinigung

Hiermit bescheinige ich, dass Frau *Xiurong Cai* innerhalb der Service Unit Biometrie des Instituts für Biometrie und klinische Epidemiologie (iBikE) bei mir eine statistische Beratung zu einem Promotionsvorhaben wahrgenommen hat. Folgende Beratungstermine wurden wahrgenommen:

- Termin 1: 24.08.2022

Folgende wesentliche Ratschläge hinsichtlich einer sinnvollen Auswertung und Interpretation der Daten wurden während der Beratung erteilt:

- Two-way ANOVA
- Two-way repeated measures ANOVA
- Graphik Darstellung
- Effektgröße

Diese Bescheinigung garantiert nicht die richtige Umsetzung der in der Beratung gemachten Vorschläge, die korrekte Durchführung der empfohlenen statistischen Verfahren und die richtige Darstellung und Interpretation der Ergebnisse. Die Verantwortung hierfür obliegt allein dem Promovierenden. Das Institut für Biometrie und klinische Epidemiologie übernimmt hierfür keine Haftung.

Datum: 17.10.2022 Name der Beraterin: Pimrapat Gebert

Pimrapat Gebert Digital unterschrieben von Pimrapat Gebert Datum: 2022.10.17 11:34:38 +02'00'

Unterschrift BeraterIn, Institutsstempel

CHARITÉ UNIVERSITÄTSMEDIZIN BERLIN
Institut für Biometrie und Klinische Epidemiologie
Campus Charité Mitte
Charitéplatz 1 | D-10117 Berlin
Sitz: Reinhardtstr. 58